A PRELIMINARY INVESTIGATION OF FOULING IN BRAZED PLATE HEAT EXCHANGERS

By

ELLISA LIM

Bachelor of Science in Mechanical Engineering

Seattle University

Seattle, WA

2006

Submitted to the Faculty of the
Graduate College of the
Oklahoma State University
in partial fulfillment of
the requirements for
the Degree of
MASTER OF SCIENCE
July, 2010

A PRELIMINARY INVESTIGATION OF FOULING IN

BRAZED PLATE HEAT EXCHANGERS

Thesis Approved:

Dr. Jeffrey Spitler

Thesis Adviser

Dr. Lorenzo Cremaschi

Dr. Daniel Fisher

Dr. Mark E. Payton

Dean of the Graduate College

ACKNOWLEDGMENTS

I am indebted to many people who have supported and helped me throughout the completion of my work. In my humble acknowledgement, I would like to convey my gratitude to them. First and foremost, I would like to express my deep gratitude to my adviser, Dr. Jeffrey Spitler, for his patience, guidance and assistance through feedbacks throughout the writing process. I am grateful for his advice and generous assistance because I have always admired his sense of perfection and intelligence. I would also like to express my sincere gratitude to my committee member, Dr. Lorenzo Cremaschi, who also serves as the co-advisor. His guidance and support have really been crucial during the difficult times and I cannot be thankful enough for the opportunity that he has given to me to work on this project. My sincere gratitude also goes to Dr. Daniel Fisher who serves as my committee member and has helped me to determine my research path in the beginning of my graduate school.

There are so many numerous wonderful people that I have encountered during my graduate school. I wish to express my gratitude to some of my colleagues and friends who have made special contributions both directly and indirectly to my work: Mike Gulizio for all the help in understanding water chemistry; Befrika Murdianti and Bee Khim for answering all my chemistry questions; Malai Ramesh who has been working patiently with me for the past two years, Ozgur Aslan who has developed the Labview program for this project, Chandan, ShanShan, Lu, Pranav, and many more for sharing all the joy and laughter during my tough times. My sincere gratitude also goes to the Indonesian community in Stillwater for the friendships and for showing me great generosity.

I would also like to extend my deep gratitude to Fareez Ismail who has constantly provided me with encouragement. He is the one who has always challenged me “to be the best I can ever be”.

Last but not least, I would like to express my deepest gratitude to my family, and especially to my father. He is the reason to why I am here today, and I am very much indebted for all the sacrifices that have allowed me pursue my education here in the US.

TABLE OF CONTENTS

Chapter **Page**

Chapter Page

LIST OF TABLES

Table **Page**

Table **Page**

LIST OF FIGURES

Figure **Page**

Figure **Page**

Figure **Page**

Figure **Page**

CHAPTER I

INTRODUCTION

1.1 Background

There are four main components in a refrigeration cycle – evaporator, compressor, condenser and expansion device. The purpose of the condenser is to reject heat that is collected from a conditioned space by the evaporator. The condenser may transfer heat directly to the environment (air-cooled condenser) or via a cooling tower or fluid cooler (water-cooled condenser). Brazed Plate Heat Exchangers (BPHE) are commonly found in refrigeration cycles used as water-cooled condensers because of their high performance. BPHE-condensers are used with cooling towers to transfer heat from the conditioned space to the atmosphere. Generally, the water side of the water-cooled condenser has the most serious fouling problem in any of the heat exchangers in building heating, ventilation, and air conditioning (HVAC) system.

Fouling is defined as unwanted deposits on the heat exchanger surfaces. The presence of fouling causes resistance on heat exchange areas and thus reduces the thermal efficiency of heat exchangers. The water-cooled condenser suffers from fouling because the cooling tower is exposed to airborne dust and microbes and the required make-up water often contains minerals.

In order to consider fouling in design of HVAC systems, fouling factors are included in the design process. Fouling factors are design estimate of thermal resistances that may occur during heat exchanger operation and are used to help select a heat exchanger with sufficient capacity. The Tubular Exchangers Manufacturers Association (TEMA) first published a table of fouling factors for different fluids in a multitude of applications in 1941. These values were created for shell-and-tube heat exchangers, which were commonly used because of their robustness (Chenoweth, 1990). In practice, the same fouling factor is applied to all different type of heat exchangers. However, the fouling factor given by TEMA might not be appropriate for BPHE because BPHE has different heat transfer characteristics from shell-and-tube heat exchangers. The air conditioning industry has used the fouling factor of 8.8×10^{-5} $m^2 \cdot °C/W$ (5×10^{-4} $hr \cdot ft^2$ F/Btu) as specified by TEMA to select heat exchangers for evaporators and condensers (ARI, 1997). Air-Conditioning & Refrigeration Institute (AHRI) Guideline E-1988 reduced the fouling factor specified by TEMA to 4.4×10^{-5} $m^2 \cdot °C/W$ (2.5×10^{-4} $hr \cdot ft^2$ F/Btu) for both evaporator and condenser selections (AHRI, 1997). The fouling factor for evaporator selection was further reduced to 1.8×10^{-5} $m^2 \cdot °C/W$ (1.0×10^{-4} $hr \cdot ft^2$ F/Btu) in AHRI Guideline E-1997 (AHRI, 1997). The revised fouling factor for condensers has not been developed yet since there have not been enough data to assess fouling factor for condensers. This thesis focuses on the design and construction of a test facility to measure fouling on the water side of a brazed - plate type condenser in cooling tower applications.

1.2 Literature Review

Before starting to construct a test facility, a fundamental understanding about the heat transfer characteristics of BPHE and fouling parameters are required. In this section, an overview of BPHE technology is presented first. This review is followed by a review of precipitation and particulate fouling.

1.2.1 Brazed Plate Heat Exchangers

The Brazed Plate Heat Exchanger (BPHE) can be considered as a relatively new advancement of the plate and frame heat exchanger. The BPHE is able to handle higher pressure and capacity without requiring as much space as the plate and frame heat exchangers. The performance of BPHEs relies on the internal geometry of corrugated plates, which often incorporate a herringbone pattern. This type of pattern is able to maximize effective surface area of the plates.

There are several stainless steel corrugated plates pressed together with spacers in between the plates. The purposes of the spacers are to support the plates and to distribute flows of one fluid or the other across a plate. Every second plate is rotated 180° from the first plate creating 3-dimensional network of pathways through which the fluid flows. Depending on the internal geometry of the plates, the flow pattern could either be in the form of “zigzag” or “double-cross” flow as shown in Fig. 1-1A and Fig. 1-1B (Luan, Zhang, Tian, & Fan, 2008). In both flow patterns, the fluid streams intersect each other at the intersection nodes as shown in Fig. 1-2. These intersections points induce the turbulent flow and at the same time increases pressure drop inside the BPHE. The stacked plates are assembled with a thin copper sheet before the unit enters a furnace.

The melted copper acts as a brazing agent to seal the edges of the BPHE plates.

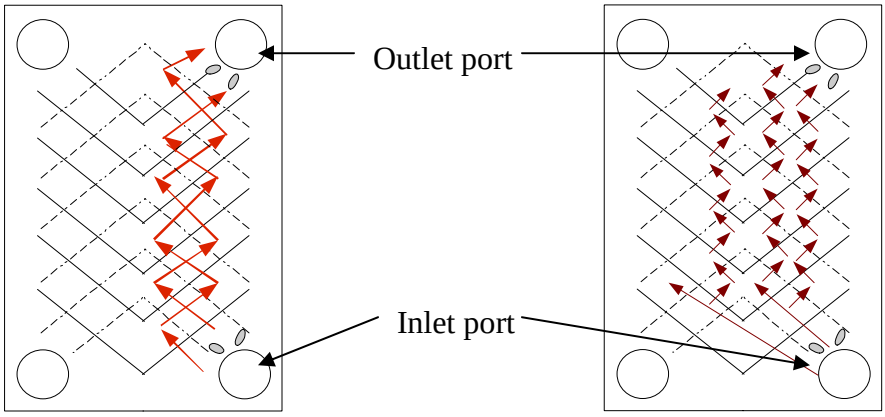

(A): Schematic of a flat plate with a double-cross flow pattern

(B): Schematic of a flat plate with a zig-zag flow pattern

Fig 1-1: Schematic of two different flow patterns inside BPHEs

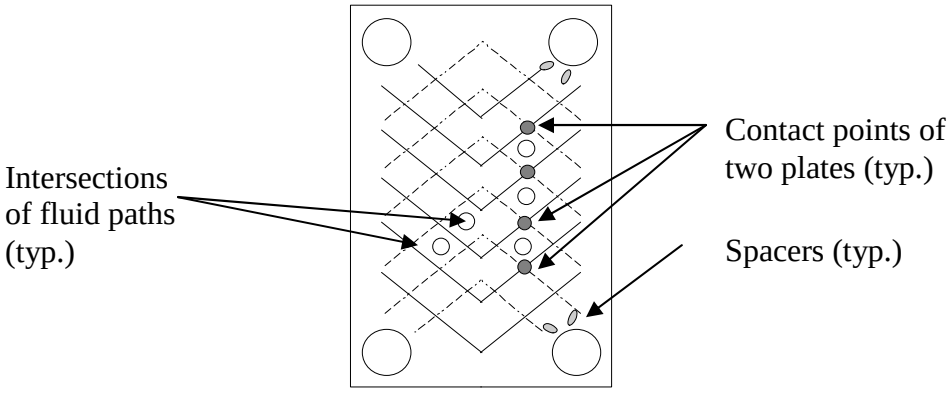

Fig 1-2: Schematic of a flat plate with a chevron angle

There are several possible arrangements inside a BPHE. The most common one is the single pass arrangement as shown in Fig. 1-3, which can be installed in either parallel or counterflow. The other possible arrangement is shown in Fig. 1-4, called multi-pass flow.

It involves running two or more parallel streams and in counter flow with respect to other parallel streams.

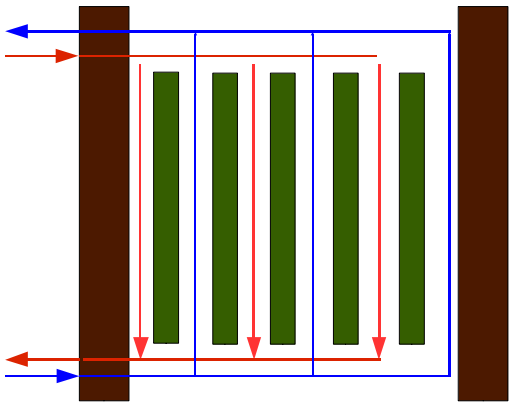

Fig. 1-3: Schematic of single pass flow arrangement

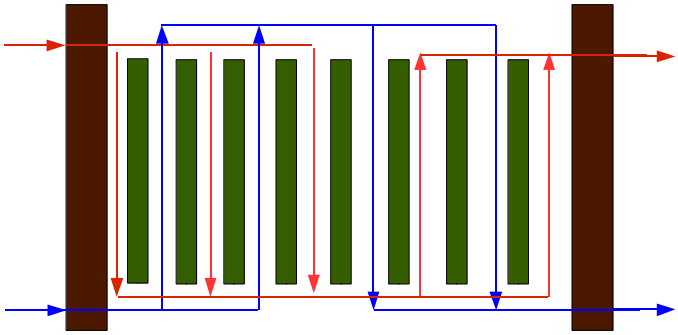

Fig. 1-4: Schematic of multi-pass flow arrangement

The thermal performance analysis of a BPHE relies on the evaluation of convective heat transfer coefficient for a given plate surface type and internal geometry. Several terms of internal geometry that used throughout this study are as follows:

1. Chevron angle (β)

   Chevron angle is an important parameter to determine thermal and hydraulic performance of BPHEs. Low chevron angle induce a higher heat transfer and pressure drop across the heat exchanger. Care must be exercised in defining a

chevron angle because chevron angle is defined differently in several literatures. In this study, the angle of herringbone pattern is measured from horizontal axis as shown in Fig. 1-5.

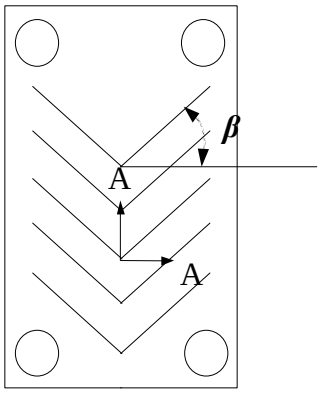

Fig. 1-5: Schematic of a BPHE plate with a herringbone pattern

2. Mean flow channel gap (*e*)

   The two plates are arranged adjacent to each other to form a space for fluid to flow. The space formed by two plates creates a complex 3D passage defined as a channel (Heggs, 2003). The mean flow channel gap is defined as the actual gap available for the flow as shown in Fig 1-6.

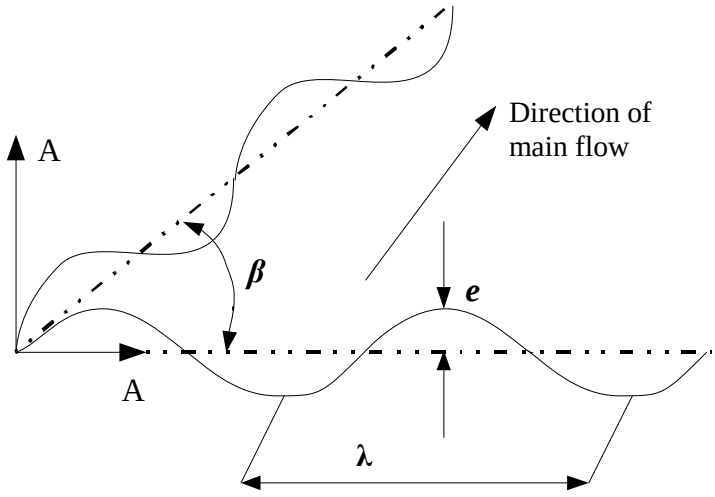

Fig. 1-6: Schematic of cross-sectional BPHE showing a flow channel

3. Enlargement factor (ϕ)

   The corrugated plates increase the overall heat transfer area compared to the flat plates. The increase of surface area is expressed as an enlargement factor. It is defined as the ratio of developed length over projected length as shown in Fig. 1-7.

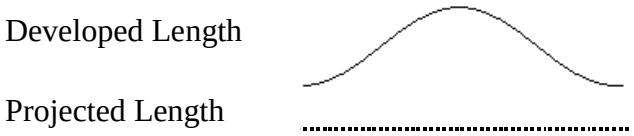

Figure 1-7: Cross sectional view of BPHE

4. Cross sectional area (A_c)

   Cross sectional area of the corrugated channel is defined as the actual flow area and can be computed using the following equation:

$$A_C = w * e \tag{1-1}$$

   where *w* is the width of the plate heat exchanger (m) or (inch)

5. Hydraulic diameter

   Hydraulic diameter is defined as:

$$d_h = \frac{2e}{\phi} \tag{1-2}$$

   When ϕ is not available, a simplified hydraulic diameter can be used for computations: $d_h = 2e$

6. Channel Reynolds number is defined as:

$$\mathrm{Re} = \frac{2 * \dot{M}_i}{\mu * w} \tag{1-3}$$

where: $\dot{M}_i$ is the channel mass flow rate $\left(\frac{kg}{s-channel}\right)$ or $\left(\frac{lb}{s-channel}\right)$

w is the width of the plate heat exchanger (m) or (inch)

μ = fluid viscosity $\left(\frac{kg}{m \ -s}\right)$ or $\left(\frac{lb}{ft \ -s}\right)$

Numerous investigators have developed correlations for estimating performance of BPHEs for single phase heat transfer. All of the correlations are functions of plates' chevron angle and Reynolds number because these are the parameters of interest that determine the performance of a BPHE. Ayub (2003) has compiled thermal and hydraulic correlations that have been developed for plate heat exchangers by several investigators. Ayub suggests using a correlation by Kumar (1984) for quick calculation and using Heavner et al. (1993), Wanniarachchi et al. (1995a), and Muley and Manglik (1999) for more elaborate calculations. These correlations can be used for plates of different manufacturers as long as the plate geometric parameters are within the limit of the validity of each correlation.

1.2.2 Fouling Background

Fouling is typically categorized by the different types of deposits. There are four different types of fouling that can be found in cooling towers:

1. Precipitation fouling: the deposition of minerals, which is caused by the reduction of mineral ions' solubility on the heat exchange surfaces.

This is often due to an inverse solubility, where solubility decreases with increasing temperature.

2. Particulate fouling: the accumulation of suspended solids on heat exchange surfaces.
3. Corrosion fouling: the accumulation of the corrosion on heat exchange surfaces.
4. Biological fouling: growth of microbiological organisms on the heat transfer surfaces. This is often referred to as “slime”.

The net fouling rate is expressed as the difference between the deposition and the removal rate (Kern, 1959):

$$\frac{dR_f}{dt} = \dot{m}_d - \dot{m}_r \tag{1-4}$$

Where: $\frac{dR_f}{dt}$ = net fouling rate

$\dot{m}_d$ = deposit rate $\left(\frac{kg}{m^2 - s}\right)$ or $\left(\frac{lb}{ft^2 - s}\right)$

$\dot{m}_r$ = removal rate $\left(\frac{kg}{m^2 - s}\right)$ or $\left(\frac{lb}{ft^2 - s}\right)$

The deposit rate depends on the type of fouling that occurs in the system and the removal rate should depend on the hardness, adhesive force of the deposit, and the shear stress on the surface of heat exchange areas. The deposit rates in a condenser utilized with a cooling tower are dominated by precipitation and particulate fouling mechanisms. Biological and corrosion fouling are usually prevented by using inhibitors. Precipitation fouling occurs simultaneously with particulate fouling in a cooling tower system because cooling tower water typically contains inversely-soluble minerals, which are originated

from the water source, dust and microbes from the atmosphere. Webb (1994) explained there are three possible trends of fouling curves as shown in Fig. 1-8.

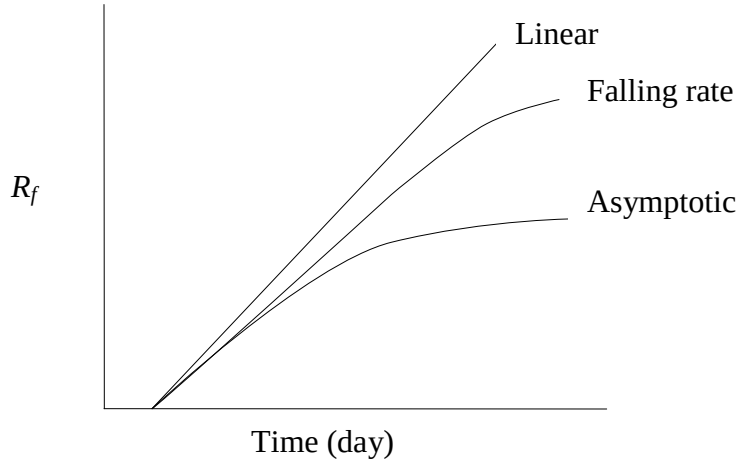

Fig. 1-8: Fouling curves

A linear growth is attained either when the removal rate is negligible or when the deposition and removal rates are constant as long as $\dot{m}_d > \dot{m}_r$. The fouling resistance will attain an asymptotic value only when $\dot{m}_d = \dot{m}_r$. It is mentioned that typically precipitation fouling follows the linear curve trend and the particulate fouling due to crystallization and corrosion follows the asymptotic curve trend. Most fouling studies report the measured fouling resistance (R_f) with respect to time for example study of alkalinity on scaling of simulated cooling tower by Morse (1977), study of particle size on particulate fouling by Chamra (1993), study of particulate fouling by Thonon (1995). Assuming uniform deposition over the heat exchanger surface, the fouling rates in Equation (1-4) can be expressed in terms of mass deposition rates (1995):

$$\frac{dm}{dt} = \dot{m} = \rho k_f \frac{dR_f}{dt} \tag{1-5}$$

Where: ρ = density of fouling deposit $\left(\frac{kg}{m^3}\right)$ or $\left(\frac{lb}{ft^3}\right)$

k_f = thermal conductivity of deposit $\left(\frac{W}{m-^oC}\right)$ or $\left(\frac{Btu}{ft-hr-^oF}\right)$

Taborek et al. (1972) have presented the first systematic investigation of fouling problem in heat exchangers with emphasis on $CaCO_3$. They explain different ways to express deposition rates depending on the deposition mechanisms. They proposed the following equations:

1. Precipitation fouling

   Precipitation fouling occurs due to crystallization on the heat transfer area. This type of fouling can be categorized as a reaction rate controlled deposition because it depends on the solubility of a mineral at a given fluid temperature. The deposition rate is given in the following equation:

$$\dot{m}_d = C_1 * (C_R)^n * \exp\left(\frac{-E}{R_g T_s}\right) \tag{1-6}$$

where: C_1 = constant

C_R = the water characterization factor, which is a function of the Langelier Index

n = the reaction order

E = the activation energy

R_g = the universal gas constant

T_s = the temperature of the fouling deposit surface (°C) or (°F)

2. For diffusion controlled deposition, which occurs in systems that have low fluid velocities and small size particles:

$$\dot{m}_d = C_3 K_d (C_b - C_s) \tag{1-7}$$

where: C_3 = constant

C_b = concentration in bulk of fluid $\left(\frac{mol}{L}\right)$

C_s = concentration at the surface $\left(\frac{mol}{L}\right)$

K_d = mass transfer coefficient $\left(\frac{m}{s}\right)$ or $\left(\frac{ft}{s}\right)$

3. For gravity controlled settling of solids, which effective for systems that have low velocities and large size particles:

$$\dot{m}_d = C_4 (\rho_s - \rho_f) \tag{1-8}$$

where:

C_4 = function of particle size, fluid velocity and viscosity

ρ_s = density of solid $\left(\frac{kg}{m^3}\right)$ or $\left(\frac{lb}{ft^3}\right)$

ρ_f = density of fluid $\left(\frac{kg}{m^3}\right)$ or $\left(\frac{lb}{ft^3}\right)$

Although a combination of different fouling mechanisms may occur, it is important to understand the individual mechanisms. In the following paragraphs, the mechanisms of precipitation, particulate, and combination of both fouling will be discussed.

1.2.2.1 Precipitation Fouling

Precipitation fouling is the most common type of fouling that can be found in cooling tower water. This type of fouling occurs when an inversely soluble mineral in the water comes out of the water and sticks on the internal surface of heat exchanger. Many researchers have reported water quality as one of the significant factors that contributes to precipitation fouling.

The quality of cooling tower water varies geographically. Several references from the literature were explored in order to understand representative particles in actual cooling tower water. Chamra (2006) presents constituents that can be found in cooling tower water as listed in Table 1-1. These constituents are classified as to their contribution to precipitation fouling, particulate fouling and deposit due to water treatment chemicals.

Table 1-1: Cooling Water Constituents (Chamra, 2006)

Cooling Water Constitutents	Inverse soluble Salts	Suspended Particles	Water Treatement Residuals
Calcium Carbonate	X		
Calcium Sulfate	X		
Magnesium Salts	X		
Silica	X		
Iron Oxidde	X		
Silt		X	
Clay		X	
Mud		X	
Natural Organics		X	
Dissolved Iron		X	
Sand		X	
Debris		X	
Corrosive Products			X
Phosphates			X
Organic Dispersants			X
Trivalent Chronium			X
Mircoorganisms			X

Many of the constituents listed in Table 1-1 are present in cooling tower because it is open to the atmosphere. The water typically contains a significant amount of dirt from the

outdoor air and substances that promote microbiological growth. In addition, most municipal water sources usually contain inversely-soluble minerals such as calcium carbonate and magnesium carbonate. Solubility of a mineral depends on three different parameters – temperature of the solution, pH of the solution, and the presence of other minerals. The temperature effect on solubility is explained in further in Fig. 1-9.

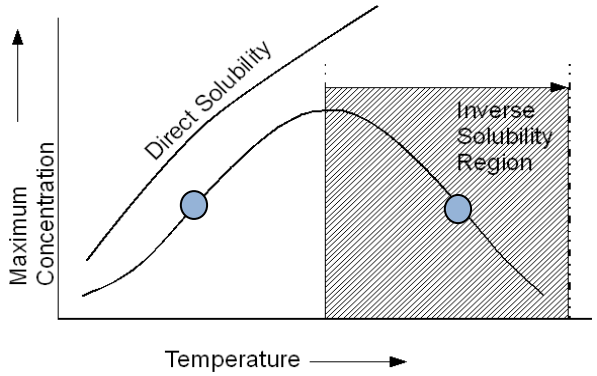

Figure 1-9: Solubility curves for two substances

Fig 1-9 shows that a directly-soluble mineral is able to dissolve more amount of that substance as the temperature of the solution is raised. Some examples of directly-soluble minerals are NaCl and $NaNO_3$. On the other hand, an inversely-soluble mineral can only increase its solubility up to a certain temperature. Beyond this temperature, the substance reaches a region where the solubility decreases with increasing temperature. If there are two solutions have the same maximum concentration of inversely-soluble minerals, the one with the higher temperature will be likely to precipitate. Examples of inversely-soluble minerals are $CaCO_3$ and $CaSO_4$. Fig. 1-10 shows how the solubility of calcium carbonate changes with the temperature of the solution.

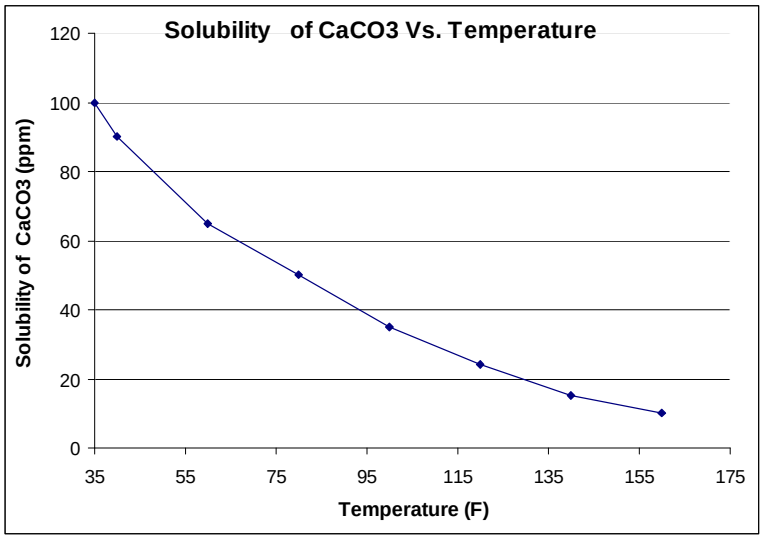

Fig 1-10: Solubility of calcium carbonate vs. temperature

Besides temperature, the solubility of an inversely-soluble mineral is also affected by the pH of the solution. For instance, $CaCO_3$ is more dissolvable in an acidic solution compared to a basic solution. Nakayama (1968) performed an experimental study of $CaCO_3$ solubility with the effect of pH. The experimental results of his study shows that the solubility of $CaCO_3$ is inversely proportional to the pH of the solution as shown in Fig. 1-11

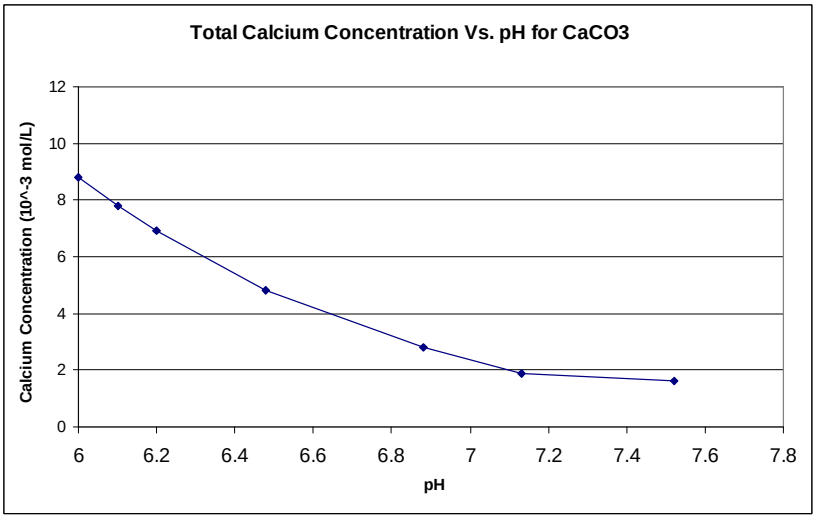

Fig 1-11: Solubility of calcium carbonate vs. pH at 25°C

Other than temperature and pH of the solution, the solubility of a mineral is also affected by the presence and quantity of other minerals. Kemmer (1988) gives an example on the effect of solubility of $CaCO_3$ with the presence of magnesium in a solution. Kemmer reported that when magnesium precipitated along with $CaCO_3$, the residual calcium in the solution may be increased (Kemmer, 1979). Another example of the effect of impurities is shown in Fig. 1-12. The plots shows that the solubility of $CaSO_4$ changes depending on the amount of NaCl in the solution (Solubilities of inorganic handbook).

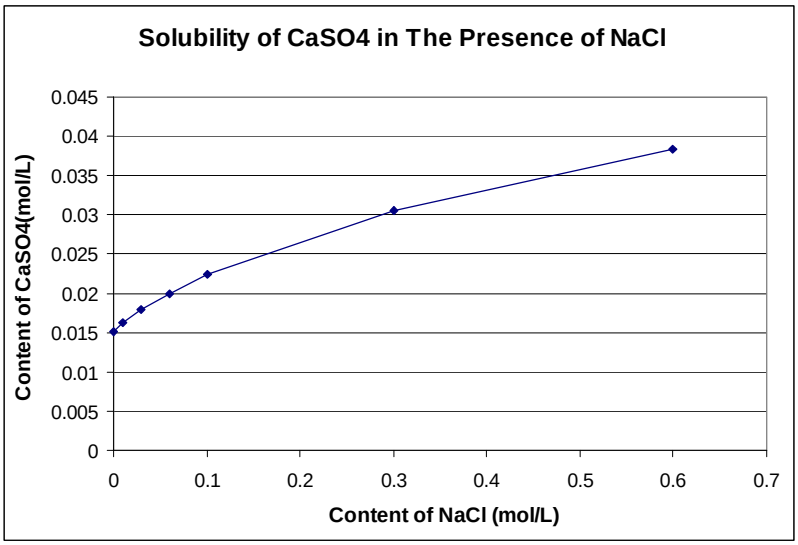

Fig. 1-12: Solubility of $CaSO_4$ vs. the amount of NaCl in the solution

A solution must reach its saturated stage before the dissolved minerals start to precipitate. It is possible for a solution to reach a supersaturated stage at which a solution contains more dissolved minerals than a saturated solution. Supersaturated solution can be attained when the solution temperature is either heated or cooled. For instance, $Na_2S_2O_3$, sodium thiosulfate, for which the solubility at 25°C is 50g $Na_2S_2O_3$ per 100 g H_2O. If 70g $Na_2S_2O_3$ is dissolved in 100g at 50°C and then the solution is cooled to room temperature, the extra 20g of mineral might not precipitate. The resulting solution is

known to be supersaturated and usually the solution is not stable. Not only temperature, but also evaporation process is able to bring the water to supersaturated stage. The evaporation process increases the concentration of the dissolved solids. If the process is continued for a sufficient period of time, it is possible for the solution to reach saturated and eventually supersaturated stage (Bott, 1994).

Although there are several inversely-soluble minerals found in typical cooling tower water, calcium carbonate ($CaCO_3$) is found to be the predominant mineral found in fouling deposits. Hence, fouling of heat exchangers by precipitation of $CaCO_3$ has been the main focus of many researchers for the past two decades. The first study performed regarding precipitation fouling was done by Langelier (1936). He proposed the "Langelier Index" now commonly known as Langelier Saturation Index (LSI). LSI is used to predict the solubility of $CaCO_3$ in water. The parameters used to determine LSI values are values of total dissolved solids, calcium hardness, total alkalinity, fluid temperature, and actual pH.

Ritter (1981) investigated precipitation fouling in tube heat exchangers using two different minerals – lithium sulfate and calcium sulfate. The circulating solution that contains inversely-soluble minerals was prepared by charging the system with distilled water and circulating the system water through a bed of minerals. The solution was circulated until the desired test condition was reached. The experiments were conducted by varying the solution velocities inside the heat exchangers between 0.6 – 13 ft/s, the water temperatures between 99 – 222°F and heat fluxes between 6 – 140 Btu/ft^2-hr. The heat transfer coefficients were determined from the inlet and exit temperature of the tube

and the measured heat inputs. The obtained results were correlated using the following parameters:

(1) Supersaturation

Supersaturation is calculated by using the solubility of the minerals corresponding to the measured temperatures using the following equation:

$$S = \frac{\Delta C}{C_s} \tag{1-9}$$

where: ΔC = concentration difference between circulating solution concentration and saturated concentration at the heat surface (weight %)

C_s = saturated concentration at the heat surface (weight %)

(2) Mass transfer coefficient (k_l)

The mass transfer was computed using the Colburn analogy for turbulent flow inside tubes:

$$\frac{k_l}{G}\left(\frac{\mu}{\rho D_l}\right)^{2/3} = \frac{h}{c_p G}(\mathrm{Pr})^{2/3} = \frac{f}{2} \tag{1-10}$$

where: k_l = mass transfer coefficient $\left(\frac{m}{s}\right)$ or $\left(\frac{ft}{s}\right)$

G = mass velocity $\left(\frac{kg}{m^2 - s}\right)$ or $\left(\frac{lb}{ft^2 - s}\right)$

μ = solution viscosity $\left(\frac{kg}{m - s}\right)$ or $\left(\frac{lb}{ft - s}\right)$

D_l = diffusivity $\left(\frac{m^2}{s}\right)$ or $\left(\frac{ft^2}{s}\right)$

ρ = density $\left(\frac{kg}{m^3}\right)$ or $\left(\frac{lb}{ft^3}\right)$

c_p = solution specific heat $\left(\frac{J}{kg-K}\right)$ or $\left(\frac{Btu}{lb-R}\right)$

h = heat transfer coefficient $\left(\frac{W}{m^2-°C}\right)$ or $\left(\frac{Btu}{hr-ft^2-^oF}\right)$

Pr = Prandtl number (-)

f = friction factor (-)

(3) Surface temperature

Surface temperature was measured by thermocouples

(4) Shear stress on deposition wall (τ)

Shear stress at the inside heat exchanger is computed by using the following equation:

$$\tau = \frac{f\rho V^2}{2} \tag{1-11}$$

where: f = friction factor

ρ = fluid density $\left(\frac{kg}{m^3}\right)$ or $\left(\frac{lb}{ft^3}\right)$

V = fluid velocity $\left(\frac{m}{s}\right)$ or $\left(\frac{ft}{s}\right)$

(5) Heat flux

Heat flux was calculated by using measured temperatures and flow rates.

(6) Reynolds number

Reynolds number is computed using the following equation:

$$\mathrm{Re} = \frac{\rho V D}{\mu} \tag{1-12}$$

where: ρ = fluid density $\left(\frac{kg}{m^3}\right)$ or $\left(\frac{lb}{ft^3}\right)$

V = fluid velocity $\left(\frac{m}{s}\right)$ or $\left(\frac{ft}{s}\right)$

μ = solution viscosity $\left(\frac{kg}{m\ -s}\right)$ or $\left(\frac{lb}{ft\ -s}\right)$

D = hydraulic diameter of the heat transfer surface (m) or (ft)

Most of the above parameters are dependent on operating temperatures and/or operating flow rates. Multiple regression methods were implemented to evaluate the importance of the listed parameters. It was found that supersaturation is the most important parameter in correlating fouling resistance for both minerals used in Ritter's experiments. The other parameters varied in importance depending on the attributes of a particular mineral. For instance, $CaSO_4$ has two different crystalline forms when it precipitates depending on the surface temperature. Each crystalline form has its own attachment force characteristics that identify whether the particles will be deposited either during crystallization or re-entrainment process. After performing analysis, fouling rate due to $CaSO_4$ is found out to be controlled by mass transfer coefficient. Thus, the fouling resistance was correlated by the mass transfer rate in the following equation:

$$R_f = C * k_l \left(\frac{\Delta C}{C_s}\right)^2 \tag{1-13}$$

where: C = $3.8(10)^{-5}$ for IP units and $1.9(10)^{-9}$ for SI units.

Li_2SO_4 fouling rate, on the other hand, was more influenced by surface temperature. The fouling curve for Li_2SO_4 data was correlated using the following equation:

$$R_f = A*\left(\frac{\Delta C}{C_s}\right)\exp\left(\frac{B}{T_s}\right) \tag{1-14}$$

where: A = 570 and B = -6540 for IP units.

A = 0.028 and B = -3630 for SI units.

Andritos et al. (1996) studied scale formation of $CaCO_3$ on tube walls under isothermal conditions. The effects of pH, supersaturation, flow velocities and liquid temperature were investigated. The experiment was performed with velocity in the range of 0.2 – 2.4 m/s, temperatures in the range of 15-55 °C, and pH values in the range of 8-13. It was noted that the deposition rate increased sharply between pH 8.5-9 and was relatively constant at pH > 9. The investigators also explained that the increase of liquid temperature promotes higher deposition rate and also shifted the onset of deposit formation to lower pH. These results confirm that an inversely-soluble mineral decreases its solubility with the increase of both fluid temperature and pH. The investigators computed the supersaturation ratio (*S*) using the thermodynamic driving force for $CaCO_3$ formation:

$$S = \left[\frac{(Ca^{2+})(CO_3^{2-})}{K_{sp}}\right]^{1/2} \tag{1-15}$$

Where: K_{sp} =solubility product $\left(\frac{mol}{m^3}\right)^2$

The deposition rates increased drastically when *S* is approximately at 7- 8 and remaining stable at higher supersaturation ratio.

Bansal et al. (1993) performed a study of precipitation fouling in a plate heat exchanger employing a liquid to liquid heat transfer process. The tested plate heat exchangers have 3 channels with 2.4 mm channel gap. Calcium sulfate solution was prepared using de-ionized water and stored in a 50 liters tank. The undissolved minerals were filtered to eliminate re-entrainment process. Effects of flow velocity, wall temperature, and $CaSO_4$ concentration on fouling rates were studied. The investigators noticed that in the beginning of the fouling process, there is hardly any removal process because the size of the crystals on the heat exchanger surface area is still small and almost unnoticeable. After a period of time, the size of the crystals will increase, resulting in more fragile crystals and higher shear force on the surface of the fouling deposit. These conditions induce the removal of crystals. The other possible condition is that as fouling thickness grows the velocity of the fluid increases because of the reduction of flow area. The increase of local velocity reduces the solution temperature by 2 to 3°C. Based on the nature of inversely-soluble salts, the decrease in temperature causes the precipitation rate of minerals to decrease as well. They concluded that these occurrences are the main reason for the decrease in precipitation fouling rate with time. The strong effect of fluid velocity on precipitation fouling has been also reported by Hasson (1962) and Watkinson and Martinez (1975)

Knudsen and Story (1978) studied the effect of heat transfer surface temperature on the scaling behavior of simulated cooling tower water. The simulated cooling tower water was obtained by concentrating municipal water to several different concentrations. Water quality needed to be held constant; however, from the test results, it was not possible to maintain a constant water quality throughout the test. The temperature of the

surface of the deposit was recorded periodically, and the run was continued until a reasonably constant fouling resistance was maintained for 50 to 100 hours. The data were fitted into Taborek's model (1972) and represented by

$$R_f^* = (3\times10^{11})\exp\left(\frac{-11000}{RT_s}\right) \tag{1-16}$$

The coefficient (3×10^{11}) in the above equation is only applicable to the test conditions used by Knudsen and Story. Equation (1-8) indicates that the surface temperature is inversely proportional to the asymptotic fouling values. Besides studying the effect of surface temperature, Knudsen and Story also observed the effect of alkalinity on asymptotic fouling resistance. In another study, Morse and Knudsen (1977) investigated further the effect of alkalinity in scaling of simulated cooling tower water. Throughout the tests, fluid velocity and heat flux were maintained at constant values, which are 0.75 ft/s and 87,600 Btu/ft^2-hr respectively. The alkalinities were varied between 116 to 187 ppm of CaCO3 at the beginning of each run. A general trend observed was that the higher the water alkalinity the higher asymptotic fouling resistance values. The change in alkalinity alters the solubility rates of other different inversely-soluble minerals in the water. By these observations, Morse and Knudsen concluded that the asymptotic fouling rates are dependent on water alkalinity, through a complex relationship of minerals' solubility in the water.

The above research was primarily experimental in nature; Hasson et al. (1970) presented a deposition fouling model that predicts the deposition rate of $CaCO_3$ using ionic diffusion theory. His model allows estimation of the scale formation caused by calcium carbonate in heat exchanger tubes given values for the pH, calcium

concentration, total alkalinity, and the fluid flow parameters. In addition, Hasson et al. consider the fluid temperature as a coupling effect of precipitation fouling process. The model is presented as follows:

$$\dot{m}_p = \frac{k_d[Ca^{2+}]}{2a}\left(-b + \sqrt{b^2 - 4ac}\right) \tag{1-17}$$

$$a = 1 - \frac{4k_2^{'}k_r}{k_1^{'}k_d}[Ca^{2+}] \tag{1-18}$$

$$b = \frac{4k_2^{'}k_r}{k_1^{'}k_d}[HCO_3^{-}] + \frac{k_{spi}^{'}k_r}{k_d}\frac{1}{[Ca^{2+}]} + \frac{[CO_2]}{[Ca^{2+}]} \tag{1-19}$$

$$c = \frac{k_{spi}^{'}}{k_d}\frac{[CO_2]}{[Ca^{2+}]} - \frac{k_2^{'}k_r}{k_1^{'}k_d}\frac{[HCO_3^{-}]^2}{[Ca^{2+}]} \tag{1-20}$$

where: $\dot{m}_p$ = mass deposition rate due to mineral precipitation $\left(\frac{kg}{m^2 - s}\right)$

$k_1^{'}$ and $k_2^{'}$ = first and second dissociation constants of carbonic acid

$k_{spi}^{'}$ = solubility product of calcium carbonate at wall temperature $\left(\frac{mol}{L}\right)$

k_r = crystallization rate coefficient with unit (mol/L). It can be computed from

$\ln k_r = 41.04 - \frac{10417.7}{T_i}$ where T_i is the temperature of fouling surface in Kelvin

k_d =mass transfer coefficient is computed from the following equation:

$k_d = 0.023v\,\mathrm{Re}^{-0.17}\,Sc^{-2/3}$ where v is flow velocity of water (m/s), *Re* is the Reynolds number, and *Sc* is the Schmidt number.

$[HCO_3^{-}] = \frac{2*TA - 10^{-14+pH}}{1 + 2*K_2^{'}10^{pH}}$ ($CaCO_3$ ppm)

$[Ca^{2+}]$ = Calcium concentration $\left(\frac{mol}{L}\right)$

Wiechers et al. (1975) reported models to compute solubility product of calcium carbonate, first and second dissociation constant of carbonic acid:

$$K_1^{'} = 10^{-\left(\frac{17052}{T_{w,avg}} + 215.21*\log(T_{w,avg}) - 0.12675*(T_{w,avg}) - 545.56\right)} \quad (1\text{-}21)$$

$$K_2^{'} = 10^{-\left(\frac{2902.39}{T_{w,avg}} + 0.02379*T_{w,avg} - 6.498\right)} \quad (1\text{-}22)$$

$$K_{spi}^{'} = 0.01183*\left(T_{w,avg} - 273\right) + 8.03 \quad (1\text{-}23)$$

Where: $T_{w,avg}$ = average fluid temperature (°C)

Hasson's model predicts scaling rates of the same order of magnitude as observed by Morse and Knudsen. These investigators studied the effect of alkalinity on the scaling of cooling tower water on a tube heat exchanger by keeping the flow rate, surface, and water temperature to be constant.

1.2.2.2 Particulate Fouling

Particulate fouling is mainly caused by suspended solids in the bulk of fluid. There are two possible different types of suspended particles in cooling towers:

1. Crystallizing particles: particles that are generated during crystallization but removed during the fouling process due to being fragile. These particles are later deposited by entrainment process.
2. Non - Crystallizing particles: any particles from the circulating water

Muller-Steinhagen and Middis (1989) investigated particulate fouling in plate heat exchangers. Flow velocity, heat flux and particle concentration were the main parameters of the investigation. The study utilizes the "washboard" type of plate heat

exchangers. The study used Al_2O_3 as the suspension foulants. The inlet temperatures and flow rates of both streams were kept constant throughout the tests. The tests were run until the fouling resistance reached an asymptotic value. The study showed the asymptotic fouling resistance decreased with increasing fluid velocity; however, the asymptotic fouling resistance was not influenced by heat flux. Muller-Steinhagen and Middis showed that the asymptotic fouling resistance for particles with 1.6 µm diameter increases linearly with particle concentration. This trend was noticed until the concentration reached to 900 ppm.

Thonon et al. (1999) performed a study on the effect of geometry and flow conditions on particulate fouling in plate heat exchangers. Thonon et al. selected $CaCO_3$ as the foulant particle in his experiment. In order to avoid crystallization inside the heat exchanger, the wall temperature was kept as low as possible. They maintained the fluid temperature between 22.0 and 24.2°C and the wall temperature was no more than 10°C greater than the fluid temperature. The corrugation angles used in the experiments were 30°, 60°, and combination of 30° and 60°. At the end of his study, he concluded that the channel geometry and the fluid velocity are the two great factors that affect fouling trend in a plate heat exchanger. Contrary to the finding of Muller-Steinhagen (1989), Thonon did not find that particle concentration significantly affects the rate of particulate fouling.

Muller-Steinhagen et al. (1988) ran tests on the influence of flow velocity and particle size on the deposition of suspended alumina particles onto heat transfer surfaces. The tests were performed using a heated cylindrical rod in an annulus and a coiled wire in the crossflow. The test conditions varied fluid velocities between 1.2 cm/s and 3.0 cm/s and heat fluxes of 14400 W/m^2 and 5500 W/m^2. Muller-Steinhagen et al. used a constant

concentration for two different particle diameters to run their tests, which were 2 μm and 0.45 μm. From the tests, the investigators showed that the asymptotic fouling resistance increased with smaller particle diameters. This conclusion is supported with the simulation results performed by Chamra and Webb (1993). They developed a semi-empirical model for liquid side particulate fouling in enhanced tubes by modifying Kern and Seaton's original model.

Several investigators have made attempts to develop models for precipitation, particulate, and combination of both precipitation and particulate fouling.
The particulate fouling deposition rate term is expressed in the following equation (Webb, 1994):

$$\dot{m}_d = K_m (C_p - C_s) \tag{1-24}$$

where: K_m = mass transfer coefficient $\left(\frac{m}{s}\right)$ or $\left(\frac{ft}{s}\right)$

C_p = the bulk concentration of particles $\left(\frac{kg}{m^3}\right)$ or $\left(\frac{lb}{ft^3}\right)$

C_s = concentration of particles adjacent to the surface $\left(\frac{kg}{m^3}\right)$ or $\left(\frac{lb}{ft^3}\right)$

Generally concentration of particles adjacent to the surface is taken to be zero. The deposition process due to particulate fouling process may be divided into two processes - the transport particles to the wall and the adhesion of particles at the wall. The deposition coefficient (K_m) is categorized into three different transport mechanisms depending on the diameter size of the suspended solid particles. The dimensionless particulate relaxation time (t_p^+) is used to identify the transport mechanism.

$$t_p^+ = \frac{d_p^2 \rho_P (V^*)^2}{18\mu * V} \tag{1-25}$$

Where: V^* = friction velocity = $\bar{V} * \sqrt{\frac{f}{2}}$ $\left(\frac{m}{s}\right)$ or $\left(\frac{ft}{s}\right)$

f = fanning friction factor = $\frac{1774}{\beta^{1.026} * \mathrm{Re}}$

$\bar{V}$ = bulk fluid velocity $\left(\frac{m}{s}\right)$ or $\left(\frac{ft}{s}\right)$

d_p = suspended solids diameter (m) or (ft)

ρ_P = particle density $\left(\frac{kg}{m^3}\right)$ or $\left(\frac{lb}{ft^3}\right)$

μ = fluid viscosity $\left(\frac{kg}{m \ -s}\right)$ or $\left(\frac{lb}{ft \ -s}\right)$

Gudmundsson (1981) explains the three different transport mechanisms and Papavergos and Hedley (1984) present an empirical equation of dimensionless velocity (k_m^+) for each transport mechanism. They are as follows:

1. Diffusion

   In the diffusion regime, the suspended particles are carried to the heat exchanger wall by Brownian motion. Brownian motion is the random movement of particles in the fluid due to imbalance in the combined exerted forces on particles that are induced by the surrounding molecules. This regime occurs when $t_p^+ < 0.02$.

   Papavergos and Hedley (1984) present an empirical equation of dimensionless velocity (k_m^+) for this regime:

   $$k_m^+ = 0.07 Sc^{-2/3} \tag{1-26}$$

2. Inertia

   In the inertia regime, the particles are sufficient large to acquire momentum from the fluid to move through the viscous sublayer. This regime occurs at $0.02<t_p^+<20$. Papavergos and Hedley (1984) propose:

$$k_m^+ = 0.0035 * (t_p^+)^2 \tag{1-27}$$

3. Impaction

   In this regime where $t_p^+>20$, the particles are large enough so that the velocity of particles is approximately equal to the friction velocity. Papavergos and Hedley (1984) propose:

$$k_m^+ = 0.18 \tag{1-28}$$

For all regimes the mass transfer coefficient is then determined from the following equation:

$$K_m = V^* \cdot K_m^+ \tag{1-29}$$

The adhesion of particles to the wall is characterized by the deposit strength factor (ψ), which depends on the deposit structure, concentration, and type of suspended solids, and flow velocity. The adhesion of particles is the parameter that governs the rate of removal during fouling process. Deposit strength factor can only be deduced from the experimental data by using the following equation:

$$\psi = \tau_w \cdot \frac{R_f^*}{R_{f0}} \tag{1-30}$$

where: τ_w = wall shear stress (Pa) or (psi)

R_f^* = asymptotic fouling resistance $\left(\frac{m^2-^oC}{W}\right)$ or $\left(\frac{hr-ft^2-^oF}{Btu}\right)$

R_{f0} = initial fouling resistance $\left(\frac{m^2-^oC}{W}\right)$ or $\left(\frac{hr-ft^2-^oF}{Btu}\right)$

1.2.2.3 Combined Precipitation and Particulate Fouling

In heat exchangers connected to cooling towers, the interactions of the listed mechanisms occur at the same time. Of course, the interactions of these mechanisms affect the rate of fouling; however, the combined effects of mechanisms have not been fully understood. Yiantisios et al. (1995) proposed that presence of suspended particles may affect the rate of fouling. This claim was further studied by Bansal et al. (1997). They presented a study on the effect of suspended particles in solutions on crystallization rate. The study was performed on plate and frame heat exchanger. The calcium sulfate solution was prepared by mixing calcium nitrate and sodium sulfate in order to reduce the amount of undissolved minerals. From the study, Bansal observed that the suspended particles settle on the heat transfer surface and act as nuclei. According to several published crystallization studies, the rate of crystallization increases significantly in the presence of nuclei (Klepetsanis & Koutsoukos, 1991), (Klima & Nancollas, 1987), (Amjad, 1988). Therefore, neglecting the presence of suspended particles could cause a significant error.

Webb and Li (2000) studied fouling in enhanced tubes using actual cooling tower water. The investigated fouling mechanism is a combination of particulate and precipitation fouling. There were eight 7 enhanced tubes and 1 plain tube tested by

Webb and Li. The enhanced tubes that were selected have different combinations of helix angles (α), number of starts (N_s), and rib heights (e). The tests were conducted using the following conditions:

1. Water velocity of 1.07 m/s (3.5 ft/s), which gives Re=16,000
2. The total hardness of cooling tower water was approximately 800 ppm $CaCO_{3,}$ electrical conductivity of 1600-1800 $\mu\Omega$, and pH = 8.5

From the tests, Webb and Li observed that there were more mineral deposits found in enhanced tubes than those found in the plain tube. From this observation, Webb and Li concluded that there is a strong relationship between asymptotic fouling resistance and the internal geometry of the enhanced tubes. They fitted their asymptotic fouling resistance results in different enhanced tubes into the following correlations:

$$R_f^* = 4.64 * 10^{-3} \left(\frac{p}{e} \right)^{5.72} \qquad N_s \leq 25 \tag{1-31}$$

$$R_f^* = 1.85 * 10^{-4} \left(\frac{p}{e} \right)^{0.92} \qquad N_s > 25 \tag{1-32}$$

1.3 OBJECTIVES

Past heat exchanger fouling literature has been done. To date, there have been no reported studies of fouling in BPHE operating as condensers. Furthermore, most of the studies that have been conducted used local water sources or solutions that do not represent actual cooling tower water. The main objective of this work is to design and construct an experimental facility in order to study and evaluate waterside fouling factor on brazed plate type condensers in cooling tower applications. A secondary objective is to develop a general methodology to obtain cooling tower water with specified fouling

potential. In addition, a test methodology is also developed based on the understanding of fouling parameters from previous fouling studies.

There are three different BPHE tested in this project; the first two BPHEs have the same chevron angle and different aspect ratio (L/W) and the third BPHE has the same aspect ratio as that in the first BPHE but different chevron angle. The BPHEs will be tested using three different qualities of cooling tower water: low, medium, and high fouling potential. The compositions of minerals that define each water quality can be found in Table 2-2.

The focus of this thesis will be the development of the test facility in the water-side, the experimental apparatus and the preparation of cooling tower water. A complimentary thesis focuses on the development of the refrigerant loop side and overall experimental facility construction.

CHAPTER II

EXPERIMENTAL FACILITY

This chapter describes design, construction, and instrumentation of the test facility for the project. Design criteria, refrigeration and hydronic loops design, equipment and instrumentation are described in detail in the following sections.

2.1. Design criteria

The design of the facility depends greatly on the test conditions that are going to be implemented. Part of this project is to determine two test operating conditions – low and high heat transfer rate. The selected test operating conditions should mimic the actual operating conditions in cooling towers. AHRI 450 (2007) specifies standard rating conditions to measure performance rating of water-cooled refrigerant condensers. One of the conditions listed in AHRI 450 is adopted as the low heat flux test condition in this project. Table 2-1 provides a summary of the selected test conditions.

Table 2-1: Test conditions for high and low heat flux

Heat Flux	Saturated Condensing Temperature of the Entering Refrigerant		Minimum Actual Temperature of the Entering Refrigerant		Temperature of Entering Water		Temperature of Leaving Water		Refrigerant Mass Flow Rate		Cooling Tower Water Flow Rate	
	℉	℃	℉	℃	℉	℃	℉	℃	lb/min	kg/min	gal/min	liter/min
Low	105.0	40.6	125.0	51.7	85.0	29.4	93.0	33.9	3.5	1.6	4.6	17.4
High	120.0	48.9	120.0	48.9	85.0	29.4	100.0	37.8	6.9	3.1	4.6	17.4

To create a high flux test condition, there are several parameters that can be changed from the low heat flux condition in order to achieve high heat flux. They are as follows:

1. Increase the cooling tower flow rate by keeping the refrigerant condition the same as in the low heat flux condition.
2. Reduce entering water temperature to test condenser to 27.2°C (81°F) and keep the same refrigerant test conditions as listed under low heat flux.
3. Increase the refrigerant saturated temperature and keep the entering water temperature to the test condenser at 29.4°C (85°F).

The feasibility of the first option was verified by checking the manufacturer's data. Using the available data from the manufacturer, Fig 2-1 (a), (b), and (c) were plotted. If the refrigerant condition is kept to be the same as in the low heat flux test condition, the cooling tower flow rate needs to be increased significantly in order to achieve high heat flux. Increasing flow rate causes an increase in pressure drop across the condenser as shown in Fig. 2-1. For instance, to obtain heat flux of 6000 Btu/hr-ft^2 for BPHE model BPHE-A2, the required flow rate needs to be at 16 gal/min. Since, this option would require a high pumping capacity, this option is not desirable.

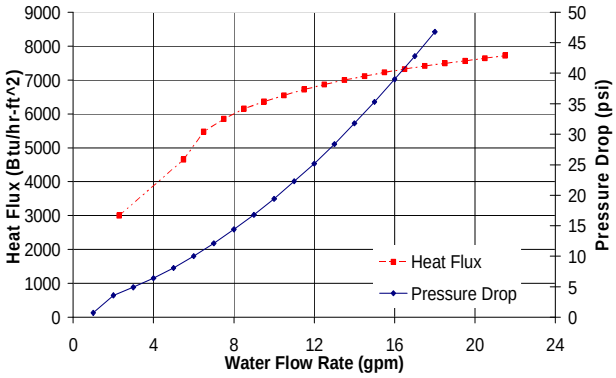

(A): Heat flux vs. water flow rate for BPHE model BPHE-A4

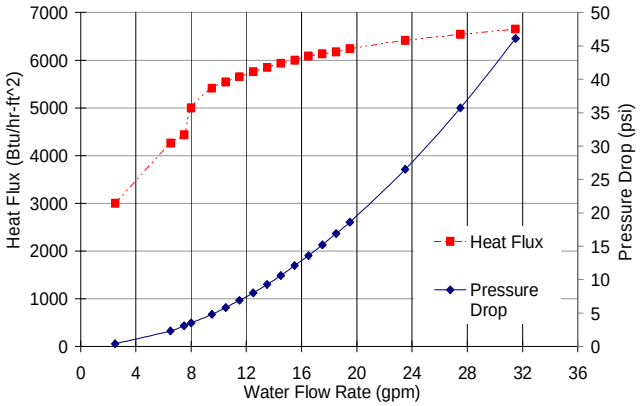

(B): Heat flux vs. water flow rate for BPHE model BPHE-A2

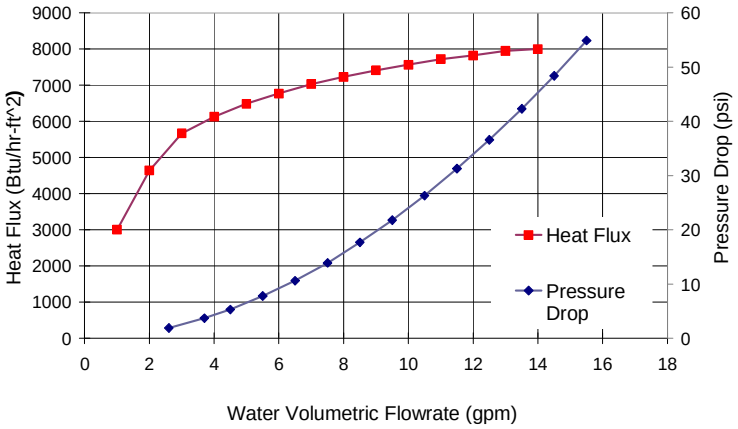

(C): Heat flux vs. water flow rate for BPHE model BPHE-A3

Fig. 2-1: Heat transfer rate and pressure drop for the selected BPHEs

Option 2 is not desirable because it does not reflect the actual operating condition for cooling towers. Hence, to achieve high heat flux, option 3 was selected. In option 3, the refrigerant condensing temperature has to be increased to 48.9°C (120°F) and the entering vapor temperature to the test BPHE is set at 85°C (185°F).

Another important part of this project is to determine the water qualities of the cooling tower water that will be implemented in the tests. The cooling tower water should be a good representative of actual cooling tower water that varies geographically. The water used in the tests is categorized into three different fouling potentials – low, medium, and high. Each fouling potential has a certain mineral concentrations that determine the water quality. As discussed in the previous chapter, high fouling potential water is more unstable compared to the low fouling potential water because it has reached its supersaturated stage. Hence, slight change of temperature or pH is able to alter solubility level of dissolved minerals in the water. Table 2-2, which was provided by the Project Monitoring Subcommittee, lists the three different water qualities that were desired for this study. In the event, it was not possible to create cooling tower water with the specified chemistries. This is discussed in detail in chapter 3.

Table 2-2: Water chemistry for three different fouling potential

Fouling Potential	Total Hardness	Calcium (as CaCO3)	Magnesium (as $CaCO_3$)	"M" Alkalinity (as $CaCO_3$)	Chloride	Silica	Sulfate	Specific Conductance
low	240	180	59	96	< 200	5.7	72	TBD
medium	480	360	119	192	< 200	11.4	144	TBD
high	640	480	158	256	< 200	15.2	192	TBD

Fouling Potential	pH	Total Iron	Copper	TDS	Total Suspended Solids	P-Type Alkalinity	LSI
low	7.80	0.15	0.03	1140	< 100	0	0.198
medium	8.60	0.30	0.06	1500	< 100	0	1.864
high	9.30	0.40	0.08	1800	< 100	0	2.803

2.2 TEST FACILITY OVERVIEW

The overall dimension of the test facility is 3.2m W x 2.9m H x 1.2m D (10.5'W x 9.5'H x 4'D) and it includes five different fluid loops:

1. Refrigerant loop

The refrigerant loop is conditioned to deliver constant heat transfer to the water side of the test condenser

2. Cooling tower loop

   This loop is charged with cooling tower water and measurements are taken continuously to monitor the fouling growth on the water-side of the test condensers.

3. Evaporator loop

   This loop is connected to an evaporator to maintain condensing pressure of refrigerant.

4. Superheater loop

   This loop is connected to a superheater to maintain degree of refrigerant superheat at the inlet of the test condenser. The inlet refrigerant temperature to the test condenser has to have 18.3°C (65°F) of superheat.

5. Chilled water loop

   This loop is connected to a sub-cooler in refrigeration cycle and a post-cooler in cooling tower loop to provide cooling.

The facility was designed to be able to maintain relatively constant test conditions throughout the tests and prevent any catastrophic failures that will disrupt the tests. Fig. 2-2 shows the configuration of the test facility and Fig. 2-2 shows the picture of the test facility.

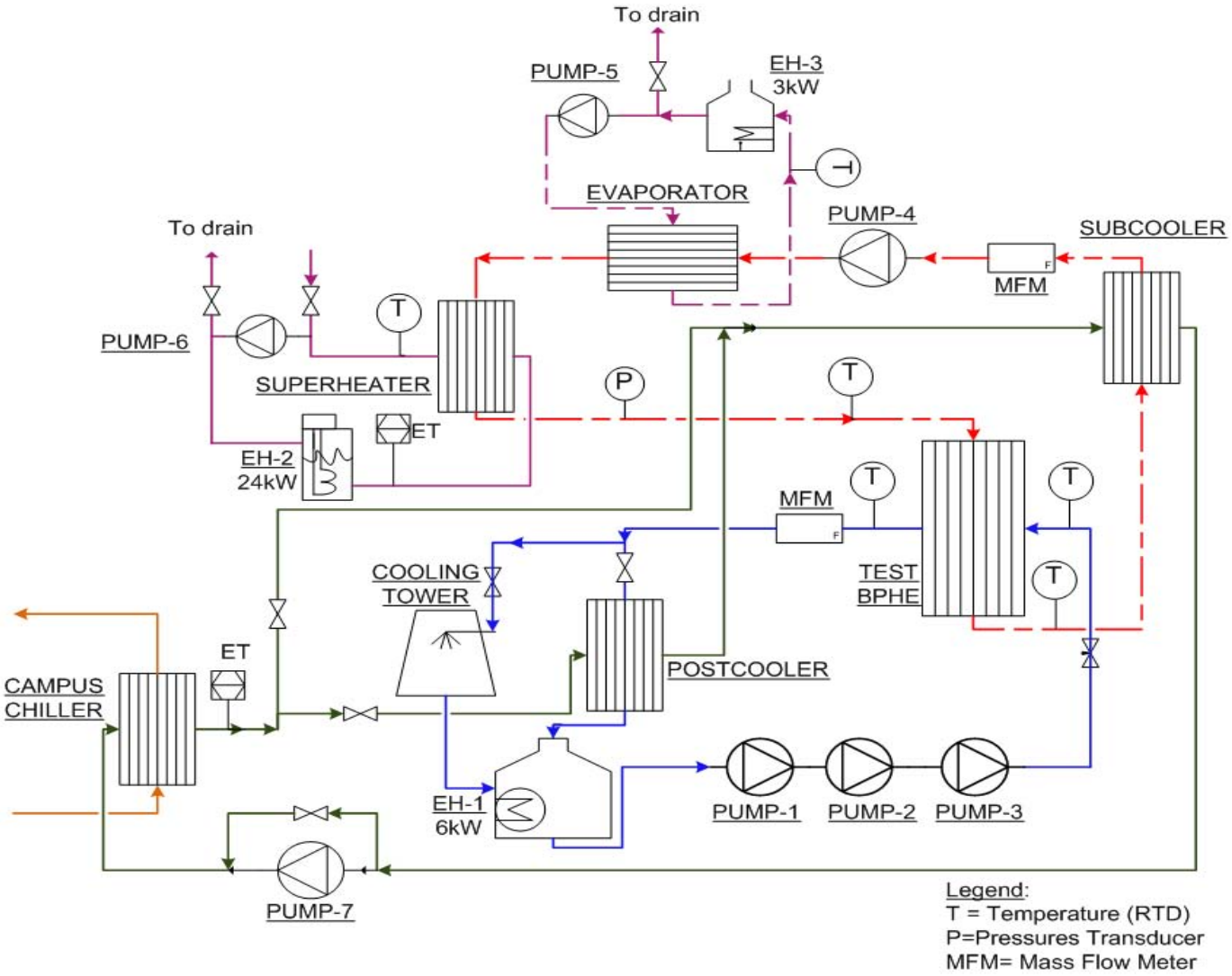

Fig.2-2: Schematic of the test facility

Fig. 2-3: Photo of test facility

Data Acquisition

In this project, the data acquisition (DAQ) system consists of a PXI (PCI eXtensions for Instrumentation) model 1031, an SCXI (Signal Conditioning eXtensions for Instrumentation) chassis model 1000 that can accommodate 4 modules as shown in Fig. 2-4. The SCXI chassis is designed to power and control four modules. There are three types of modules installed in the SCXI and each one is designed for a specific task and connected to a terminal block. The purpose of terminal blocks is to wire all the external signals, such as pressure transducers, thermocouples, and Resistance Temperature Detectors (RTDs). The type of modules and terminal blocks used are described as follows:

1. Module SCXI 1102 attached to SCXI 1303 terminal block (2 pairs)

   Module SCXI 1102 is a voltage input module that is able to measure voltage input range of ± 10V. This module is accompanied with a terminal block model SCXI 1303. This terminal block is equipped with a built-in cold-junction temperature sensor and a thermistor to compensate the temperature gradient between terminals and the cold junction sensor. SXCI 1303 temperature sensor outputs 1.91 to 0.58 V from 0 to 55°C (32 to 131°F) with accuracy ± 0.5°C (0.9°F) from a temperature range of 15°C to 35°C (59°F to 95°F).

2. Module SCXI 1581 attached to SCXI 1300 terminal block

   This module is a 32-channel current excitation module that acts as a 100 µA current excitation sources, with accuracy ± 0.05%. This module is attached to an SCXI 1300 terminal block, which is a general purpose terminal block with an onboard temperature sensor for cold-junction compensation. The accuracy of this cold junction is ± 1.3°C (2.34°F) from 0 to 50°C (32 to 122°F) and output 0 to 0.5 V from 0 to 50°C (32 to 122°F).

3. Module SCXI 1102 attached to SCXI 1308 terminal block

   This module is used to read input signals of 4-20 mA and 0 – 5 Vdc.

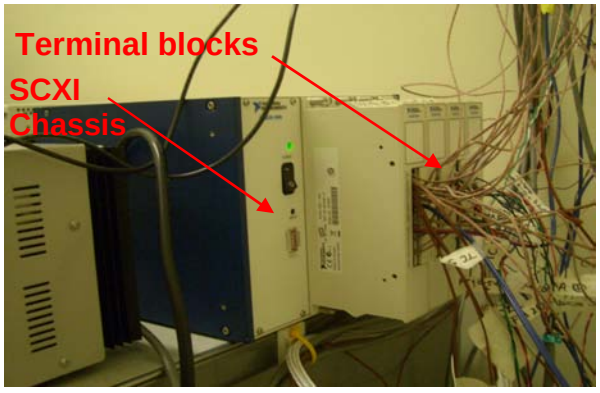

Fig 2-4: Photo of terminal blocks installed in SCXI chassis

The connection between DAQ hardware and PC is established using NI LabVIEW software. It is a graphical programming environment to read, store, and visualize the measurements. LabVIEW's tasks are to analyze an input from the process and produce an output based on the control algorithm.

2.3 REFRIGERATION LOOP DESIGN

The purpose of the refrigerant loop is to supply constant heat transfer on the refrigerant side of the test condensers. In this section an overview of the refrigeration loop is given. A detailed description of the refrigeration loop design and construction is covered by Ramesh (2010). The refrigeration loop, which utilizes R134a, consists of an evaporator, a superheater, a test condenser, a metering valve, and a gear pump. The purpose of the evaporator is to maintain the desired condensing pressure. This is accomplished by connecting one side of the heat exchanger to one of the heating hydronic loops. The same heating concept is applied to the superheater. The superheater is designed to maintain 65°F of superheat before the R134a enters the test condenser. A temperature sensor and two Setra model 206 pressure transducers with pressure of 0 – 250 psi and 0-500 psi were located right at the inlet of test condenser to monitor the temperature and pressure respectively. After exiting the condenser, there is another temperature sensor to monitor the outlet temperature. Then, the refrigerant is directed to a sub-cooler that cools down the refrigerant before it enters the pump. Refrigeration cycle of the system is plotted using EES (Engineering Equation Solver) and shown in Fig. 2-5.

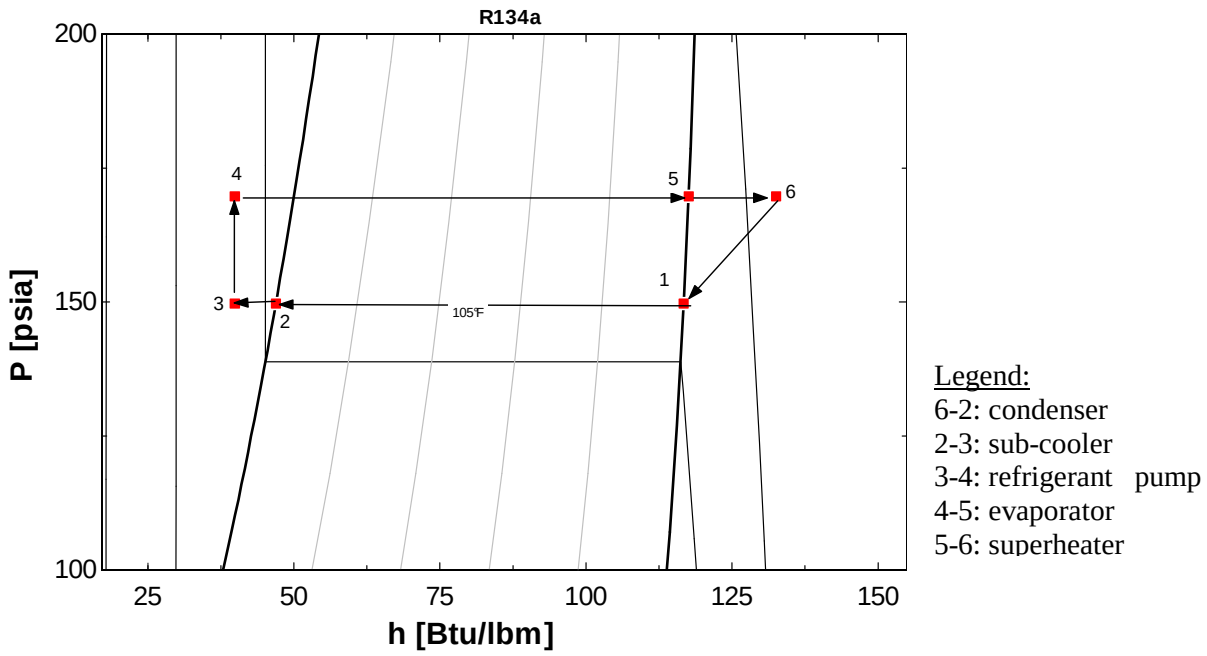

Fig 2-5: Pressure vs. enthalpy diagram for R134a in the system

2.4 COOLING TOWER LOOP DESIGN

The purpose of the cooling tower loop is to simulate a heat transfer process in actual condensers serve by cooling towers. A cooling tower was installed in this loop mainly to concentrate the water not to reject heat from the test condenser. The main design of the cooling tower loop must be able to accommodate a range of heat transfer capacity and minimize the uncertainties in measuring fouling. Minimizing the uncertainties can be done by utilizing highly accurate instruments. The following sections explain the design of the loop and the instruments used in the system. Fig. 2-6 shows the cooling tower loop, which consists of two BPHEs – a test condenser and a post-cooler, a cooling tower, a flow meter, and a solution tank as a reservoir for cooling tower water.

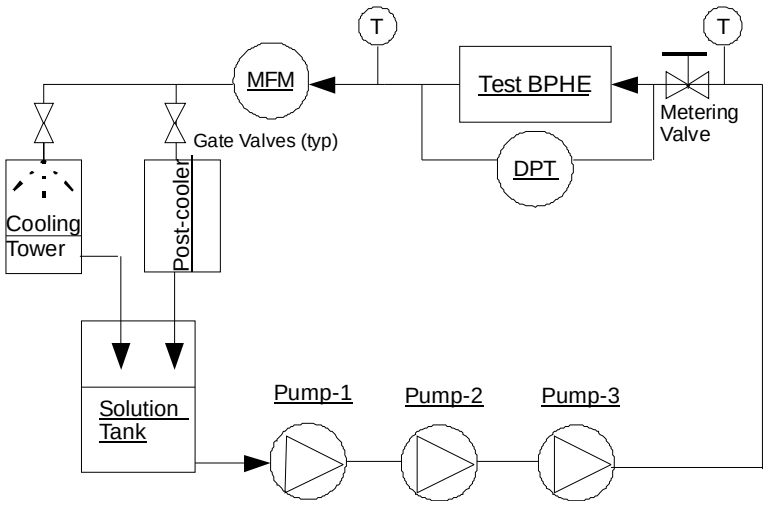

Fig 2-6: Schematic of cooling tower loop

The water is pumped through the test condenser and around the cooling tower loop by three pumps that were installed in series. There are two temperature sensors positioned in-stream: the first one (RTD-1) is to measure the inlet temperature of the water and the second one (RTD-3) is to measure the outlet temperature of the test condenser. The second one was positioned 15 – 16 inches away from the outlet of test BPHE to make sure that the water temperature is uniform when measurements are taken. A manual metering valve was installed before the test condenser to set the desired flow rate, which is measured by a flow meter located after the test condenser. After the test condenser, water can be directed to either a post-cooler or a cooling tower by adjusting gate valves that were installed before these two components.

The final design shown in Fig. 2.6 incorporates significant modifications from the original design:

1. Eliminating a bypass BPHE

   Bypass BPHE was initially set in parallel to the test BPHEs to reduce contamination in the test BPHE during the start-up. During the start-up, all

the water was directed to bypass BPHE. During the initial calibration, it was found out that the bypass BPHE did not serve a purpose because the equilibrium conditions of the refrigerant and cooling tower water were shifted during the transition from bypass BPHE to the test BPHE. This transition caused additional calibration to re-set the system to the desired test conditions.

2. Testing one test condenser instead of two condensers at the same time

   Another major change is that the test facility was previously designed to test two test condensers at the same time when they were tested under low heat transfer rate test condition. However, during system calibration, the test conditions could not be maintained when two test condensers were tested at the same time.

3. Installation of a cooling tower

   The addition of cooling tower is integrated just towards the end of the completion of test facility construction. The purpose of cooling tower is to create high fouling water quality through an evaporation process.

4. Addition of a pump for cooling tower loop

   Initially cooling tower loop utilized two pumps. The addition of the third pump is required because over the course of experiments, the flow rate of cooling tower water cannot be maintained

2.4.1 Hydronic Pump selection

The cooling tower pumps were selected after completing design of cooling tower loop. In order to select the pumps, pressure drop due to friction in pipe, fittings, and

other components were calculated by using Equations (2.1) and (2.2). The flow rate as specified in table 2-1 is used in the pressure drop calculation.

$$\Delta P_{major} = f \frac{L}{D} \frac{\overline{V}^2}{2g_c} \tag{2-1}$$

$$\Delta P_{\min or} = k\rho \frac{\overline{V}^2}{2g_c} \tag{2-2}$$

where: f = Moody friction factor

ΔP_{major} = pressure drop in fittings (Pa)

$\Delta P_{\min or}$ = pressure drop in pipes (Pa)

D = pipe diameter (m)

g_c = constant (1 in SI unit)

k = minor loss coefficient

$\overline{V}$ = fluid velocity (m/s)

ρ = fluid density (kg/m³)

The value of Moody friction factor can be obtained from either a Moody chart or Churchill correlation (McQuiston, 2005). The Churchill correlation (1977) for the friction factor is expressed in the following equation:

$$f = 8\left[\left(\frac{8}{\mathrm{Re}_D}\right)^{12} + \frac{1}{(A+B)^{1.5}}\right]^{1/12} \tag{2-3}$$

$$A = \left\{2.457 \ln\left[\frac{1}{\left(7/\mathrm{Re}_D\right)^{0.9} + \left(0.27\varepsilon/D\right)}\right]\right\}^{16} \tag{2-4}$$

$$B = \left(\frac{37530}{\mathrm{Re}_D} \right)^{16} \tag{2-5}$$

where: Re_D = Reynolds number

ε = pipe roughness (mm or in.)

D = pipe diameter (m or in.)

The total pressure drop in the system was calculated by summing the pressure drops due to pipes, fittings, a mass flow meter (MFM) and BPHEs. GEA heat exchanger selection software (http://www.flatplate.com) was used to obtain pressure drop for test BPHEs and post-cooler. Pressure drop across a MFM was also obtained from the manufacturer's catalog and is listed in the Table 2-3.

Table 2-3: Pressure drop of a MFM by Micromotion model CMF 050 (Data obtained from manufacturer via e-mail)

Flow rate (lb/min)	Pressure Drop (psi)
45.00	2.24
38.80	1.76
36.12	1.56
31.86	1.27
27.24	1.01

Since the flow rate of the water will be set at a constant value throughout the experiments, constant speed centrifugal pumps were selected. The total head loss in the system is 59.7 feet at 4.6 gpm. The selected pumps are in-line pumps with model TACO 1400-50. The electrical specification for this pump is 115Volt/ 5.0Amps. Two pumps were initially installed in series to provide sufficient pressure rise at the desired flow rate.

After the addition of a cooling tower in the system, the head loss has increased and installation of a third pump was required in the system. Fig. 2-7 shows the pump curves for different combinations.

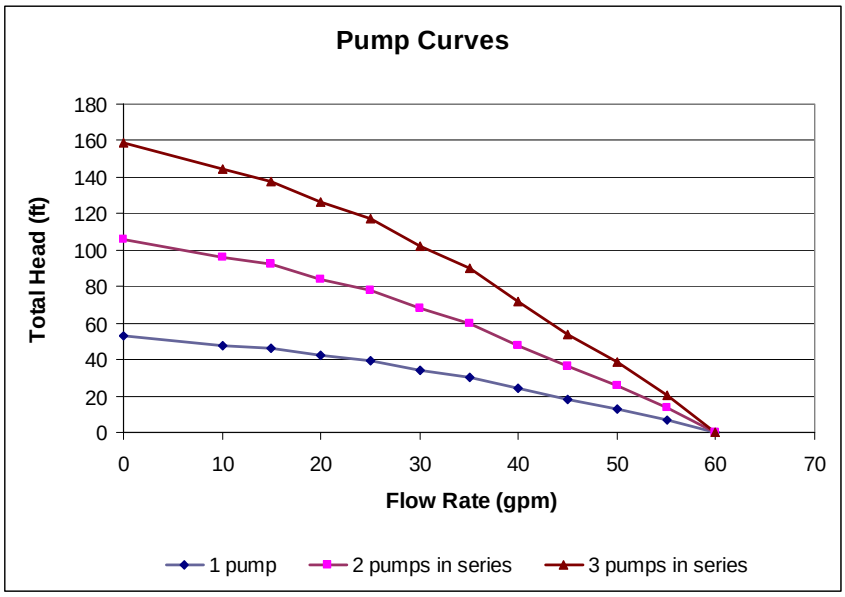

Fig. 2-7: Taco pump curves

2.4.2 RTD (Resistance Temperature Detectors)

Temperature measurement on the water side of the condenser is very critical because the growth of the mineral deposit is monitored by the outlet temperature at the test BPHEs. It is expected that the outlet temperature to decrease over time as the thickness of the mineral deposit on the plates increases. Since temperature measurements are very critical, 4-wire RTDs were selected for the cooling water side. The three RTDs are model P-M-1/10-1/8-6-0-P-3 by OMEGA. The probes are 6” in length with 1/8” probe diameter. They can sustain a temperature range of -50 ~ 100 °C (-58 ~ 212 °F).

2.4.3 Test Brazed Plate Heat Exchangers

Four different geometries of BPHE were selected based on the given performance rating by the manufacturer, GEA. Table 2-4 summarizes the geometries of the selected BPHE.

Table 2-4: Test BPHE dimensions

Model	Overall dimension	No. of Plates	Corrugation/ Chevron Angle (°)	Corrugation/ Chevron depth, inch (cm)	Corrugation/ Chevron pitch, inch (cm)
BPHE-A1	5.1" W x 13.3" H x 1.6" D (12.95 cm W x 33.78 cm H x 4.06 cm D)	14	60	0.079 (0.20)	0.236 (0.60)
BPHE-A2	5.1" W x 13.3" H x 1.6" D (12.95 cm W x 33.78 cm H x 4.06 cm D)	14	27	0.079 (0.20)	0.236 (0.60)
BPHE-A3	5.1" W x 21.0" H x 1.1" D (12.95 cm W x 53.34 cm H x 2.79 cm D)	8	27	0.079 (0.20)	0.236 (0.60)
BPHE-A4	9.8" W x 20.3" H x 0.7" D (24.89 cm W x 51.56 cm H x 1.78 cm D)	6	27	0.079 (0.20)	0.25 (0.64)

BPHE-A2, BPHE-A3, and BPHE-A4 have different aspect ratios, which is defined as the ratio of overall length to width of the heat exchangers. BPHE-A1 and BPHE-A2 have the same aspect ratio but different corrugation angles. The selected BPHEs should be able to be tested under two different heat transfer rate – low and high heat flux, and three different water qualities – low, medium, and high potential fouling. A photo of the BPHEs is shown in Fig. 2-8.

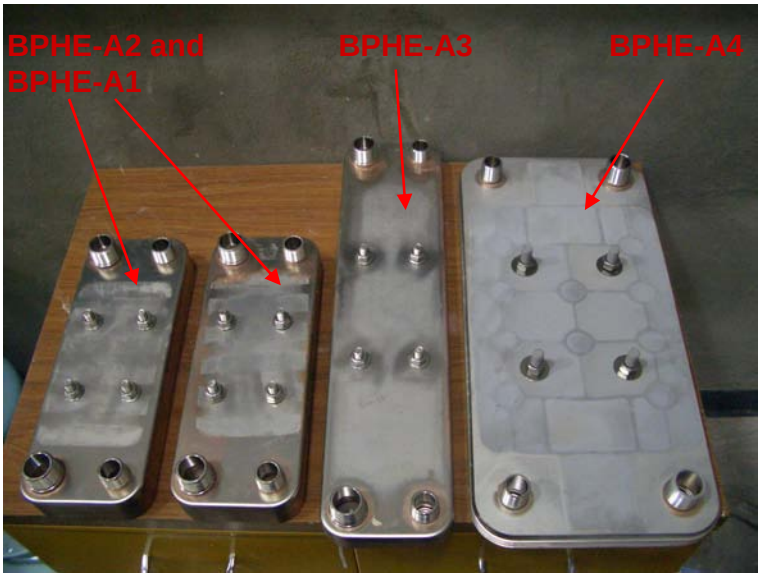

Fig 2-8: Four test BPHE models

2.4.4 Differential Pressure Transducer (DPT)

A differential pressure transducer is installed to measure the change of pressure drop across the test BPHE. It has been reported for enhanced type water cooled condensers that the pressure drop increased no more than 2% going from clean to fouled condition (Chamra, 2005, Li, 1998). Since the effect of fouling on pressure drop is very small, a DPT with high accuracy was selected. The transducer is manufactured by Validyne with model number P855D-1-N-1-26-S-4-A. The pressure transducer has nominal range between ± 0.08 psid to ±3200 psid and it is calibrated by the manufacturer to pressure range of 0-15 psi with accuracy ± 0.015 psi. The pressure transducer sends output signal of 0 to 5 Vdc to a data acquisition system.

2.4.5 Mass Flow Meters (MFM)

A Coriolis mass flow meter was selected from Micro Motion, Inc. The sensor is ELITE series with model CMF050M320NRAAEZZZ with transmitter

2700C12BBAEZZZ. CMF 050 is able to measure flow rate ranging from 0.45 kg/min (1.0 lb/min) to 27.2 kg/min (60.0 lb/min) with accuracy ± 0.10% at the operating flow rate. Table 2-5 shows the pressure drop and accuracy change under different flow rates based on using water as a working fluid.

Table 2-5: Accuracy of CMF 050 with different flow rates (Micromotion, 2010)

Flow Rate (lb/min)	Mass Flow Accuracy (± % of Rate)	Pressure Drop (psi)	Velocity (ft/s)
60.00	0.10	3.679	12.39
54.10	0.10	3.087	11.17
48.20	0.10	2.545	9.95
42.30	0.10	2.053	8.73
36.40	0.10	1.611	7.52
30.50	0.10	1.221	6.30
24.60	0.10	0.881	5.08
18.70	0.10	0.589	3.86
12.80	0.10	0.340	2.64
6.90	0.10	0.133	1.42
1.00	0.60	0.005	0.21

2.4.6 Post-cooler

The purpose of the post-cooler is to reject heat from the water that has been added by the test condenser. In an actual cooling tower loop, the post-cooler simulates the heat transfer process that occurs inside a tower. The model BPHE that was selected for post-cooler is GB400H-14. Fig. 2-9 shows the photo of the post cooler connected to the chilled water line.

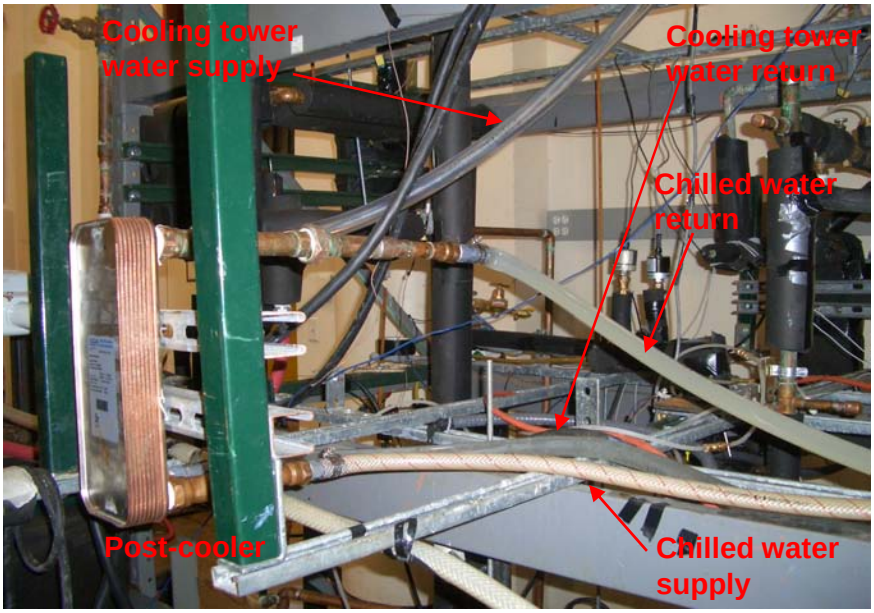

Fig 2.9: Photo of post-cooler connected to chilled water loop

Flexible hoses were used to connect both chilled water and cooling tower sides to post-cooler. This allows easy removal of the post cooler for maintenance and cleaning.

2.4.7 Cooling Tower

Since the post-cooler is able to reduce the temperature of the fluid, the cooling tower is actually not required for heat rejection in the system. However, after numerous trials to re-create high fouling potential water, it was concluded that the high fouling potential water cannot be simply created by mixing different chemicals. In order to reach high fouling potential water, the cooling tower water is first mixed at a low fouling potential, then concentrated by cycling through the cooling tower. Make-up water at a low fouling potential is charged to the system to compensate the loss due to evaporation. Therefore, a cooling tower was added towards the end of the test facility construction to create high fouling potential of water.

The cooling tower is constructed inside a 105 gallon polyethylene tank that has dimension 58.42cm D x 165.1cm H (23in D x 65in H) and with 20.32cm (8in) diameter opening at the top. There is a 1.91 cm (0.75 in) PVC pipe inserted through the sidewall at the top of the tank and the end of the pipe was capped. Two flat spray brass nozzles were installed in series along the PVC pipe to spray the water downward. The nozzles have 0.64 cm (¼ in) NPT male connection with 80° deflection angle. A 20.32cm (8in) diameter flexible duct was used to connect the top of the tank to the fan, which is supported on the nearest test stand. Although the fan is equipped with a variable frequency drive, the frequency is set to be constant at 50 Hz throughout the experiments to ensure consistency in airflow rate. The air intakes of the cooling tower were located 53.34cm (21in) from the bottom of the basin and they were made by drilling three 3.34cm (1.315in) diameter openings that are evenly distributed around the tank. To prevent the sprayed water escaping the tower through the air intake openings, the openings were fitted with 2.54cm (1in) PVC elbows and extended vertically using 2.54cm (1in) PVC pipes. At the end, the openings were sealed to avoid any leakage.

The fan pulls the air across the dropping water to remove the heat from the test BPHE. A wire mesh screen was placed at the top of the nozzles to prevent any water droplets entering the fan. The flow rate from the test condenser to the cooling tower is set at 0.00379 m^3/min (1 gal/min) during the start-up. This flow rate gives evaporation rate of 0.076 m^3/day (20 gal/day) under typical laboratory conditions.

The cooling tower sits on a stand so that the tank is lifted 1.346m (53in) above the ground as shown in Fig. 2-10. This design allows the pressure due to water column to direct the water back to the solution tank without using additional pump.

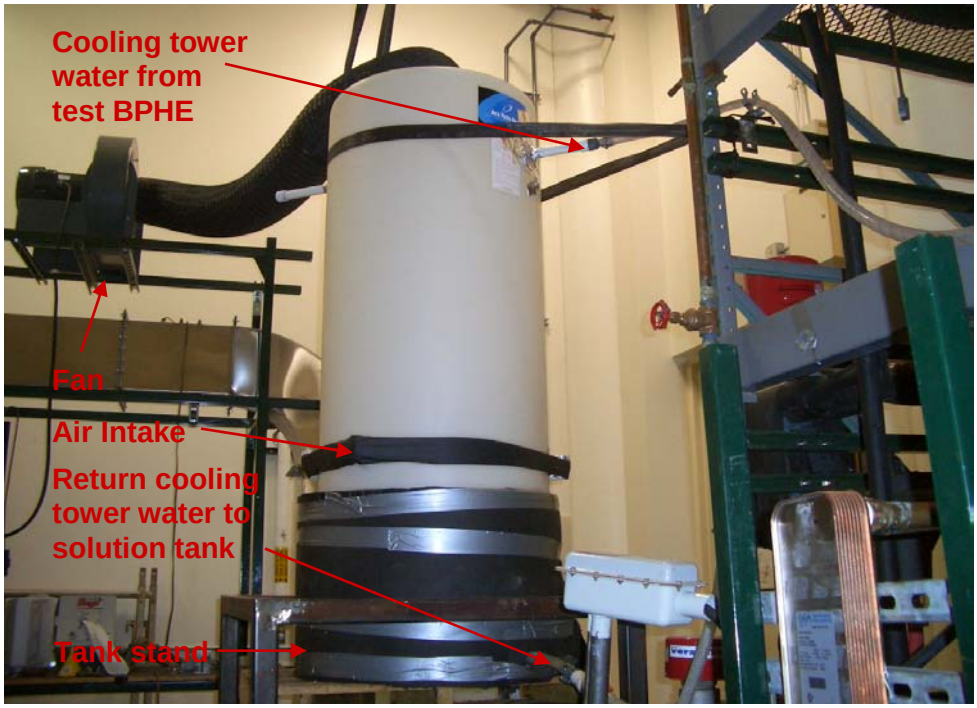

Fig. 2-10: Final cooling tower construction

2.4.8 Electric Heater in a Solution Tank

After the post-cooler, the water is directed to the solution tank in which the water from the cooling tower returns to. A 0.644 m^3 (170 gal) tank was installed in-line as a reservoir to store cooling tower water. The tank is also used as a charging location to charge make-up water. A 6 kW immersion heater by Chromolox was installed in the solution tank to maintain the water temperature at the inlet of BPHE at 29.4°C (85°F). The model of the immersion heater is KTLS-360A-036 and it has an electrical requirement of 480V/3PH/3.61A. The heater is connected to an SCR Power Pak controller model Mmax2-3-01-1-1-1, with maximum load current rating of 30 Amps. This controller utilizes zero voltage switching technique to modulate power by receiving

input signal of 0-5 V from the DAQ. Another two identical controllers were connected to the heaters that were installed in evaporator and superheater loop which will be discussed in later section. Fig 2-11 shows photos of one of the SCR controllers and electrical boxes in which the SCR controllers were mounted. These electrical boxes were mounted inside a control room.

Fig. 2-11: Photos of a heater controller and control boxes

The heater is indirectly controlled by the output from RTD that is located at the inlet of the test BPHE. The temperature read by this RTD is sent to the DAQ and then compared with the set point temperature, which is specified by users. If the temperature of the water is lower than the set point temperature, Labview sends signal to the SCR controller to deliver more power to the heater. The SCR controller is able to communicate with Labview because the controller accepts signals in 4 ~ 20 mA, 0 ~ 5 Vdc, and 0 ~ 10 Vdc.

2.5 Evaporator loop

The purpose of the evaporator loop is to bring the condition of the refrigerant from sub-cooled to a saturated vapor condition. The water in the evaporator loop is

circulated using a Dayton pump model 6K582A. A 3-kW electric heater is placed inside a 30 gal conical tank to maintain constant water temperature. The main reason to use a water tank in this loop is that to obtain a stabilized water temperature since the fluctuation in water temperature affects the constancy of refrigerant pressure. Essentially, the refrigerant condensing pressure is set by adjusting the water temperature in this loop. Water temperature is measured using an in-stream RTD placed at the outlet of the evaporator. The water temperature set point is manually adjusted to reach the desired condensing pressure on the refrigerant side. A piping schematic of the evaporator loop is shown in Fig. 2-12.

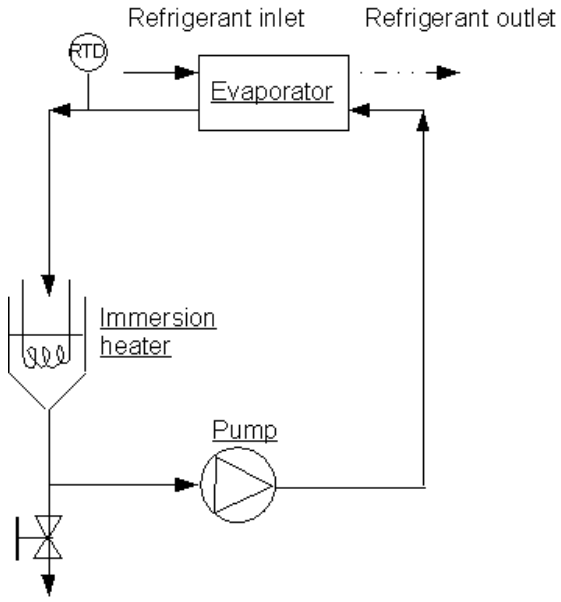

Fig. 2-12: Evaporator loop

2.6 Superheater loop

The purpose of the superheater loop is to condition the refrigerant from saturated vapor to superheated vapor prior to the entering of the test condenser. The refrigerant inlet temperature has to have 18.3°C (65°F) of superheat before entering the test condenser. Therefore with the refrigerant inlet temperature has to be maintained at

76.77°C (170°F), the water temperature in the superheater loop has to be set at approximately 81.11°C (178°F). Due to the high working temperature and safety reasons, the superheater loop was designed to be a closed-loop system. Water is circulated with Grundfos pump model UP 26-99F and heated with a 24-kW in-line heater by Chromalox. This heater is connected to an SCR Power Pak controller model Mmax2-3-01-1-1-1 to regulate the output power to the heater. Fig. 2-13 shows the schematic of the superheater loop.

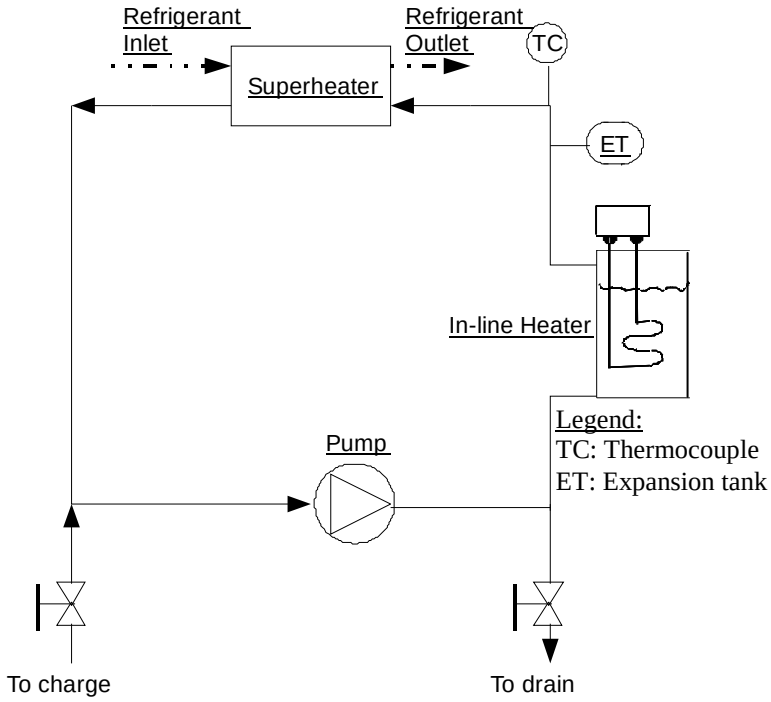

Fig. 2-13: Superheater loop

At the outlet of the in-line heater, an in-stream J-type thermocouple was installed to monitor the water temperature. The monitored temperature was set as the cut-off temperature for the heater in order to avoid overheating. Since this is a closed loop and it operates at high temperature, a diaphragm-type of expansion tank by Bell and Gossett, model HFT-15 was installed at the outlet of the heater to accommodate volume change in

the system. A brazed plate type of heat exchanger by GEA model GB400L-14 was installed to exchange heat from the superheater loop to the refrigerant. Two ball valves were installed at the pump inlet and outlet to easily purge the system when it is necessary.

2.7 Chilled water loop

The main purpose of the chilled water system is to reject heat from both the refrigerant and the cooling tower loops. Additionally, this loop also eliminates using excessive amount of domestic cold water to reject heat from the sub-cooler and post-cooler. There are three different heat exchangers connected to chilled water loop as listed in Table 2-6.

Table 2-6: List of BPHE models in chilled water loop

Component Names	Model	Overall dimension	No. of Plates
Post-cooler	GB400H-14	5.1" W x 13.3" H x 1.6" D	14
Campus cooler	FP 5 x 12 - 28	4.9 " W x 12.2" H x 2.9 " D	28
Sub-cooler	GB200H-6	3.4 " W x 8.9" H x 0.9" D	6

Schematic of chilled water system is shown in Fig. 2-14.

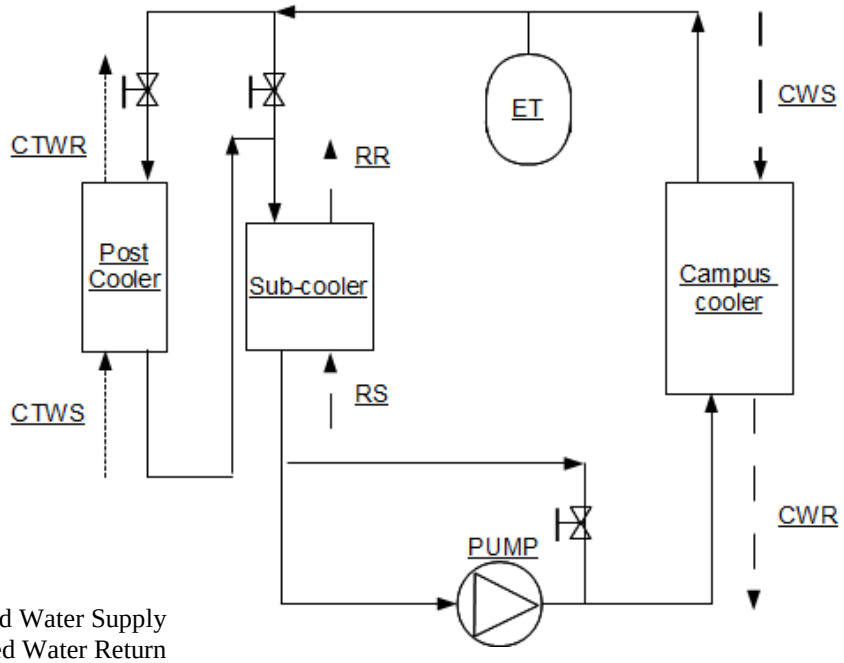

Legend:
CWS: Chilled Water Supply
CWR: Chilled Water Return
RS: Refrigerant Supply
RW: Refrigerant Return
CTWS: Cooling Tower Water Supply
CTWR: Cooling Tower Water Return
ET: Expansion Tank

Fig: 2-14: Schematic of chilled water loop

The water in chilled water loop is circulated using a Dayton pump model 6K582A. The flow distribution between the post-cooler and sub-cooler can be regulated manually by gate valves to meet the cooling demand. For refrigerant loop, the refrigerant temperature at the exit of condenser is lowered by 5.56 - 11.11°C (10 – 20°F) before it enters the refrigerant pump. This process ensures the refrigerant is in the sub-cooled or liquid condition before entering the pump. For cooling tower loop, the heat from test condenser needs to be dissipated to the chilled water loop by the post-cooler. After passes through the post-cooler, the chilled water enters sub-cooler before it is directed to campus cooler BPHE that rejects heat to campus chilled water. Fig. 2-15 shows connection of this BPHE to campus chilled water system.

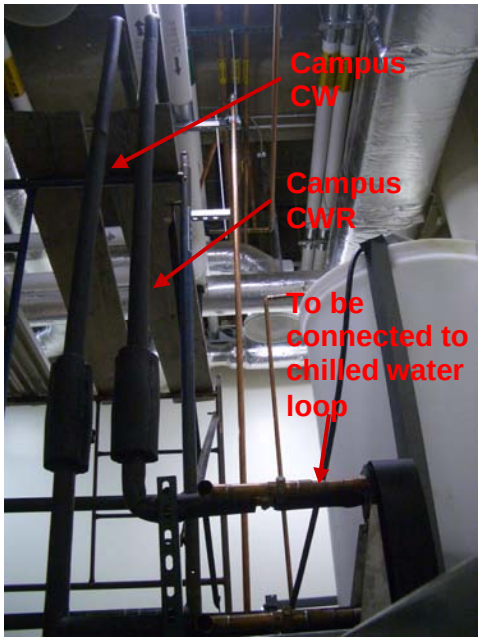

Fig. 2-15: Photo of campus chilled water system

The chilled water supply temperature comes in at approximately 5°C (41°F) and the return temperature has to be at about 13.33°C (56°F). There is an expansion tank installed at the outlet of the campus cooler to allow thermal expansion of the chilled water that potentially could damage the piping system.

2.8 Safety

Since the design of test facility incorporates heaters to maintain the cooling tower temperature and to condition the refrigerant loop, a few safety precautions are integrated and controlled by LabVIEW. The safety precautions for the heaters are triggered by the installed thermocouples on heating elements. The maximum cut-off temperature is set at 190°F. The cooling tower pumps are connected to a relay switch will shut down the pumps during the emergency shut down. All the temperature and flow rates constraints can be adjusted by users. The DAQ will shut down the system in case any of the following conditions occur:

1. Heating elements of the heaters reach the cut-off temperature. This could occur were the pumps that are installed in the evaporator and superheater loops fail.
2. One of the cooling tower pumps fails.
3. The cooling tower loop runs out of water.

The safety shut-down includes turning off the cooling tower pumps, refrigerant pump, two immersion heaters, and an in-line heater. After the shut down, the LabView program will send email for notifications. At last, LabView program will stop monitoring and recording any data.

CHAPTER III

WATER CHEMISTRY

The ultimate objective of this project is to study the effect of water quality on fouling of brazed-plate type condensers that are connected to cooling towers. The study of water quality is required to be able to create cooling tower water. The original request-for proposals (RFP-1345) specified the chemical makeup of three different solutions to be employed in this study. Each of the three solutions is supposed to be representative of water quality that can be found in cooling towers that are located in the United States. However, as explained later in this chapter, the solution cannot be made exactly as specified.

Table 3-1: Water chemistry for three different fouling potential (RFP-1345)

Fouling Potential	Total Hardness	Calcium (as CaCO3)	Magnesium (as $CaCO_3$)	"M" Alkalinity (as $CaCO_3$)	Chloride	Silica	Sulfate	Specific Conductance
low	240	180	59	96	< 200	5.7	72	TBD
medium	480	360	119	192	< 200	11.4	144	TBD
high	640	480	158	256	< 200	15.2	192	TBD

Fouling Potential	pH	Total Iron	Copper	TDS	Total Suspended Solids	P-Type Alkalinity	LSI
low	7.80	0.15	0.03	1140	< 100	0	0.198
medium	8.60	0.30	0.06	1500	< 100	0	1.864
high	9.30	0.40	0.08	1800	< 100	0	2.803

As shown in Table 3-1, the three solutions have fouling potentials characterized as low, medium, and high. Each fouling potential level is described by the amount of alkalinity, total hardness, LSI (Langelier's Saturation Index), and other values. In the next section, these terms are discussed in detail. A complete procedure to create high fouling potential water and water analysis of the cooling tower water are also discussed in the following sections.

3.1 Water Characteristics

Natural water contains several dissolved salts, most of which are inversely soluble. As mentioned earlier, although there are several inversely-soluble salts found in typical cooling tower water, calcium carbonate ($CaCO_3$) is usually the predominant component found in fouling deposits. In the following sections, water characteristics that define water quality are discussed.

3.1.1 Alkalinity

The precipitation of $CaCO_3$ originates from the presence of calcium, (Ca^{+2}) and carbonate (CO_3^{-2}) ions in the water. $CaCO_3$ in the water originates from sedimentary rocks, accelerated by the dissolved carbon dioxide (CO_2). CO_2 is responsible in the formation of $CaCO_3$ in the water by several stages of chemical reactions. The formation of CO_3^{-2} ions can be explained in the following dissociation process that starts from the occurrence of $CO_{2(g)}$ in the water:

$$CO_{2(g)} \leftrightarrow CO_{2(aq)} \tag{3-1}$$

Once CO_2 is dissolved in the water, it forms bicarbonate (HCO_3^-) as expressed in the following equilibrium equation:

$$CO_{2(aq)} + H_2O \leftrightarrow H_2CO_3 \quad (3\text{-}2)$$

Since the above process is kinetically slow, only a small fraction of $CO_{2(aq)}$ is converted into carbonic acid (H_2CO_3). The rest of the carbon dioxide remains as $CO_{2(aq)}$ molecules. The H_2CO_3 in the product side of Equation (3.2) is further dissociated in two steps:

$$H_2CO_3 + H_2O \leftrightarrow H_3O^+ + HCO_3^- \quad (3\text{-}3)$$

$$HCO_3^- + H_2O \leftrightarrow H_3O^+ + CO_3^{2-} \quad (3\text{-}4)$$

Alkalinity is due to the bicarbonate (HCO_3^-) and carbonate (CO_3^-) ions from the product side of Equation (3-3) and (3-4) respectively, depending on the water pH. Alkalinity acts as a buffer of a solution to resist against pH change and it is expressed in terms of equivalent mg/liter of $CaCO_3$ (commonly stated as "ppm *as* $CaCO_3$"). In other words, if a drop of acid are added to a solution that has high alkalinity, the pH of the solution does not change until a few more drops of acid is added to the solution. Alkalinity can be reported as "M"Alkalinity and "P"alkalinity. Methyl Orange ("M" alkalinity or also known as total alkalinity) specifies the amount of dissolved bicarbonate (HCO_3^-), carbonate (CO_3^-) and hydroxyl (OH^-) ions that present in natural water. The amount of bicarbonate and carbonate are determined by a titration method with using a 0.02 N sulfuric acid (H_2SO_4). Table 3-4 gives some details of procedure in obtaining concentration of HCO_3^- and CO_3^-.

In pH range of 8.2-9.6, both HCO_3^- and CO_3^- typically exist together in natural water; however, OH^- ions can be measured only when pH is above 9.6. In pH range of 8.2-9.4, "P" and "M" alkalinities can be calculated after the concentration ratio of HCO_3^- and CO_3^- are known (Kemmer, 1979):

$$P = \frac{[CO_3^-]}{2} \tag{3-5}$$

Where: P = "P" alkalinity (ppm as $CaCO_3$)

$[CO_3^-]$ = concentration of carbonate (mol/L)

$$M = [HCO_3^-] + [CO_3^-] \tag{3-6}$$

Where: $[HCO_3^-]$ = concentration of bicarbonate (mol/L)

M = "M" alkalinity (ppm as $CaCO_3$)

3.1.2 Water Hardness

Total hardness is one of the important water characteristics. The carbonate ions in the product side of the equilibrium equation in Equation (3.4) interact with any positively charged ions (cations) presents in the water. Examples of cations are Ca^{2+} and Mg^{2+} ions. If these ions present in the water, they will bond together with CO_3^{2-} to form deposits of $CaCO_3$ and $MgCO_3$.

Total hardness is primarily used to quantify the amount of calcium carbonates and magnesium carbonates in the water. It is classified subjectively because the classification

varies with reference. Table 3-2 shows one of the water hardness classifications provided by the USGS (U.S Geological Survey):

Table 3-2: Water Hardness Classification (Briggs, 1977)

Hardness (ppm as $CaCO_3$)	Classification
0-60	Soft
61-120	Moderately Hard
121-180	Hard
above 181	Very Hard

The higher the total hardness indicates the greater amount minerals contained in the water. Total hardness is typically reported as milligrams per liter *as* $CaCO_3$. Thus, to quantify the actual amount of Ca^{2+} ions that exist in the water, the following conversion is used:

$$Total\ Hardness \times \frac{40 mg Ca^{2+}}{100 mg CaCO_3} = \frac{mg}{L} Ca^{2+} \qquad (3\text{-}7)$$

Where: Total Hardness = concentration expressed in $\left(\frac{mg}{L}\right)$ *as* $CaCO_3$

Water hardness in cooling towers originates from the water source and is then increased by the evaporation process. As water is evaporated, it becomes more concentrated and often the water reaches a concentration level in which the solubility of the minerals is reached. At this point the water is already saturated with the minerals. Therefore, a slight temperature or pH increase can result in precipitation, as can a local high temperature within the system.

Total hardness is affected by the solubility of dissolved salts in the water. That is the maximum amount of salts in a specified amount of solute. Solubility is expressed in grams per liter of solution. The precipitation of a salt can be predicted by using solubility product, which is defined as the maximum product of the concentrations of cations and

anions that can be contained in a solution at a certain temperature. For instance, for calcium carbonate, the expression of solubility product is:

$$\left[Ca^{2+}\right]\times\left[CO_3^{2-}\right]=K_{sp}\ =3.8\text{x}10^{-9}\ \text{at}\ 25°\text{C} \qquad (3\text{-}8)$$

Where: [ ] is the concentration of the ion (moles/liter)

K_{sp} is the solubility product $\left(\frac{moles^2}{liters^2}\right)$

At a specific temperature, if the product of calcium and carbonate ions exceeds the K_{sp} value, then solid of $CaCO_3$ will precipitate out until the product of the two ions is equal to K_{sp} . However, the precipitation of a substance in a solution is more difficult to be predicted than the solubility product concept expressed in Equation (3.8) may suggest. The solubility product is affected by several factors - temperature, pH, presence and amount of other ions. For example, Fig. 3-1 shows the solubility of calcium ions is affected simultaneously by temperature and presence and amount of carbonate ions.

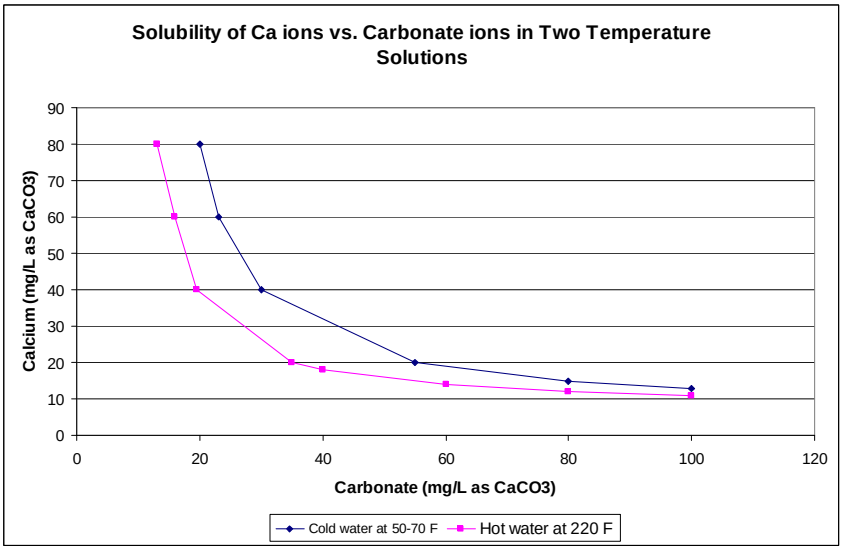

Fig. 3-1: Plot of calcium ions vs. carbonate ions in saturated $CaCO_3$ solution in hot and cold solution temperature (Kemmer, 1979)

The plot shows that addition of carbonate ions in the solution reduces the solubility of calcium ions. In addition, it also shows that the solubility of each ion is inversely proportional to the temperature of the solutions. If the above plot is translated into solubility product as a function of the amount of carbonate ions, the following plot is obtained:

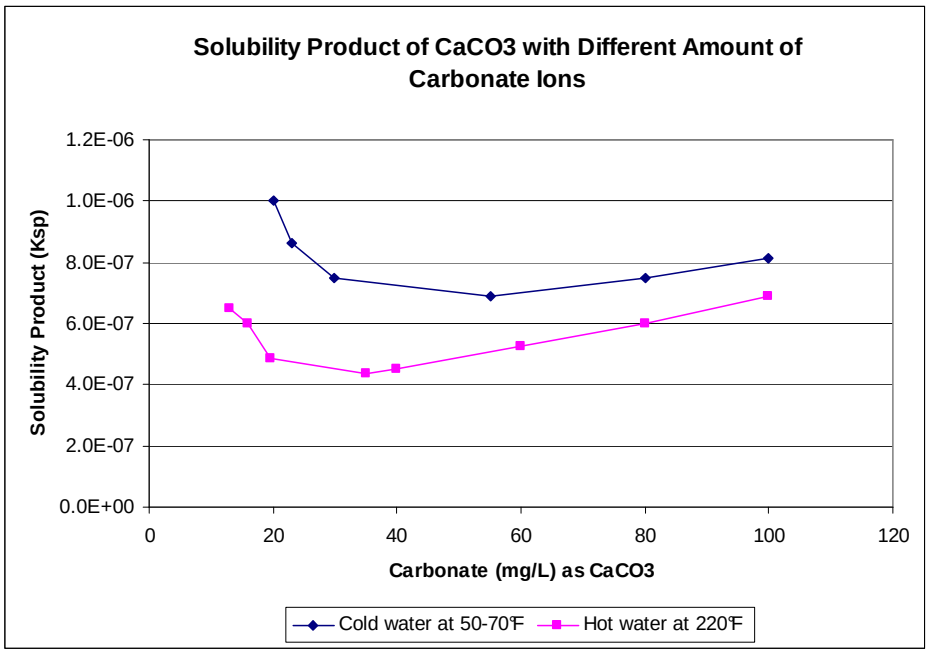

Fig. 3-2: Solubility product vs. amount of carbonate ions in the solution

Fig 3-2 shows that the calculated K_{sp} decreases if amount of calcium ions is decreased and additional carbonate ions present in the solution up to a certain point. Beyond this point, the K_{sp} of the salt increases with the addition of carbonate ions although the solubility product of the $CaCO_3$ salt remains constant. Since the calculated Ksp values are still higher than the Ksp value in equation 3-8, precipitation of $CaCO_3$ occurs in the solution. The higher the calculated Ksp value indicates the higher amount of precipitation in the solution.

3.1.3 Langelier Saturation Index (LSI)

Saturation index is commonly used as a parameter that defines the quality of water. Langelier (1936) attempted to formulate a way to determine calcium carbonate saturation in natural water in terms of pH, calcium concentration, alkalinity, total salinity, and temperature, which later became known as Langelier Saturation Index (LSI). To the present time, LSI has been used extensively in the water industry to determine the saturation level of calcium carbonates in a water sample. Saturation Index is defined as the difference between actual pH of the water sample and its computed saturation pH (pH_s), which is the pH at which calcium concentration in a given sample is in equilibrium with the total alkalinity. Essentially, the index is the logarithm of the ratio of hydrogen ion concentration in equilibrium conditions to the actual hydrogen ion concentration. It is expressed in the following equation:

$$\text{LSI} = pH_{actual} - pH_{saturation} = \log\frac{1}{(H^+)} - \log\frac{1}{(H_s^+)} = \log\frac{\left(H_s^+\right)}{\left(H^+\right)} \qquad (3\text{-}7)$$

Where: LSI = Langelier Saturation Index (-)

$\left(H^+\right)$ = concentration of hydrogen $\left(\frac{mol}{L}\right)$

$\left(H_s^+\right)$ = saturated hydrogen concentration $\left(\frac{mol}{L}\right)$

The saturation pH is given by:

$$pH_{saturation}\ (pH_s) = (pK_2^{'} - pK_s^{'}) + pCa^{+2} + pAlkalinity \qquad (3\text{-}8)$$

Where: $pK_2^{'} = -\log(K_2^{'}) = -\log\frac{\left[H^+\right]\cdot\left[CO_3^{-2}\right]}{\left[HCO_3^-\right]}$ $\left(\frac{mol}{L}\right)$

$$pK_s^{'} = \left[Ca^{+2}\right] \cdot \left[CO_3^{-2}\right] \qquad \left(\frac{mol}{L}\right)^2$$

$$pAlkalinity = -\log\left[Alkalinity\right] \text{ (ppm as } CaCO_3\text{)}$$

Positive LSI index numbers specify over-saturation that indicates fouling is potentially formed on the pipe or heat exchanger surfaces on which the water has contact. On the other hand, negative index numbers indicates under-saturation or in other words the water has the tendency to dissolve the existing carbonates in the water resulting in corrosion in the system. Table 3-2 characterizes LSI values.

Table 3-2: LSI Characterizations (Pearson, 2010)

LSI	SCALING CONDITIONS	
3.0+	---------->	Severe Scale Formation
2.0 - 2.9	---------->	Very Strong Scale formation
1.0 - 1.9	---------->	Strong Scale Formation
0.5 - 0.9	---------->	Moderate Scale Formation
0.2 - 0.4	---------->	Slight Scale Formation
0.1 to -0.1	---------->	Little to No Scale Formation (stable)
-0.2 to -0.4	---------->	Slight Tendency to Dissolve Scale (corrosive)
-0.5 to -0.9	---------->	Moderate Tendency to Dissolve Scale (corrosive)
-1.0 to -1.9	---------->	Strong Tendency to Dissolve Scale (corrosive)
-2.0 to -2.9	---------->	Very Strong Tendency to Dissolve Scale (corrosive)
-3.0 or <	---------->	Severe Tendency to Dissolve Scale (corrosive)

Several investigators performed studies to improve the saturation index developed by Langelier. Larson and Buswell (1942) developed a different method to compute pH_s, it is as follows:

$$(pH_s) = A + B - \log(Ca^{+2}) - \log(Alkalinity) \qquad (3\text{-}8)$$

Where: A and B = constants (can be found in Faust, 1998)

(Ca^{2+}) = concentration of calcium $\left(\frac{mol}{L}\right)$

In this project, the saturation pH values are computed using the following equation (*):

$$pH_S = 12.18 + 0.1 \cdot \log(TDS) - 0.0084 \cdot (T_{water}) - \log(Ca) - \log(M_{alkalinity}) \quad (3\text{-}9)$$

Where: TDS = Total Dissolved Solid (ppm)

T_{water} = water temperature (°F)

Ca = calcium concentration (ppm as $CaCO_3$)

$M_{alkalinity}$ = "M" alkalinity (ppm as $CaCO_3$)

The LSI calculations are performed in an MS Excel spreadsheet as shown in Fig. 3-3

Water Indices Calculations Spreadsheet

FORMULAE NOTES:				WATER ANALYSIS:			
LSI =	pH - pH(s)			pH	9.22		
RSI =	2*pH(s) - pH			"M" ALKALINITY	106.0	ppm	
PSI =	2*pH(s) - pH(calc)			Ca^{+2} HARDNESS	416.1	ppm	
pH(s) = 12.18 + 0.1*(logTDS) - 0.0084*F - log(Ca) - log(M)				CONDUCTIVITY	2150	µS/cm	
"CALCULATED" pH = 1.465 * log["M"] + 4.54				(Highest) Water Temperature	89	(°F)	
					Raw	**Cycled**	
				"CALCULATED" pH ---------->	7.51	7.51	
				* Actual (if known) Cycled Water pH ---------->		**0.0**	
				**Cycles of Concentration to be used ---------->		**1.0**	
INDICES CALCS:		**Raw**	**Cycled**	**pH(s)** (pH of saturation)	---------->	**7.11**	**7.11**
Ca^{+2} Hardness calcs =		2.62	2.62	**LSI** (Langelier's Index)	---------->	2.11	0.40
"M" Alkalinity calcs =		2.03	2.03	**RSI** (Ryznar Index)	---------->	4.99	6.70
TDS (Cond. X 0.7) calcs =		0.32	0.32	**PSI** (Practical Index)	---------->	6.70	6.70
Temperature calcs =		0.75	0.75				

Fig 3-3: Screenshot of MS Excel used to calculate LSI

Other saturation index models were used to compute LSI values based on the amount of constituents in low, medium, and high fouling potential water given in Table 3-1. Resulting LSI values are compared in the following table:

Table 3-3: Comparison of LSI values

	LSI Source			
Water Profile:	1205RP [1]	LSI_RSI[2]	edstrom[3]	Sam Faust[4]
High Fouling Potential	2.803	2.598	2.658	2.659
Medium Fouling Potential	1.995	1.781	1.841	1.868
Low Fouling Potential	0.478	0.266	0.326	0.352

Sources:

(1) Chamra, 2006

(2) Pearson, 2010
(3) Edstrom (http://www.edstrom.com)
(4) Sam Faust, 1998

From the table above, it can be seen that there is a small variation in the computed LSI using different saturation index equations. One LSI model might give more conservative values compared to the others; however, they are still within an acceptable range.

3.2 Initial Attempts to Create High Fouling Potential Water

The requirement in this project is to create cooling tower water based on the fouling potential that is provided by the PMSC in Table 3-1. The initial attempt to create high fouling potential water involved dissolving *CaSO4* and $MgSO_4$ in a 0.00378 m^3 (5 gal.) batch of Reversed Osmosis (RO) water that is available from lab. These salts were selected because they are more soluble than $CaCO_3$ and $MgCO_3$. This was followed by an aeration process with carbon dioxide ($CO_{2(g)}$) process because CO_2 can dissolve into bicarbonate (HCO_3^-) and eventually carbonate (CO_3^-) in water as it is shown in Equation (3.2) to (3.4). The carbonate should bond with the calcium ions (Ca^{2+}) from $CaSO_4$ and magnesium ions (Mg^{2+}) from $MgSO_4$ to form $CaCO_3$ and $MgCO_3$ in the solution. These reactions are expressed in the following equilibrium equations:

$$2H_3O^+ + CO_3^{2-} + CaSO_{4(aq)} \leftrightarrow CaCO_3 + 2H_3O^+ + SO_4^{2-} \qquad (3\text{-}10)$$

$$2H_3O^+ + CO_3^{2-} + MgSO_{4(aq)} \leftrightarrow MgCO_3 + 2H_3O^+ + SO_4^{2-} \qquad (3\text{-}11)$$

After preparing several water samples, the water analysis test reports showed that the minerals were completely dissolved; however, the pH of the solution was only 6.3, which is lower than the desired pH value of 9.3 for the high fouling potential water. The low pH was caused by the undissociated $CO_{2(aq)}$. Increasing pH of the solution was

attempted by performing an aeration process using compressed air. This process was able to remove the excess $CO_{2(aq)}$ because the pH increased to 8.3. However, once the pH reached 8.3, further aeration process was not effective. Thus, the only way to increase the pH to reach the desired pH was by adding a base, potassium hydroxide (*kOH*). Nevertheless, once the solution pH was successfully increased, precipitation began to occur and alkalinity level started to drop.

A second approach to obtain high fouling potential water was to use the water from cooling towers that are located in Oklahoma State University (OSU). The requirements of high fouling potential water can be satisfied by addition of reagents to reach the desired water hardness. However, the water in the OSU cooling towers had been pre-treated with fouling inhibitors to minimize precipitation or any other reactions that contribute to fouling. Therefore, utilizing OSU cooling tower water to run the tests is not desirable because the use of inhibitors can alter the results of water quality studies.

After numerous attempts to create high fouling potential water, the following observations were made:

1. The inversely-soluble minerals can be dissolved in acidic solution, but once after the pH is increased, precipitation occurs immediately.
2. Creating water that is saturated with inversely-soluble minerals is difficult, because precipitation occurs immediately as the pH or the water temperature is slightly increased. The change in pH or temperature shifts the equilibrium of the minerals.

3. Addition of different minerals can change the solubility of a mineral. For example, Hydroxide is able to increase pH solution; however, it can precipitate magnesium carbonate.
4. Table 3-1 states that high fouling potential water has no P-alkalinity at pH = 9.3. This is contrary to the definition of P-alkalinity as discussed in the previous section because at pH = 9.3, carbonates (CO_3^-), which contributes to P-alkalinity exists together with bicarbonates (HCO_3^-) in water.

Thus, it is concluded that the high fouling potential water cannot be created by simply mixing different chemicals in RO water without using any water treatments to prevent precipitation.

3.3 Procedure to create high fouling potential water

A new test protocol was created to create high fouling potential cooling tower water by employing an evaporation process. The high fouling potential cooling tower water is created by cycling low fouling potential water through a "cooling tower", as described in section 2.4.7. The low potential water contains the constituents specified in Table 3-1. The reagent grade chemicals used to create low fouling water are $CaCl_2$, $MgSO_4$, and $Ca(OH)_2$. The amount of each reagent is calculated in an Excel spreadsheet that is set up to calculate the amount of each ion in a substance. The quantity of each substance to create low fouling potential water is listed as follows:

1. $MgSO_4 = 90 \left(\frac{mg}{kgH_2O} \right)$

2. $CaCl_2 = 156.34 \left(\frac{mg}{kgH_2O} \right)$

3. $Ca(OH)_2 = 28.97 \left(\frac{mg}{kgH_2O} \right)$

The reagents are dissolved in 1.041 m^3 (275 gallon) of RO water, which is stored in a 300 gallon batch tank. Eventually, the prepared cooling tower water that is stored in a batch tank is used to charge the system at the beginning of the experiment as well as to replace the water loss due to evaporation. Since the make-up water contains some minerals, it is expected that the concentration of minerals in the system gradually increases over time. As a result, the water in the system is going to be saturated and therefore precipitation is very likely to occur at the hottest part of the system. In actual cooling tower operations, the water is typically bled from the system to remove the concentrated water. This process is known as blowdown process. In this experiment, blowdown process is not implemented in the system. Therefore, the water quality that is used in the tests represent the worst possible water quality in actual cooling towers.

This project is mainly focuses on precipitation and particulate fouling. Hence, during the preparation of low fouling potential water, sodium Tolytriazole (TTA) and chlorine are added to the water to prevent corrosion and microbial deposits. A step-by step procedure to prepare 1.041 m^3 (275 gallon) of low fouling potential water is described as follows:

1. Place a plate on the scale and turn on the scale. Make sure the scale reads “0”
2. Prepare the following chemicals:
    a. Magnesium Sulfate: 93.69 g
    b. Calcium chloride: 162.75 g

c. Calcium hydroxide: 30.2 g

3. Dissolve each measured reagent at one time into the RO water
4. Turn on the pump and recirculate the water inside the batch tank. Make sure that the pump has been cleaned by running clean water through it for the first 1 minute.
5. While circulating the water inside the batch tank, add 343.75 mL(330 ppm) of TTA and 206.25 mL (198 ppm) of Clorox bleach.
6. Circulate the water for another 20 minutes.
7. Charge 80 gallon of low fouling water into the system.
8. After charging the water, test the pH. Most likely pH will be approximately 8.8. If pH is below 9, add Potassium Hydroxide to increase pH.

3.4 Water analysis

A water sample is taken after the first time low fouling potential water is prepared to ensure the desired water quality is reached. Once the system runs, water samples are taken weekly to monitor the water quality. The water analysis is performed by the Soil, Water, and Forage Analytical Laboratory (SWFAL) in OSU. Fig 3-4 shows the photo of Inductively Coupled Plasma (ICP) mass spectrometry and pH meter that are used by SWFAL to run water analysis.

Fig 3-4: Photo of ICP and pH meter

ICP mass spectrometry is a device that quantifies the presence of ions in a water sample by measuring the emitted wavelength from the excited ions. The pH meter consists of a glass electrode and an electronic meter that measures and display the pH of a solution. Table 3-4 lists the procedures and methods of calculation to analyze other water properties. The test results are reported in ppm or (mg/L) units.

Table 3-4: Water testing procedures

Analysis	Procedure
pH	Direct electrode reading of water samples
CO_3	Titrate with 0.02 N H_2SO_4 to pH 8.3, CO3= mL titrant x 0.02 x 6000/ml sample
HCO_3	Titrate with 0.02 N H_2SO_4 to pH 8.3 to 4.5, HCO3= mL titrant x 0.02 x 12,200/ml sample
EC (Electrical Conductivity)	Direct electrode reading of water samples
Na, Ca, Mg, K	Direct reading on ICP
SO_4	Direct reading on ICP
Cl	Automated ferricyanide
TSS (Total Soluble Salts)	EC x 0.66
SAR (Sodium Absorption Ratio)	0.043498 x Na/ [(0.04990 x Ca +0.08229 x Mg/2)1/2
PAR (Potassium Absorption Ratio)	$0.025577 \times K/[(0.0499 \times Ca + 0.08229 \times Mg)/2]^{1/2}$
Na %	0.043498 x Na/(0.043498 x Na +0.08229 x Mg +0.04990 x Ca)
Hardness	(0.04990 x Ca +0.08229 x Mg)x 50

Source: OSU Soil, Water, and Forage Analytical Laboratory

Since it is important to maintain the desired pH, pH of the solution is monitored daily by using a handheld pH meter. This pH meter is frequently calibrated in buffer solutions. If the cooling tower water pH drops to below 9.0, a concentrated *kOH* solution is added to the water until the pH reaches 9.3 or higher. The amounts of minerals in the system are calculated based on the test results from SWAFAL. An excel spreadsheet is set up to calculate the concentration of calcium and magnesium ions in the system using the total volume in the system and the added volume of the make-up water. The concentration of calcium ion along with the alkalinity and the electrical conductivity values that are

obtained from the SWAFAL test results are inserted into Equation (3-9) to compute saturation pH. The LSI is expected to gradually increase throughout testing of one BPHE as make-up water is constantly added to the system to replace the evaporated water. Fig. 3-5 shows a plot of LSI vs. time for one of the experiments.

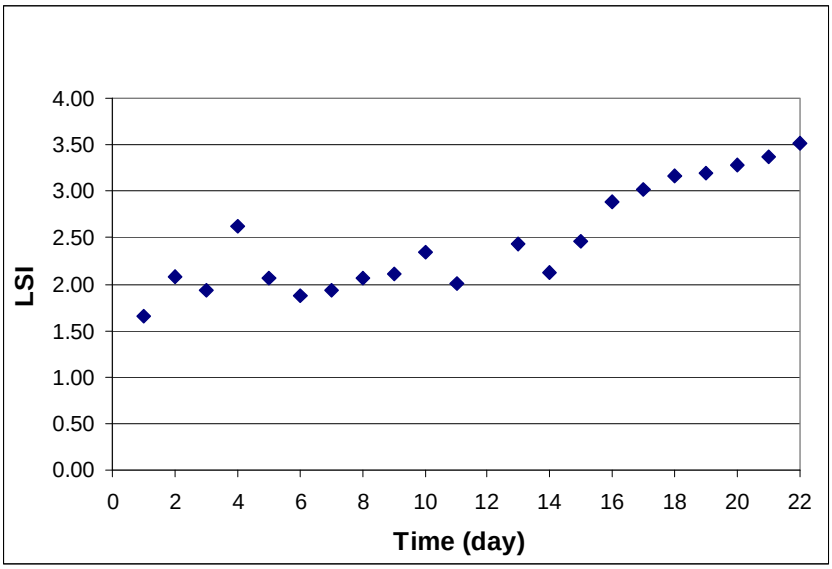

Figure 3-5: LSI vs. time for BPHE-A3 test

CHAPTER IV

EXPERIMENTAL ANALYSIS

4.1 Overview

Tests are conducted for extended period, on the order of 30-55 days. Test conditions drift slightly over time. For reasons that will be explained in the next section, it is necessary to adjust the test conditions to obtain nearly uniform refrigerant saturation pressure, inlet water temperature, entering refrigerant temperature to the test BPHE, and water and refrigerant mass flow rates. This is done once a day before an intensive 3-hour data collection period. For a low heat flux test, the refrigerant inlet temperature to the test condenser is set to 76.67°C (170°F) to maintain 18.3°C (65°F) of superheat. This is done by adjusting the water temperature in the superheater loop. The condensing pressure is set at 1032.1 kPa (149.7 psi) by adjusting the water temperature in the hot water evaporator loop. The saturation temperature is obtained from the R134a property table once the saturation pressure is known. The flow rate of the refrigerant is set to 1.59 kg/min (3.5 lb/min) by adjusting the refrigerant pump rpm. The inlet water temperature to the BPHE is set to 29.44°C (85°F) by adjusting an immersion heater set point temperature and the water flow rate from the cooling tower. A needle valve that was installed at the inlet of the test BPHE was regulated until the flow rate reaches 17.6 kg/min (38.8 lb/min). After the test condition stabilizes, data are collected for 3 hours

with a sampling rate of 2 seconds. Thus, each data set contains 5400 readings of temperatures, flow rates, and pressures. This data set is then used to compute overall heat transfer coefficient (UA) and fouling resistance. For the other 21 hours each day, data are recorded with a sampling rate of 5 minutes. This allows us to monitor and analyze the system if the conditions shift drastically. The intensive data collection periods are performed daily until the fouling resistance curve reaches an asymptotic value, which is referred as the asymptotic fouling factor.

4.2 Overall Heat Transfer Coefficients (UA) Computation

In order to compute the overall heat transfer coefficients, the first step is to calculate heat transfer rate on the water-side of the test condenser:

$$\dot{q} = \dot{m}_{water} \cdot c_p \cdot (T_{ExWT} - T_{EwT}) \tag{4-1}$$

Where: $\dot{q}$ = heat transfer rate (kW) or (Btu/min)

$\dot{m}_{water}$ = mass flow rate (kg/s) or (lb/min)

c_p = specific heat of water (kJ/kg-K) or (Btu/lb-°F)

T_{ExWT} = Exiting Water Temperature (°C) or (°F)

T_{EwT} = Entering Water Temperature (°C) or (°F)

Log Mean Temperature Difference (LMTD) for a counter flow heat exchanger is traditionally defined as:

$$LMTD = \frac{(T_{h,i} - T_{c,o}) - (T_{h,o} - T_{c,i})}{\ln\left(\frac{T_{h,i} - T_{c,o}}{T_{h,o} - T_{c,i}}\right)} \tag{4-2}$$

where: $T_{h,i}$ = inlet hot fluid temperature (°C) or (°F)

$T_{h,o}$ = outlet hot fluid temperature (°C) or (°F)

$T_{c,i}$ = inlet cold fluid temperature (°C) or (°F)

$T_{c,o}$ = outlet cold fluid temperature (°C) or (°F)

However, per AHRI 450 (2007), LMTD for a water-cooled refrigerant condenser is computed with the following equation of LMTD:

$$LMTD = \frac{\left(T_{sat} - T_{ExwT}\right) - \left(T_{sat} - T_{EwT}\right)}{\ln\left(\frac{T_{sat} - T_{Exwt}}{T_{sat} - T_{EwT}}\right)} \tag{4-3}$$

Where: *LMTD* = Log Mean Temperature Difference (°C) or (°F)

T_{sat}= refrigerant saturated temperature (°C) or (°F)

T_{ExWT} = Exiting Water Temperature (°C) or (°F)

T_{EwT} = Entering Water Temperature (°C) or (°F)

The AHRI definition of LMTD eliminates the effect of superheat and sub-cooled regions in condensers. This standardized LMTD calculation method is used in practice to size condensers because different types of heat exchangers may have different degrees of superheat and sub-cooling. Through some observations, which will be discussed later in Chapter 5, the tested BPHE have differing sizes of superheat and sub-cooled regions. Since, in this project, the refrigerant enters the test condenser at superheated condition and exits at sub-cooled condition or saturated liquid depending on the test BPHE, the standardized LMTD calculation method does not give accurate representations of the actual performance of test BPHE. Two other methods to calculate LMTD are proposed and discussed in the next chapter.

The overall heat transfer coefficient is then calculated by using the following equation:

$$UA = \frac{\dot{q}}{LMTD} \tag{4-4}$$

Where: UA= overall heat transfer coefficient in clean condition $\left(\frac{W}{^{o}C}\right)$ or $\left(\frac{Btu}{hr-^{o}F}\right)$

$\dot{q}$ = heat transfer rate from Equation (4-1) (W) or (Btu/min)

LMTD = Log Mean Temperature Difference from Equation (4-2) or (4-3) (°C) or (°F).

In this chapter, only the AHRI approach (Equation (4-3)) for calculating LMTD is used. During the 3-hour test period, the conditions of both the refrigerant and cooling tower loops have to be set and maintained close to the desired test conditions. However, some fluctuations in the refrigerant pressure readings and in water mass flow rates inevitably occur during the test. Thus, the averaged measurement readings might not correspond precisely to the same test condition as when the clean UA value is taken. A slight fluctuation in refrigerant pressure and water flow rate could lead to potentially large errors in the computed fouling resistance. Fig. 4-1 is obtained using data from the first day of testing BPHE-A2. The facility is set up according to the low heat flux test condition, while varying the saturation pressure from 149.3 psi to 144.8 psi. The readings are recorded for 10 minutes, and then averaged to compute UA values using Equation (4-1), (4-3), and (4-4).

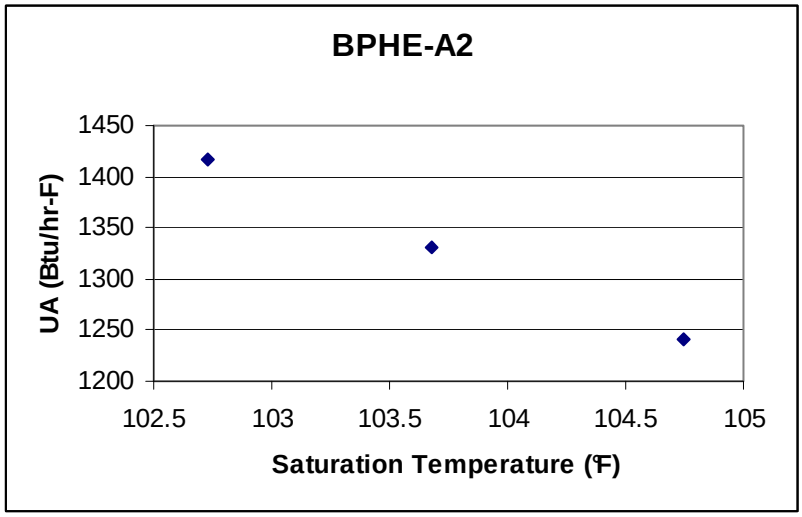

Fig 4-1: Plot of fouling resistance with different refrigerant saturation temperatures

The plot shows that UA values based on the AHRI LMTD are inversely proportional to the saturation pressure. The difference of 1.07°F in saturation temperature reduces UA values from 1330 to 1242 Btu/hr-°F.

To further study the effect of fluctuation of saturation pressure, an EES model of the heat exchanger was developed. The refrigerant entering temperature to the BPHE and flow rate is set to 76.67°C (170°F) and 1.59 kg/min (3.5 lb/min) respectively. The saturation pressure was varied between 1025.25 kPa (148.7 psi) to 1039.04 kPa (150.7 psi). At the median saturation pressure 1032.15 kPa (149.7 psi), the corresponding saturation temperature is 40.56°C (105°F). The water mass flow rate is fixed at 17.6 kg/min (38.8 lb/min) and the entering water temperature set at 29.44°C (85 °F). Heat transfer on the refrigerant side is computed by using the following equation:

$$\dot{q} = \dot{m}_{ref} \cdot \left(h_{ref,in} - h_{ref,out} \right) \tag{4-5}$$

Where: $\dot{q}$ = heat transfer rate of heat exchanger (kW) or (Btu/min)

$\dot{m}_{ref}$ = refrigerant mass flow rate (kg/min) or (lb/min)

$h_{ref,in}$ = enthalpy of entering refrigerant (kJ/kg) or (Btu/lb)

$h_{ref,out}$ = enthalpy of exiting refrigerant (kJ/kg) or (Btu/lb)

Fig. 4-2 shows a R134a T-s diagram that plots the conditions of the refrigerant at the inlet and outlet of the BPHE.

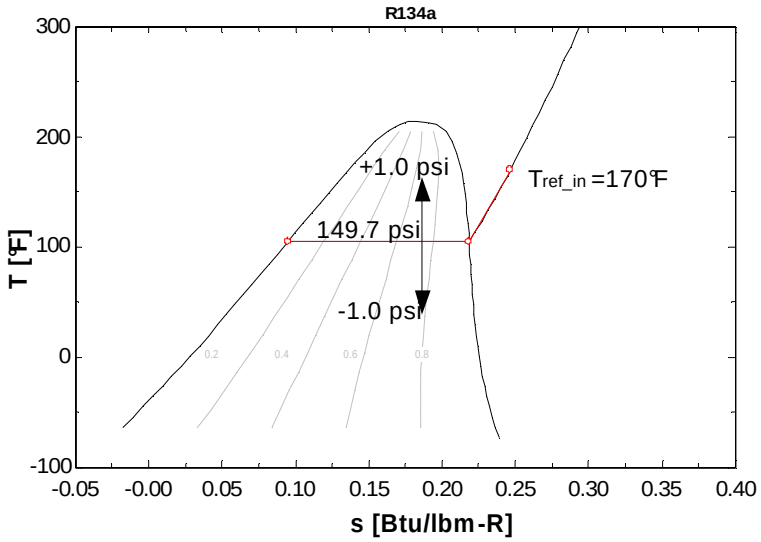

Fig. 4-2: T-s diagram of R134a

The exiting refrigerant condition is taken to be always at saturated liquid stage, so there is no sub-cooling effect. Thus, the exiting water temperature, the LMTD per AHRI definition and the UA values can be computed using Equation (4-1), (4-3), and (4-4). Fig. 4-3 shows the heat transfer process between refrigerant and water in the BPHE model.

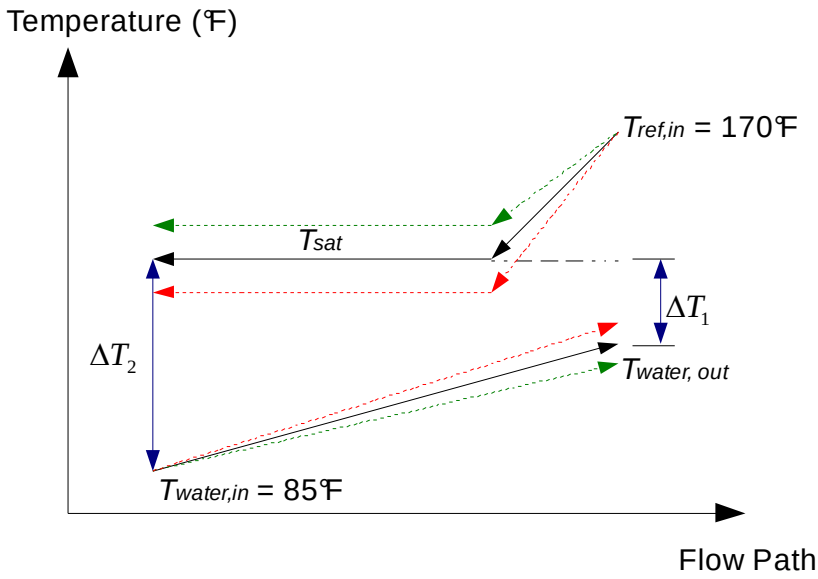

Fig. 4-3: Schematic of heat transfer process between R134a and water

The difference between desired saturation temperature and the exiting water temperature is denoted as ΔT_1 and the difference between desired saturation temperature and entering water temperature is denoted as ΔT_2. The output from the model is summarized in Table 4-1.

Table 4-1: Output from EES model to verify the effect of pressure fluctuation

P_{sat} (psi)	Degree of superheat (°F)	Heat Transfer Rate (Btu/hr)	T_{sat} (°F)	$LMTD_{(AHRI)}$ (°F)	ExWT (°F)	UA (Btu/hr-°F)
148.7	65.47	18212	104.5	15.29	92.83	1191
148.9	65.38	18203	104.6	15.38	92.83	1184
149.1	65.29	18195	104.7	15.48	92.82	1176
149.3	65.2	18186	104.8	15.57	92.82	1168
149.5	65.11	18177	104.9	15.66	92.82	1160
149.7	65.02	18169	105	15.76	92.81	1153
149.9	64.93	18160	105.1	15.85	92.81	1146
150.1	64.84	18152	105.2	15.95	92.8	1138
150.3	64.75	18143	105.3	16.04	92.8	1131
150.5	64.66	18135	105.3	16.13	92.8	1124
150.7	64.57	18126	105.4	16.23	92.79	1117

As can be seen from Table 4-1, when saturation pressure is equal to 149.7 psi, the computed water outlet temperature is 92.81°F. As P_{sat} is increased by 1 psi, the outlet water temperature decreases by 0.02°F and the heat transfer decreases by 0.24%. The LMTD values that are computed by AHRI definition show an increase of 2.90%, while the computed UA values show a decrease from 1153 to 1117 Btu/hr-°F or 3.12%. The corresponding UA values are used to compute fouling resistance using an equation that is discussed in section 4.4. The decrease of UA values indicates a fouling resistance of 1.29 x 10^{-4} hr • ft^2 F/Btu, which is 48.4 % of the specified fouling factor by TEMA (2.5 x 10^{-4} hr • ft^2 F/Btu). As a 1 psi drift in saturation pressure causes an error in the UA (based on the AHRI LMTD) computation that results in a ~ 50% error in the expected fouling factor, it is crucial that the saturation pressure be carefully controlled for all intensive data correction periods.

4.3 Clean UA Values Correction Method

As seen in the last section, the sensitivity of the computed UA values to the saturation pressure is very high. Even once all the flows and temperatures have been set prior to the daily intensive data collection procedure, as described in Section 4.1, the saturation pressure and water flow rate drift some during the three-hour collection period. This drift has the potential to cause a significant error in the computed UA, and hence in the inferred fouling factors. Therefore, three approaches have been developed to compensate for this drift in conditions.

4.3.1 Moving Average Method

The first method is referred to here as the "moving average" method. On the first day of testing a new BPHE, prior to the 3 hour intensive data collection period, the system is set to the desired test conditions as described in Section 4.1. During the set-up, the cooling tower fan should also be operating. There are 5400 data points for each measurement at the end of the collection period. The goal of the moving average method is to find a subset of the data points during which time the experimental facility closely matches the desired averages of saturation pressure, water mass flow rate, and inlet water temperature to the test BPHE.

To speed up the process of finding the subset, a computer code was developed in FORTRAN, which is presented in Appendix A. There are six measurements (P_{sat} , $T_{water, in}$, $T_{water, out}$, $T_{Ref, in}$, $T_{Ref, out}$, and $\dot{m}_{water}$) are needed to compute UA. The program reads a data file (data.csv) that contains these measurements for 5400 intervals. The user chooses a subset size (number of readings). Then a series of moving averages are computed for the subset size. If the condition of the system is relatively stable throughout the 3 hour test period, the typical size of the subset is 1750 data points with 5400 data readings. A subset size of 1750, there will be 3650 moving averages. The output of the program is saved in a file named slidingwindow.csv file. The next step is to manually scan the moving averages. If the averaged desired P_{sat} and $\dot{m}_{water}$ cannot be found in the output file, the subset size needs to be adjusted until the desired P_{sat} and $\dot{m}_{water}$ are contained in the output file. Once the size of subset is found, users are able to find more than one moving average set that give the desired P_{sat} and $\dot{m}_{water}$. However, one moving average set may have higher or lower inlet water temperature and refrigerant

flow rate compared to the other moving averages. It is important to select the moving average data set that is nearly the same as the desired test conditions for data reduction. Once a moving average set is selected, these values are used to compute overall heat transfer with using equations of (4-1), (4-3), and (4-4). The computed UA value is taken as the reference clean UA value. The same procedure is then applied to compute UA values in the subsequent days. Though the selection of averaged data set in output file is currently done manually, a potential future improvement would be to automatically identify the moving average set with the best P_{sat}, $\dot{m}_{water}$, and $T_{water,\,in}$.

4.3.2 Clean UA Values Correlation Method

The second method, referred to here as the "clean UA correlation method", utilizes a set of data collection periods on the first day of testing new BPHE. During the collection periods, P_{sat} and $\dot{m}_{water}$ are intentionally varied. These results are then correlated to give a clean UA as a function of P_{sat} and $\dot{m}_{water}$.

At the initial start-up, the system is set to the desired test condition except for the refrigerant saturation pressure and water mass flow rate. Water mass flow rate is set to 38.2 lb/min while fixing the saturation pressure to 145 psi. To ensure that no fouling occurs during the collection of clean baseline UA values, all cooling tower water is directed to post-cooler. At this point, the cooling tower fan is turned off to significantly minimize evaporation. The chilled water flow is adjusted accordingly to accommodate cooling for both cooling tower water and refrigerant. After the system stabilizes, the readings are recorded for 20 minutes with sampling rate of 2 seconds. At the end of the recording, the readings are averaged and used to compute clean UA values using Equation (4-1), (4-3), and (4-4). The saturation pressures are chosen to bracket the target

pressure ± 3 psi. The water flow rates are chosen to bracket the expected decrease in water flow rate over a test period.

At the end of a series of data collection period, the computed UA values are fitted as functions of refrigerant saturation pressure at two different water flow rates. Each correlation is developed based on one constant water mass flow rate with at least three different values of P_{sat}. For each test BPHE, there are at least two correlations for two different water mass flow rates. Fig. 4-4 shows the clean baseline UA values for test BPHE-A1, BPHE-A2, and BPHE-A3 respectively.

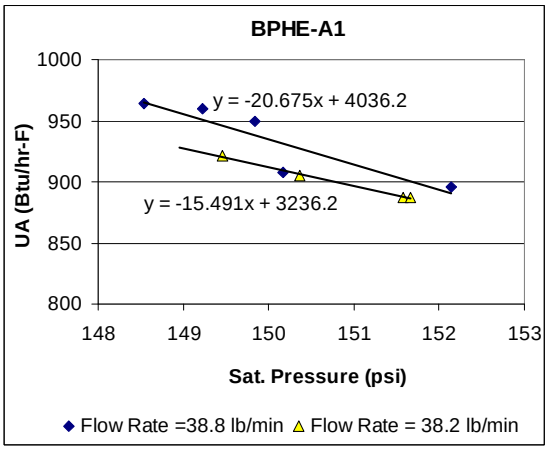

(a)

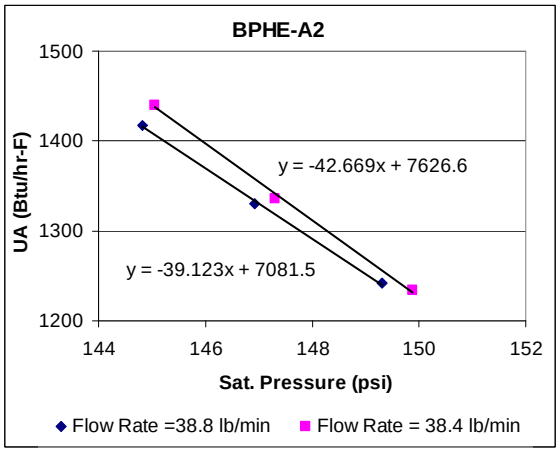

(b)

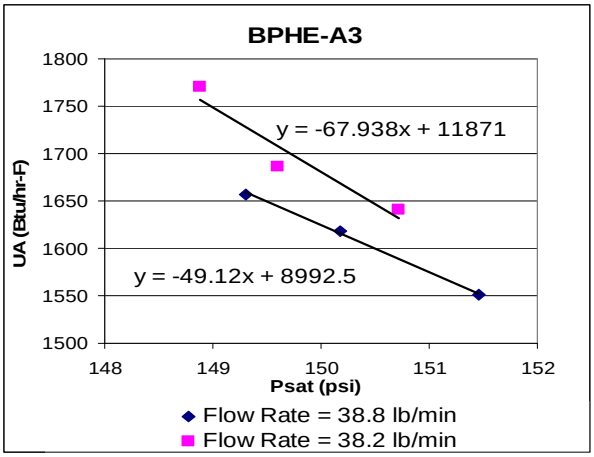

(C)

Fig. 4-4: Clean UA values for test BPHE model BPHE-A1, BPHE-A2, and BPHE-A3

For the following days, after system is set up according to the test conditions that are described in Section 4.1, data are collected each day using the 3-hour period of intensive collection period. Then, the readings for each measurement are averaged. Before computing the fouling resistance, the clean reference UA value is obtained from the appropriate correlation by substituting the averaged saturation pressure into the correlation. If the water mass flow rate deviates from the targeted 38.8 lb/min, then the reference UA value needs to be interpolated between the two correlations. To compute the fouling resistance each day, the UA in the fouled condition is compared to the corrected clean reference UA value that determined with the correlations. The reference UA values correct the variation of test conditions when the measurements are taken at slightly different condensing pressures and water mass flow rates.

4.3.3 Hybrid Method

In practice, combining the two above methods gives the best results. The hybrid method utilizes both the moving average and the UA correlation method to find clean reference UA values. Correlations are developed as described in Section 4.3.2. Then the daily results are analyzed as described in Section 4.3.1. The clean reference UA for the selected moving average set is determined by the method as described Section 4.3.2. The data are collected using the same intensive data collection procedure. At the end of the collection period, the collected data are first processed by moving average method, as described in Section 4.2.1, to find a moving average set that gives desired P_{sat} and $T_{water, in}$. Once the right data set is found, the deviation of water mass flow rate is corrected using the correlation method by substituting the moving average P_{sat} into the appropriate correlation to get the clean reference UA value. The same procedure is done on the

consecutive days every after the 3-hour data collection period to obtain clean reference UA values.

4.4 Fouling Resistance Computation

In this project, fouling resistance is calculated by using the following equation:

$$R_f = A_{ht,nom} \cdot \left(\frac{1}{UA_f} - \frac{1}{UA_c} \right) \tag{4-6}$$

Where: R_f = fouling resistance $\left(\frac{m^2 - {}^oC}{W} \right)$ or $\left(\frac{hr - {}^oF - ft^2}{Btu} \right)$

UA_f = overall heat transfer coefficient in fouling condition

$\left(\frac{W}{{}^oC} \right)$ or $\left(\frac{Btu}{hr - {}^oF} \right)$

UA_c= overall heat transfer coefficient in clean condition

$\left(\frac{W}{{}^oC} \right)$ or $\left(\frac{Btu}{hr - {}^oF} \right)$

$A_{ht,nom}$ = nominal heat transfer area (m^2) or (ft^2)

The simplest way to compute fouling factor is to assume that the changes in convective resistances in both water and refrigerant are negligible. The computation of fouling resistance can be more complex if the convective resistances vary as fouling resistances increases. Another way to compute fouling resistance in BPHE, which will need further investigation, is to consider the changes of convective resistances. In this case, the UA values in clean and fouled condition would need to be computed by using different convective coefficient values. The equation to compute UA value is shown in Equation (4-7).

$$\frac{1}{UA_T} = \frac{1}{h_w \cdot A_w} + \frac{R_m}{A_{ht}} + \frac{R_f}{A_{ht}} + \frac{1}{h_R \cdot A_R} \tag{4-7}$$

Where: UA_T = total overall heat transfer coefficient $\left(\frac{W}{^oC}\right)$ or $\left(\frac{Btu}{hr-^oF}\right)$

h_w = convective coefficient in water side $\left(\frac{W}{m^2-^oC}\right)$ or $\left(\frac{Btu}{hr-ft^2-^oF}\right)$

R_m = thermal resistance due to surface in between the two working fluids

$\left(\frac{m^2-^oC}{W}\right)$ or $\left(\frac{hr-ft^2-^oF}{Btu}\right)$

R_f = fouling resistance on water side $\left(\frac{m^2-^oC}{W}\right)$ or $\left(\frac{hr-ft^2-^oF}{Btu}\right)$

h_R = convective coefficient in refrigerant side $\left(\frac{W}{m^2-^oC}\right)$ or $\left(\frac{Btu}{hr-ft^2-^oF}\right)$

A_{ht} = nominal heat transfer area (m^2) or (ft^2)

A Wilson plot procedure can be used to obtain h_w and h_R. In fact, convective resistance on water-side may change as mineral deposits grow and reduce the flow area. Fouling resistance also indirectly impacts the refrigerant convective resistance because as fouling resistance increases, the quality of the refrigerant at the outlet of the test BPHE is increased.

In this project, only Equation (4-6) used to compute fouling factors. These fouling resistances can be thought as “effective fouling factors” as fouling may affect the convective resistances in the tested BPHE. The computed fouling resistance in equation (4-6) does not solely quantify mineral deposit, but also may include the change of convective coefficients in both refrigerant and water side.

4.5 Calibration

As discussed above, fouling factor computation relies on the following measurements:

- Inlet water temperature (labeled as RTD-1 in Labview)
- Outlet water temperature (labeled as RTD-3 in Labview)
- Water mass flow rate (labeled as MFM-2 in Labview)
- Refrigerant pressure (labeled as PT2 in Labview)
- Inlet refrigerant temperature (labeled as RTD-4 in Labview)
- Outlet refrigerant temperature (labeled as RTD-5 in Labview)

The measurements of inlet and outlet refrigerant temperatures at the test BPHE are only used to compute LMTD with the two proposed non-AHRI computation methods that are described in Chapter 5. This section describes the calibration of each device and an overall check on the calibration. The next section describes the uncertainty analyses.

4.5.1 RTD Calibration

The accuracies of RTDs are very crucial to fouling resistance computations. The effect of RTD accuracy on fouling resistance is explained in design uncertainty analysis section. Before the initial use and every beginning of a new test, the RTDs installed in the cooling tower loop are calibrated using five temperature points to verify the accuracy of the instruments. The RTDs are specified to have "1/10 DIN" accuracy, which means they have nominal resistance of 100 Ω ± 0.012Ω at 0 °C. The relation between resistance and temperature is given by the Callendar-Van Dusen equation:

$$R_t = R_0 (1 + A*t + B*t^2) \text{ for } t \geq 0°C \quad (4\text{-}8)$$

Where: R_0 = nominal resistance at 0 °C

A = 0.03908 per DIN EN 60751

$B = -5.77 \cdot 10^{-7}$ per DIN EN 60751

The nominal resistance does not include the resistance caused by the wire length; therefore; re-calibration is needed to adjust the R_0 value in the Labview program. The RTDs are calibrated using a constant temperature chiller. Users can adjust the temperature of the water bath in 0.1°C (0.18°F) increments. The RTDs were inserted in the calibration bath that was already set to 0°C (32°F). After the bath temperature stabilized, the value of R_0 was adjusted until the temperature read by each RTD was 0.002°C (32.004°F). RTD that is located at the inlet of the test BPHE (labeled as RTD-1 in Labview program) was calibrated in the temperature range of 28.3 – 30.6°C (82.94 – 87.08°F) and the outlet RTD (labeled as RTD-3 in Labview program) was calibrated in the temperature range of 31.1 – 35.0 °C (87.98-95°F). The bath temperature was gradually increased in 1°C (1.8°F) temperature increment. Every time the temperature was increased, the temperatures are allowed to stabilize before readings taken by the DAQ were finalized. RTDs that measure the inlet refrigerant temperature (labeled as RTD-4 in Labview) and outlet refrigerant temperature (labeled as RTD-5 in Labview) of the test BPHE have only been calibrated once at the beginning of the project. Both RTD were calibrated in the temperature range 20.1°C – 50°C. RTD-1 was calibrated to ± 0.05°C (0.09°F) and RTD-3 was calibrated to ± 0.05°C (0.09°F). RTD-4 and RTD-5 were calibrated to ± 0.014°C (0.025°F) and ± 0.011°C (0.02°F) respectively. In the future, calibrations for RTD-4 and RTD-5 are required because these temperatures are used in the proposed LMTD calculation as discussed in the next chapter.

4.5.2 Pressure Transducer Calibration

The pressure transducer was calibrated by the manufacturer. According to the calibration certification, the transducer is calibrated by applying pressure from 2.20 to 251.64 psi. The measured voltage output is read between 0.15 to 5.13 Vdc. The accuracy of the pressure transducer is ±0.13% F.S or ±0.325 psi at 1032.1 kPa (149.7psi)

4.5.3 Water Mass Flow Meter Calibration

The water mass flow meter by Micro Motion, Inc. was calibrated by manufacturer using 3 calibration points: 5.67 kg/min (12.47 lb/min), 28.35 kg/min (62.37 lb/min), and 56.7 kg/min (142.74 lb/min). The associated errors are 0.034, 0.051, and 0.005%.

Another calibration was performed in the lab by using a tank that has already volume marks on the side of the tank and a stopwatch. The stopwatch and water pumps were started simultaneously and tank was filled to a predetermined point. Once the point was reached, the stopwatch and the water pumps were stopped. The mass flow rate was calculated by dividing the volume as indicated on the side of the tank with time. The result was compared with the flow rate that was shown by the flow meter transmitter. The specified accuracy of the mass flow rate by the manufacturer is ±0.03%.

4.6 Uncertainty Analysis

The experimental uncertainty was calculated by the method of propagation uncertainty in which uncertainty of each measurement is considered. Propagation uncertainty allows an inclusion of different instrument accuracies as described the following:

$$Y = f(X_1, X_2, X_3, ...) \tag{4-9}$$

where: Y = the variable that is computed from the n measured variables

X_n = the n^{th} measured variable

Uncertainty analysis for this project is done by using EES. EES implements a method for determining an uncertainty propagation as described in NIST Technical Note 1297 (Taylor, 1994). The uncertainty of the computed variable is estimated as follows:

$$U_Y = \sqrt{\sum_{i=1}^{n} \left(\frac{\partial Y}{\partial X_i} \right) U_x^2} \tag{4-10}$$

Where: U_Y = the uncertainty of the calculated variable

U_x = the uncertainty of the measured variable

$\frac{\partial Y}{\partial X_i}$ = the sensitivity coefficient of calculated variable with respect to variable x_i

This method of uncertainty analysis was applied in the design and experimental uncertainty analysis. The uncertainty of the fouling resistance is estimated by using Equation (4-12):

$$e_{R_f} = \pm \sqrt{\left(\frac{\partial R_f}{\partial T_{ExWT}} e_{T_{ExWT}} \right)^2 + \left(\frac{\partial R_f}{\partial T_{EWT}} e_{T_{EWT}} \right)^2 + \left(\frac{\partial R_f}{\partial \dot{m}_{water}} e_{m_{water}} \right)^2 + \left(\frac{\partial R_f}{\partial P_{sat}} e_{P_{sat}} \right)^2} \tag{4-11}$$

Where: $\frac{\partial R_f}{\partial T_{ExWT}}$ = sensitivity coefficient due to exiting water temperature

$\frac{\partial R_f}{\partial T_{EWT}}$ = sensitivity coefficient due to entering water temperature

$\frac{\partial R_f}{\partial \dot{m}_{water}}$ = sensitivity coefficient due to water mass flow rate

$\frac{\partial R_f}{\partial P_{sat}}$ = sensitivity coefficient due to refrigerant saturation pressure

$e_{T_{ExWT}}$ = accuracy of an RTD (°C) or (°F)

$e_{m_{water}}$ = accuracy of a mass flow meter (kg/s) or (lb/min)

$e_{P_{sat}}$ = accuracy of a pressure transducer (kPa) or (psi)

$e_{T_{EWT}}$ = accuracy of an RTD (°C) or (°F)

Each of the accuracies given above and those computed below are given at the 95% confidence level.

4.6.1 Sample Uncertainty Analysis

In this section the uncertainty analysis is illustrated with sample values of measured variables. A BPHE condenser model was developed in EES to perform uncertainty analysis. The model's inputs are:

- Inlet water temperature
- Outlet water temperature in clean condition
- Outlet water temperature in fouled condition
- Water flow rate
- Refrigerant flow rate
- Saturation pressure
- Entering refrigerant temperature to the BPHE model

The model computes LMTD, UA, and fouling resistance values using Equation (4-1), (4-3), and (4-4). Sample measurement values were input for test condenser model BPHE-A2 with low heat flux test conditions:

- Inlet water temperature to the test BPHE = 29.44°C (85°F),
- Water mass flow rate = 17.67 liter/min (4.67 gpm)
- Refrigerant inlet temperature = 76.67 °C (170°F),
- Refrigerant mass flow rate = 1.59 kg/min (3.5 lb/min)
- Saturation pressure = 1032.1 kPa (149.7psi).

From the saturation pressure, the condensing refrigerant temperature is obtained from the R134a property table. The clean outlet water temperature is 34.06°C (93.3°F) as specified by the BPHE manufacturer for model BPHE-A2 (GEA, 2010) under the specified both refrigerant and water conditions. The nominal area of heat transfer is 0.427 m^2 (4.6 ft^2) for this particular model. Table 4-2 summarizes the accuracies of other devices that are used in the sample uncertainty analysis.

Table 4-2: List of Measuring Device Uncertainty

Instrument	Relative Uncertainty	Absolute Uncertainty
Refrigerant mass flow meter (MFM-3)	±0.10%	
Water mass flow meter (MFM-2)	±0.03%	
Ref. inlet temperature (RTD-4)		±0.1℃ (0.2 ℉) *
Ref. outlet temperature (RTD-5)		±0.1℃ (0.2 ℉) *
Water inlet temperature (RTD-1)		± 0.05℃ (0.09 ℉)
Water outlet temperature (RTD-3)		± 0.05℃ (0.09 ℉)
Refrigerant pressure transducer (PT-2)	±0.13%	

* Not yet recalibrated to give ±0.05°C (0.09°F) accuracy, but this is recommended

The Effect of RTD Accuracy on Fouling Resistance Uncertainty

Using the EES model, the RTD accuracy effect on fouling resistance values was studied. To simulate fouling, the outlet water temperature in fouled condition was reduced by 0.72°C (1.3°F) from the clean outlet water temperature. The accuracies of other instruments are set according to Table 4-3 and the accuracy of the four RTDs is varied from ±0.11°C (0.2°F) to ±0.05°C (0.09°F). Table 4-3 summarizes the results:

Table 4-3: Effect of RTD accuracy on fouling factor uncertainty

RTD Accuracy, ℃ (℉)	% Rf Uncertainty
0.11 (0.2)	22.76
0.056 (0.1)	11.38
0.05 (0.09)	10.25

The uncertainty of fouling resistance is reduced from 22.76% to 10.25% when accuracy RTD is improved from ±0.11°C (0.2°F) to ± 0.05°C (0.09°F). From the analysis, it is necessary to implement RTDs that have good accuracy in the system to accurately measure a small water temperature decrease at the outlet of the BPHE.

Pressure Measurement Contribution to Fouling Resistance Uncertainty

The contribution of saturation pressure accuracy in the uncertainty of overall heat transfer coefficient computation is evaluated. The accuracy of ±0.05°C (0.09°F) for RTDs is used in the evaluation. The other device uncertainty is listed in Table 4-2. The conditions of the refrigerant and water are set to the low heat flux test condition, while the outlet water temperature is decreased from 34.06°C (93.3°F) in clean condition to 33.86°C (92.94°F) in fouled condition. The uncertainty of the overall heat transfer coefficient is calculated as follows:

$$e_{UA} = \pm\sqrt{\left(\frac{\partial UA}{\partial T_{ExWT}} e_{T_{ExWT}}\right)^2 + \left(\frac{\partial UA}{\partial T_{EWT}} e_{T_{EWT}}\right)^2 + \left(\frac{\partial UA}{\partial P_{sat}} e_{P_{sat}}\right)^2 + \left(\frac{\partial UA}{\partial \dot{m}_w} e_{\dot{m}_w}\right)^2} \quad (4\text{-}12)$$

Where: $\frac{\partial UA}{\partial T_{ExWT}}$ = sensitivity coefficient due to exiting water temperature

$\frac{\partial UA}{\partial T_{EWT}}$ = sensitivity coefficient due to entering water temperature

$\frac{\partial UA}{\partial \dot{m}_w}$ = sensitivity coefficient due to water mass flow rate

$\frac{\partial UA}{\partial P_{sat}}$ = sensitivity coefficient due to refrigerant saturation pressure

$e_{T_{ExWT}}$ = accuracy of an RTD (°C) or (°F)

$e_{m_{water}}$ = accuracy of a mass flow meter (kg/s) or (lb/min)

$e_{P_{sat}}$ = accuracy of a pressure transducer (kPa) or (psi)

$e_{T_{EWT}}$ = accuracy of an RTD (°C) or (°F)

The sensitivity coefficients due to the measured variables were obtained from the EES model by inserting the test conditions as specified above. The resulting UA value in fouled condition is 638.91±5.41 W/°C (1203±7.348 Btu/hr-°F). The percentage of contribution from the uncertainty of the measured variable in the total uncertainty is calculated by using Equation (4-12)

$$\%\text{ of uncertainty due to } T_{ExWT} = \frac{\left(\frac{\partial UA}{\partial T_{ExWT}} e_{T_{ExWT}}\right)^2}{(e_{UA})^2} = 66.03\%$$

$$\% \text{ of uncertainty due to } T_{EwT} = \frac{\left(\frac{\partial UA}{\partial T_{EWT}} e_{T_{EWT}}\right)^2}{(e_{UA})^2} = 24.07\%$$

$$\% \text{ of uncertainty due to } P_{sat} = \frac{\left(\frac{\partial UA}{\partial P_{sat}} e_{P_{sat}}\right)^2}{(e_{UA})^2} = 9.87\%$$

$$\% \text{ of uncertainty due to } \dot{m}_{water} = \frac{\left(\frac{\partial UA}{\partial \dot{m}_w} e_{\dot{m}_w}\right)^2}{(e_{UA})^2} = 0.03\%$$

The percentages show that with an RTD accuracy of ± 0.05°C (0.09°F), the uncertainty of the overall heat transfer coefficient is mainly affected by the measurement of outlet water temperature, followed by the measurement of inlet water temperature, refrigerant saturation pressure, and water flow rate.

The Effect of the Water Outlet Temperature Reduction due to Fouling on Fouling Resistance Uncertainty

As previously mentioned, the water temperature at the outlet of the BPHE is expected to decrease as fouling resistance increases. The effect of outlet water temperature reduction on fouling resistance uncertainty is studied. To simulate fouling, the outlet water temperature is varied from 34.06 °C (93.3°F) to 32.22 °C (90.0°F), while the other conditions are kept constant. The accuracy of each measuring device used in this analysis is listed in Table 4-3. Fig.4-5 shows the predicted of simulated fouling resistance and the uncertainty of the corresponded fouling resistance in respect to the change of exit water temperature between clean and fouled condition ($T_{ExWT,c} - T_{ExWT,f}$).

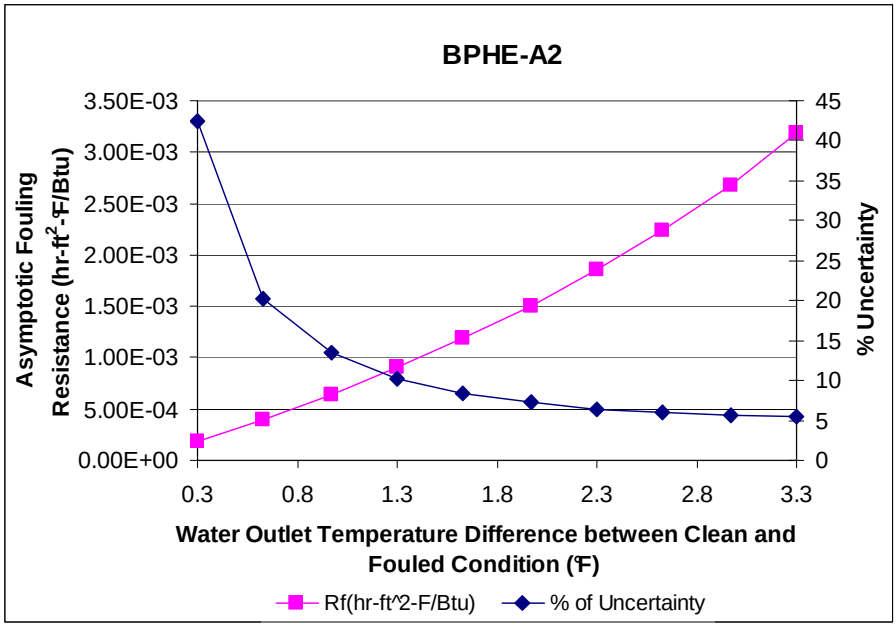

Fig 4-5: Predicted Fouling Resistance vs. Change of Outlet Water Temperature

It can be seen from the plot that the uncertainty of fouling resistance varies from 42.5% to 5.38% depending on the temperature difference between the exiting water temperature in clean and fouled conditions. The uncertainty of fouling resistance decreases as the difference of exiting water temperature between clean and fouled conditions increases. Fouling resistance of 4.4 x 10^{-5} m^2 • °C/W (2.5 x 10^{-4} hr • ft^2 F/Btu), as specified by TEMA, occurs when the outlet water temperature is decreased by 0.22°C (0.40°F) from the clean condition. The corresponded uncertainty fouling resistance is ± 35.7%.

4.6.2 Uncertainty Analysis for first three experiments

The purpose of an experimental uncertainty analysis is to find the uncertainty of the experimentally determined fouling resistance. The experimental uncertainty analysis was performed by substituting the averaged measurements, which obtained by previously-mentioned data collection procedure, into the input parameters. The data

collection was taken under the low heat flux test condition as described in Section 4.1. This analysis utilizes the same EES model. The reference clean UA values that have been corrected using one of the three methods mentioned in Section 4.2 are set as input parameters to calculate fouling resistance values. The following uncertainty of each device needs to be inserted into the model in order to evaluate the uncertainty of fouling resistance:

Table 4-4: Uncertainty of Measurement Device

Instrument	Relative Uncertainty	Absolute Uncertainty
Refrigerant mass flow meter (MFM-3)	0.10%	
Water mass flow meter (MFM-2)	0.03%	
Ref. inlet temperature (RTD-4)		±0.1℃ (0.2 ℉)
Ref. outlet temperature (RTD-5)		±0.1℃ (0.2 ℉)
Water inlet temperature (RTD-1)		±0.06℃ (0.11 ℉) (1) ±0.05℃ (0.09℉) (2)
Water outlet temperature (RTD-3)		±0.08℃ (0.144 ℉) (1) ±0.05℃ (0.09℉) (2)
Refrigerant pressure transducer (PT-2)	0.13%	

(1) RTD accuracy in the first two test BPHE (BPHE-A1 and BPHE-A2)
(2) RTD accuracy in the third test BPHE (BPHE-A3)

Test BPHE model BPHE-A1 and BPHE-A2 are tested based on the RTD accuracy ± 0.06°C for RTD-1 and ±0.08°C for RTD-3. RTD-1 and RTD-3 then were calibrated to ±0.05°C before BPHE-A3 was tested. RTD-4 and RTD-5 need to be recalibrated in the future to ensure good accuracy. The computed parameters are fouling resistance, LMTD and UA values in fouled conditions. Table 4-5 summarizes the uncertainty of the asymptotic fouling resistance for the tested BPHE.

Table 4-5: Uncertainty of Asymptotic Fouling Resistance

Model	($T_{ExWT, clean}$ - $T_{ExWT,fouled}$), ℉ (℃)	Asymptotic Fouling Resistance, hr-℉-ft^2/Btu (m^2-℃/W)	Uncertainty (%)
BPHE-A1	1.74 (0.97)	0.001991 (0.000351)	13.25
BPHE-A2	0.19(0.11)	0.00011864 (0.0000209)	64.09
BPHE-A3	0.17(0.094)	0.00019842(0.000035)	26.56

As seen in Table 4-5 the uncertainty of asymptotic fouling resistance is reduced significantly if the difference of exiting water temperature in clean and fouled condition increases.

4.7 Heat Balance Check

A further check on the uncertainty analysis involves performing a heat balance on the cooling tower loop, replacing the BPHE with an in-line heater. The heat input of the 1500 W in-line heater can be accurately measured with a watt transducer. The cooling tower loop was charged with city water. The water temperature at the inlet of the heater and the flow rate were set at constant conditions. The water was set to 3.21 kg/min (7.06 lb/min) and the water temperature at the inlet of the heater was maintained at 15.6°C (60°F) by setting constant 115 V voltage to the heater. Once the condition stabilizes, readings were taken for 10 minutes with sampling rate of 60 seconds. Average values were taken from the data set and then used to compute heat transfer rate using the following equation:

$$\dot{q} = \dot{m}_{water} \cdot c_p \cdot (T_{ExWT} - T_{EwT}) \tag{4-13}$$

Where: $\dot{q}$ = heat transfer rate (kW) or (Btu/min)

$\dot{m}_{water}$ = mass flow rate (kg/s) or (lb/min)

c_p = specific heat of water (kJ/kg-K) or (Btu/lb-°F)

T_{ExWT} = Exiting Fluid Temperature (°C) or (°F)

T_{EwT} = Entering Fluid Temperature (°C) or (°F)

The amount of heat transfer that was calculated using Equation (4-9) was verified by using a watt transducer by Ohio Semitronics model PC5-118D. The transducer has an output signal of 0-10 V for range of 0-1500 W witch accuracy ±12.5 W. Fig. 4-6 shows the connection diagram of the watt transducer.

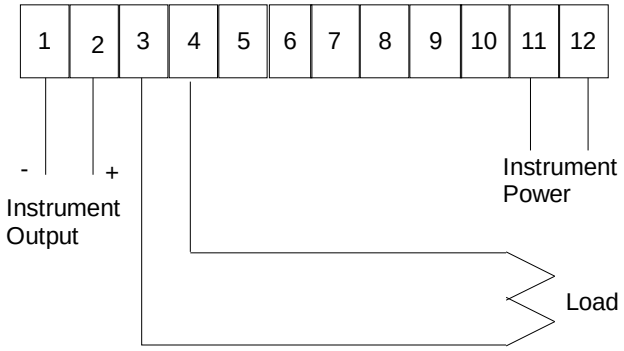

Fig. 4-6: Watt transducer connection diagram

The total of the heat transfer rate was compared with the power output by the in-line heater. The same procedure and conditions were applied to the second heat balance check, except the flow rate was set to 48.84 lb/min. The results were summarized in Table 4-6.

Table 4-6: Summary of heat balance check results

Run	Water Flow Rate (lb/min)	Temp. Difference between outlet and inlet (F)	Heat Transfer Rate =m*cp*ΔT (Btu/min)	Heat Transfer Rate (kW)	Measured Power by Watt Transducer (kW)	Difference between calculated and measured power (kW)
1	48.835	1.619	79.064±4.88	1.390±0.086	1.470±0.0074	0.08
2	7.063	11.586	81.832±0.706	1.439±0.012	1.465±0.0073	0.026

To have 95% level confidence, the following expression must be correct:

$$\left|Q_{measured} - Q_{calculated}\right| \le 2\sqrt{e_{Qmeasured}{}^2 + e_{Qcalculated}{}^2} \qquad (4\text{-}14)$$

Where: $Q_{measured}$ = measured heat transfer by a watt transducer (kW) or (Btu/min)

$Q_{calculated}$ = computed heat transfer (kW) or (Btu/min)

$e_{Qmeasured}$ = errors due to a watt transducer

$e_{Qcalculated}$ = errors due to temperature and flow rate measurements

For the first run:

$$0.08 \le 2\sqrt{0.086^2 + 0.0074^2}$$

$$0.08 \le 0.17$$

For the second run:

$$0.026 \le 2\sqrt{0.012^2 + 0.0073^2}$$

$$0.026 \le 0.028$$

Since the difference between the computed and measured heat transfer rate is less than the 2 standard deviation for both runs, the measurements are at 95% confidence level.

CHAPTER V

EXPERIMENTAL RESULTS

The first section of this chapter describes a detailed test procedure that explains the different evaporation processes during the tests. The latter section discusses the experimental results for the three BPHEs and followed by the two proposed LMTD calculation methods.

5.1 Test Procedure

There are at least two different evaporation phases occurring throughout the testing of a BPHE, during which the conditions of the facility need to be maintained close to the desired test conditions as described in Section 4.1 and the intensive 3 hour data collection periods need to be performed daily. High potential fouling water is obtained by the following evaporation processes:

1. Phase I: evaporation process without make-up water

   On the first day of phase I, 378.5 liters (100 gal.) of low fouling potential water from a batch tank is charged into the solution tank. At the initial start-up, the system is set to the desired test conditions except for the refrigerant saturation pressure and water mass flow rate. Then, the collection of clean UA values occurs to obtain data needed for one of the UA correction methods described in Section 4.3.2. After gathering the clean UA values, water mass flow rate to the cooling

tower needs to be adjusted to 1 gpm to give approximately 68.1 liters/ day (18 gallons/day) of evaporation rate. Then, the intensive data collection period can be started for day 1. The goal of phase I is to increase the concentration of salts in the water by evaporating low fouling potential water. Hence, in this phase, there is no make-up water introduced into the system. A sample of low fouling potential water from the batch tank needs to be sent to SWFAL lab for analysis in order to know the initial salt concentrations. From the initial salt concentrations and the amount of water in the system, salt concentrations in the cooling tower loop can be computed on the succeeding days. Once the calcium concentration, the "M" alkalinity, the electrical conductivity (EC), water temperature and the actual pH values are known, saturation pH can be computed to obtain LSI values. It is important to maintain pH water to ≥ 9.3 as specified in the original request-for proposals (RFP-1345) for high fouling potential water because the computed LSI values are very sensitive to the water pH level.

2. Phase II: evaporation process with make-up water

   This phase starts on the third day after approximately 136.3 liters (36 gal.) of water is evaporated. Low fouling make-up water is charged into the system at the end of the third day to compensate the water loss. In the following days, make-up water is charged into the cooling tower loop once in two days to bring back the amount of water in the loop to ± 378.5 liters (100 gal.). Every week, a water sample from the system is sent to the SWFAL lab to monitor the alkalinity and electrical conductivity level. The amount of evaporated water is recorded to

monitor the evaporation rate and to compute salt concentrations. Water pH is continuously maintained ≥ 9.3 throughout this process.

3. Phase III: minimal evaporation process and no make up water

   In phase III, the cooling tower fan is turned off to minimize the evaporation process and make-up water is no longer charged into the system. This phase was performed only in testing test condenser model BPHE-A1 to study the effect of evaporation process on the fouling curve.

5.2 Experimental Results

During the evaporation process, the water is evaporated, leaving behind the dissolved salts. The more water that is evaporated, the higher the ratio of salt concentration in the remaining water in the system. This ratio keeps increasing with the addition of make-up water because the low fouling potential water used as make-up water contains dissolved salts. LSI values can be computed by taking the difference between the actual measured water pH and the saturation pH, which is a function of calcium concentration, alkalinity, electrical conductivity, and temperature of the water. LSI values are computed throughout the tests of three test BPHEs and plotted in Fig. 5-1.

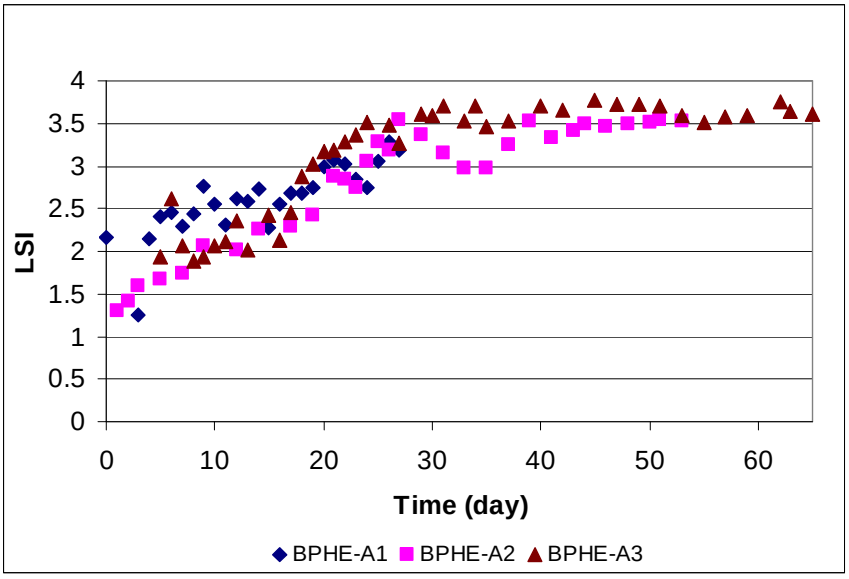

Fig. 5-1: Computed LSI vs. time during the tests

Phase I took the first two days of each test. Evaporation Phase II was begun on day 3 although at this point the LSI was still under 2 for BPHE-A1 and BPHE-A2. As expected, the LSI gradually increases as make-up water is added to replace the water loss. During Phase II, the water becomes saturated with the inversely-soluble salts such that precipitation is induced on the warmer surfaces in the system, i.e. the test BPHE. LSI ≈3, which indicates a strong scale formation in the system, is reached at day 20 ± 2 days.

Daily LSI values for each test cannot be set to be the same LSI values for all three tests because the evaporation rate for each test is slightly different even though the water flow rate to the cooling tower is set to 1 gal/min at the beginning of each new test. Evaporation rates depend on humidity and ambient temperature in the lab, which are not precisely controlled.

Overall Heat Transfer Coefficients

The overall heat transfer coefficients (UA) values are computed using water-side heat transfer rate and the LMTD equation specified by AHRI (Equation 4-3). Inlet water

temperature, water mass flow rate, and refrigerant saturation pressure are maintained as close as possible to the desired test conditions while the 3 hour intensive data collection periods are performed while the outlet water temperature is monitored closely. Fig. 5-2 shows the computed UA values for each day.

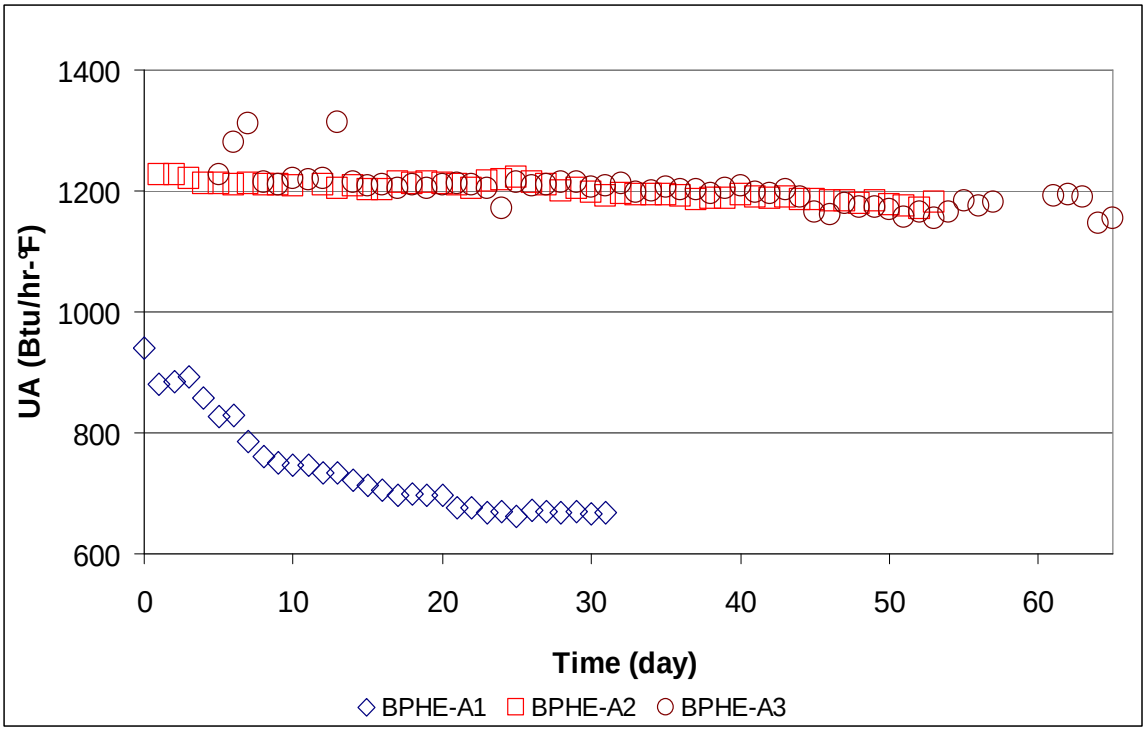

Fig. 5-2: Overall heat transfer coefficients vs. time for three test BPHEs

A decrease in overall heat transfer coefficient signifies an increase in fouling resistance in a heat exchanger. It is expected that UA value of a BPHE decreases as mineral deposits on heat exchange surface areas grow. As seen in Fig. 5-2, in clean condition, the UA value of BPHE-A1 is 182.5 W/°C (346 Btu/hr-°F) lower than BPHE-A2 and BPHE-A3. As a result, exiting water temperature for BPHE-A1 is 0.77°C (1.38°F) lower than that of the other two BPHEs. From inversed solubility theory, it might be inferred that fouling resistances in BPHE-A2 and BPHE-A3 should become higher because of the internal

surface temperature. To the contrary, the UA value of BPHE-A1 decreases more than the other heat exchangers. At the end of the tests, UA value in BPHE-A1 is reduced by 143.5 W/°C (272 Btu/hr-°F); whereas UA values for BPHE-A2 and BPHE-A3 are reduced by 23.21 W/°C (44 Btu/hr-°F) and 38.01 W/°C (72.06 Btu/hr-°F) respectively.

Fouling Resistance

At the end of an intensive data collection period, one of the methods of computing the reference UA value is applied in the data reduction process. The Hybrid method of computing the reference UA is used to compute fouling resistance for BPHE models BPHE-A1 and BPHE A-2 and the moving average method is used to compute fouling resistance for BPHE-A3. Although the hybrid method gives the best results in computing clean reference UA values, it cannot be used to evaluate fouling resistance for BPHE-A3 because the refrigerant mass flow rates deviated by ±0.1 lb/min during the clean UA collection period and during the first 4 days of intensive data collection periods. Fouling resistance for BPHE-A3 is then computed using the moving average method and by taking UA value that is computed for day 5 as the clean reference UA value. UA value for day 5 is selected to be the clean UA value because the measured refrigerant flow rate on that day matches with the desired refrigerant flow rate. Fig 5-3 shows the fouling curves for three test BPHEs in logarithmic scale.

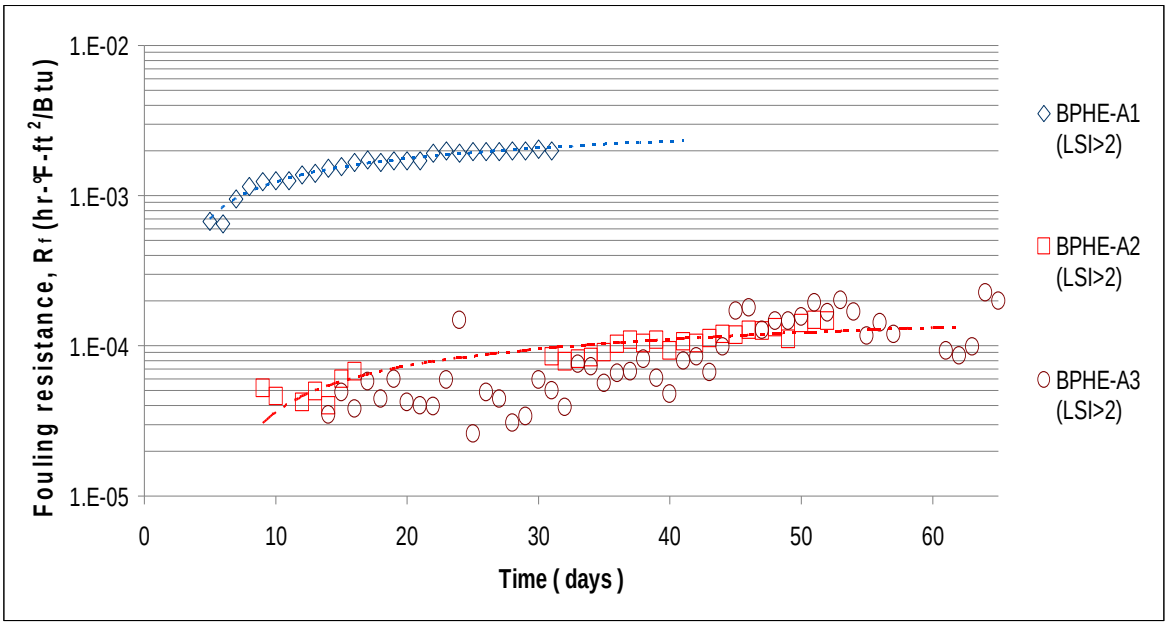

Fig. 5-3: Fouling curves for BPHE-A1, BPHE-A2, and BPHE-A3 in logarithmic scale

Fig. 5-4 shows three fouling curves in non-logarithmic scale to emphasize on the negative fouling resistances in the beginning of the tests for model BPHE-A2 and BPHE-A3.

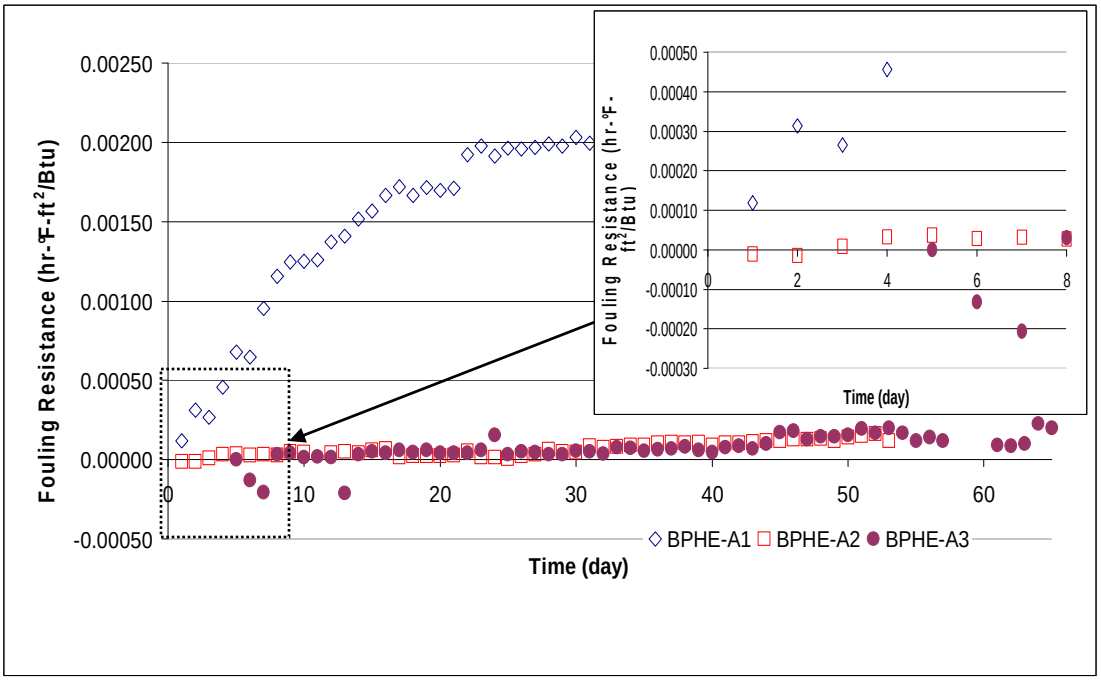

Fig. 5-4: Fouling curves for BPHE-A1, BPHE-A2, and BPHE-A3 in non-logarithmic scale

On the first two days of testing BPHE-A2 and BPHE-A3, the computed fouling resistances are negative. This time period is known as the initiation period, in which the conditions for fouling are being established. The decrease of fouling resistances during initiation period is presumed to be caused by the initial presence of deposits. As discussed in the literature review, as deposits penetrate the viscous sub-layer, the water flow characteristic becomes more turbulent and increases the convective heat transfer at the solid/liquid interface. As a result, the overall heat transfer coefficient increases, and the computed fouling resistance becomes negative. On day 10 of testing BPHE-A3, the computed fouling resistance was negative. On that day, the refrigerant mass flow rate was also 0.01kg/min (0.02 lb/min) higher than the desired flow rate; as a result, the exiting water temperature was increased by 0.33°C (0.6°F). An increase of exiting water temperature on day 10 does not indicate a deposit removal process, but simply an error in the measurements.

The tests are terminated when a fouling resistance has reached an asymptotic value. The asymptotic fouling resistance for BPHE-A1, BPHE-A2, and BPHE-A3 are 0.000351 m^2-°C/W (1.991x10^{-3} hr-°F-ft2/Btu) and 0.0000209 m^2-°C/W(1.186 x 10^{-4} hr-°F-ft2/Btu), and 0.000035 m^2-°C/W (1.984 x 10^{-4} hr-°F-ft2/Btu) respectively. Table 5-1 summarizes the overall plate geometries, test conditions, and the findings of the tests.

Table 5-1: Summary of results

	BPHE-A1		BPHE-A2		BPHE-A3	
Dimensions						
Overall Dimensions, in (cm)	5.1 W x 13.3 H x 1.6 D (12.95 W x 33.78 H x 4.06 D)		5.1 W x 13.3 H x 1.6 D (12.95 W x 33.78 H x 4.06 D)		5.1 W x 21 H x 1.1 D (12.95 W x 53.34 H x 2.79 D)	
Nominal Area, ft^2 (m^2)	4.6 (0.427)		4.6 (0.427)		3.9(0.362)	
Chevron Angles (°)	60		27		27	
Pitch, in (cm)	0.236 (0.60)		0.236 (0.60)		0.236 (0.60)	
Corrugation Depth, in (cm)	0.079 (0.20)		0.079 (0.20)		0.079 (0.20)	
Independent variables held constant	Clean initial conditions	Fouled cond.	Clean initial conditions	Fouled cond.	Clean initial conditions	Fouled cond.
Entering Water Temperature (EWT), °F (℃)	85 (29.44)	85 (29.44)	85 (29.44)	85 (29.44)	85 (2 9.44)	85 (29.44)
Sat. Condensing Temperature (SCT) ,°F (℃)	105 (40.56)	105 (40.56)	105 (40.56)	105 (40.56)	105 (40.56)	105 (40.56)
Degree of superheat for entering ref.,°F(℃)	65 (18.3)	65 (18.3)	65 (18.3)	65 (18.3)	65 (18.3)	6 5 (18.3)
Water flow rate (at 3 GPM/ton), GPM (liter/min)	4.67 (17.67)	4.67 (17.67)	4.67 (17.67)	4.67 (17.67)	4.67 (17.67)	4.67 (17.67)
Ref. mass flow rate, lb/min (kg/min)	3.5 (1.59)	3.5 (1.59)	3.5 (1.59)	3.5 (1.59)	3.5 (1.59)	3.5 (1.59)
Velocity in PHE, ft/s (m/s)	0.63 (0.19)	0.63 (0.19)	0.63 (0.19)	0.63 (0.19)	1.09 (0.33)	1.09 (0.33)
Dependent variables						
Heat Flux, Btu/hr-ft^2 (W/m^2)	3328.7 (10500)	2507.5 (7910)	4136.3 (13050)	4014.7 (12660)	4886.1 (15414)	4645 (14653)
Heat Transfer Rate (water-side measured), Btu/hr (W)	15312 (4490)	11534.4 (3380)	19027 (5580)	18467.8 (5410)	19056(5585)	18116(5309)
Leaving Water Temperature, °F(℃)	91.8 (33.22)	90.02 (32.23)	93.13 (33.96)	92.94 (3 3.86)	93.13 (33.96)	92.79 (33.77)
ΔT Water across PHE, °F(℃)	6.66 (3.7)	4.92 (2.73)	8.12 (4.51)	7.87 (4.37)	8.1 3 (4.52)	7.73(4.29)
ΔT water outlet between clean and fouled conditions, °F(℃)	0	1.74 (0.97)	0	0.19 (0.11)	0	0.40(0.22)
T ref. vapor entering to the PHE,°F(℃)	170 (76.67)	170 (76.67)	170 (76.67)	170 (76.67)	17 0 (76.67)	170 (76.67)
Leaving refrigerant quality [-]	Saturated liq.	0.44	Subcooled	Subcooled	Subcooled	Subcooled
Exiting Refrigerant Temperature, °F (℃)	105.6 (40.8 9)	108.32 (42.4)	88.06 (31.14)	89.59 (31.99)	85.54 (29.74)	85.47(29.71)
UA value (AHRI), Btu/hr-°F (W/℃)	941.45 (500)	668.84 (350)	1226.629 (650)	1182. 39 (620)	1226.94 (647.2)	1154.85 (609.2)
LMTD (AHRI), °F(℃)	16.26 (9.03)	17.25 (9.58)	15.51(8.62)	15.62 (8.68)	15.53 (8.63)	15.69 (8.72)
Asymptotic Fouling resistance (AHRI), hr-°F-ft^2/Btu (m^2-K/W)	0	0.001991 (0.000351)	0	0.00011864 (0.0000209)	0	0.00019842 (0.0000349)
UA value (Overall), Btu/hr-°F (W/℃)	349.99 (180)	250.48 (130)	832.54 (440)	724.08 (380)	1263.52 (666.5)	1235.61 (651.8)
LMTD (Overall), °F(℃)	43.75 (24.31)	46.05 (25.79)	22.85 (12.80)	25.51 (14.29)	15.34(8.52)	14.66(8.14)
Asymptotic Fouling resistance (Overall), hr-°F-ft^2/Btu (m^2-K/W)	0	0.001166 (0.000205)	0	0.0008802 (0.000155)	0	0.000103(0.00 00181)

Effect of internal geometry

Inside a BPHE, alternating plates are stacked together to form a network of contact points. These contact points support the two plates and increase the degree of turbulence. There are several plate parameters that can enhance heat transfer, such as chevron angle, corrugation depth, and flow distribution. Chevron angle is by far known as the key variable that controls heat transfer enhancement and fouling resistance of a BPHE (Thonon, et al., 1999).

There are two different plate chevron angles tested – 60° and 27°. Fig. 5-3 shows that when the three BPHEs are tested under the same test conditions, asymptotic fouling resistance in BPHE-A1 with a 60° of chevron angle is almost ten times more than those of the two BPHEs that have 27° of chevron angle. A similar result was found by Thonon et al. (1999). They found the asymptotic fouling resistance of a plate heat exchanger with a 60° chevron angle was almost ten times higher compared to the one with 30° chevron angle (note that Thonon et al. used the opposite convention for definition of chevron angle, but it is given here as the angle measured from horizontal axis). The reason for lower fouling resistance in the 27° chevron angle has not been fully understood because the physical nature of the flow pattern caused by internal surface geometry of these test BPHEs has not been fully investigated. A hypothesis is that a BPHE with a low chevron angle has higher degree of turbulence and therefore better removal of fouling deposits. This is shown from the UA values that are plotted in Fig. 5-2. The high UA value indicates a better heat transfer performance, which is typically induced by a turbulent flow.

Effect of Phase III of evaporation process

Phase III of evaporation rate was implemented only during testing of BPHE-A1. The purpose is to study the evaporation effect on fouling resistance.

Phase I took the first two days of the test. During Phase II, the fouling resistance gradually increases from day 3 to day 26. After day 26, the evaporation process entered Phase III because the desired water flow rate could not be achieved due to the increased amount of deposit in the system. Evaporation rates for BPHE-A1 are recorded and plotted in Fig. 5-5

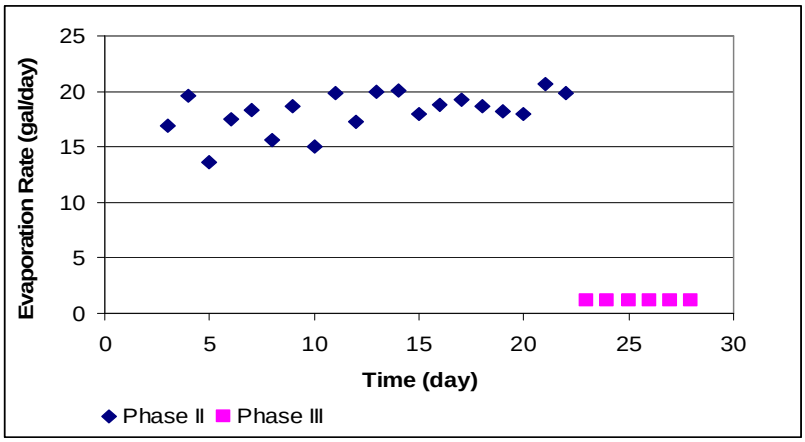

Fig. 5-5: Evaporation rate for BPHE-A1

The computed fouling resistances for BPHE-A1are plotted in Fig. 5-6.

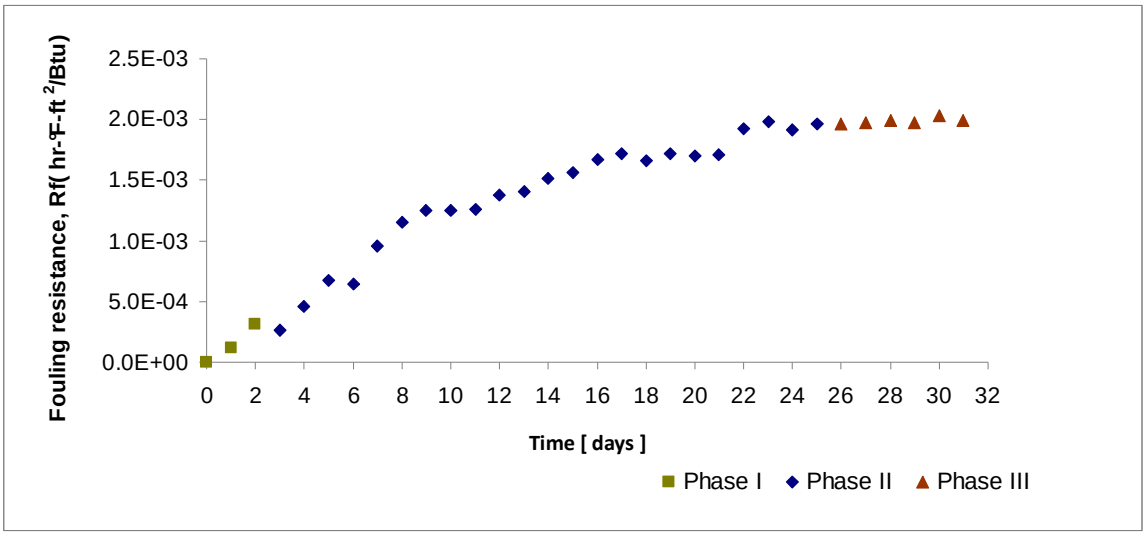

Fig. 5-6: Fouling curve for BPHE-A1

From day 26 until day 31, the cooling tower fan was turned off and make-up water was not charged into the system. In this phase, water LSI has already reached 3, which indicates a strong scale formation in the system. Yet, the fouling resistance did not increase when minimal evaporation process is enforced in the system. It is presumed that without an evaporation process and the addition of make-up water, the minerals in the system reached an equilibrium state. At this point, excess salts in the water have been completely precipitated. Hence, further precipitation did not happen in the system during Phase III. This occurrence implies that the formation of mineral deposits is indirectly dependent on the evaporation process.

Effect of removal process

At about 7:00 am, on day 11 of testing BPHE-A2, the test facility had to be shut down due to a heat-damaged polyethylene tank in the evaporator loop. A new tank was installed and the connecting piping was modified. The facility started again at about 4:00 pm the same day and the intensive data collection resumed on day 12. The fouling resistance gradually increased until day 16. At the end of day 16, the refrigerant loop was

charged with more refrigerant because the subset size to find the moving average set that matched with the desired refrigerant pressure was small. During the recharging process, the heat exchanger cooled off due to cessation of the refrigerant flow while the water flow remained on. This lasted for approximately 120 minutes. On day 17, the fouling resistance decreased as shown with an arrow in Fig. 5-7. On this day, the temperature difference across the test BPHE increased by 0.45°C (0.818°F) and the UA value also increased by 21.95 W/°C (41.6 Btu/hr-°F). The fouling resistance was increasing from day 18 until day 22. However, on day 23, another decrease of fouling resistance was observed. The temperature across BPHE increased by 0.026°C (0.046°F) and the UA value increased by 22.37 W/°C (42.4 Btu/hr-°F)

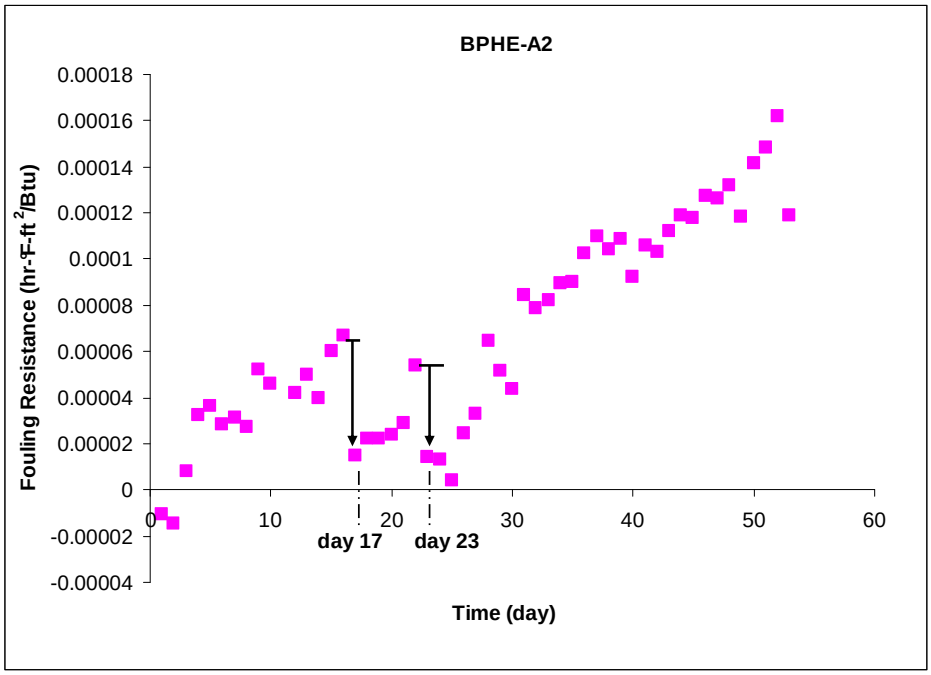

Fig. 5-7: Fouling curve for BPHE-A2

In the nature of the case, the exact reasons for these drops are unknown. At present, only hypothesis can be formed as to the cause(s). The first fouling resistance drop is suspected to be caused by the refrigerant charging period when the system had to

be stopped but the water pumps were left operating. At this period, it is assumed that deposits on the heat exchanger dissolved because the temperature of the heat exchange surface was reduced considerably after the refrigerant pump was stopped.

The second fouling resistance drop may have been caused by the presence of particles from the previous test since the system was not thoroughly cleaned before BPHE-A2 was installed in the system. The suspended solids from an earlier test might have been trapped in the crystal structures that are developed on the heat exchange surface area. The trapped particles induce fragile crystal structures; as a result the deposit on the heat exchange surface can be removed easily.

At the end of testing BPHE-A3, a "fouling destructive test" was performed. The same scenario that occurred on day 16 was simulated to re-create the same removal process. However, the pressure transducer at the inlet of BPHE broke down. So, the only way to measure the saturation pressure was by using the other transducer that was placed further from the inlet of the BPHE. The working pressure transducer is not reliable because it showed deviation of ±2.93 psi from the damaged pressure transducer. Since P_{sat} measurement is really critical in computing fouling resistance, no conclusions can be drawn from the "destructive test".

Removal process has been observed by a few researchers who performed fouling studies on plate heat exchangers (Bansal, 1993 and (Li & Webb, 2000). According to their studies, in the beginning of operation, crystals formed due to precipitation on the heat exchange surface are still small and thus the flow area has not been significantly reduced by the deposit. Removal process tends to occur after several days of operation because at this point the developed crystals are longer in shape and more fragile. In

addition, the presence of suspended solids can also be trapped in the crystal structure forming an even more fragile crystal structure. Due to the growth of deposits and the presence of suspended solids, the flow area is significantly reduced. A reduced flow area causes an increase in water velocity and hence shear stress (Bansal et al., 2001). The removal rate in the net deposition rate increases proportionally with the deposit removal rate.

Effect of velocity

Although water mass flow rate is kept constant at 17.6 kg/min (38.8 lb/min) in the three tests, water mass flow rates in the flow channel areas depend on the number of plates in a BPHE. Mass flow rate inside the channel can be computed by

$$\dot{M}_i = \frac{\dot{M}_T}{N_C} \tag{5-2}$$

Where: $\dot{M}_i$ = mass flow rate inside a channel (kg/min) or (lb/min)

$\dot{M}_T$ = total mass flow rate (kg/min) or (lb/min)

N_C = number of channels. Number of channels is equal to number of total plates divided by 2

The mass flow rate inside a channel for BPHE-A1 and BPHE-A2 are computed to be 2.513 kg/min (5.54 lb/min) and BPHE-A3 is equal to 4.40 kg/min (9.7 lb/min). As discussed in the literature review, that velocity is one of the important parameters that affect fouling in a BPHE. Velocity in a channel can be computed using Equation (5-3).

$$V = \frac{\dot{M}_i}{\rho \cdot A_c} \tag{5-3}$$

Where: V = velocity in a channel (m/s) or (ft/s)

$\dot{M}_i$ = mass flow rate inside a channel (kg/min) or (lb/min)

ρ = water density (kg/m^3) or (ft^3/min)

A_c = channel area. $A_c = b \cdot e$ (m^2) or (ft^2)

b = the width of the BPHE (m) or (ft)

e = corrugation depth (m) or (ft)

Velocity in BPHE-A1 and BPHE-A2 are computed to be 0.192 m/s (0.63 ft/s) and the velocity of BPHE-A3 is 0.332 m/s (1.09 ft/s). Thonon et al. (1995) and Bansal et al. (2001) mentioned that asymptotic fouling resistance is inversely proportional to the fluid velocity in a BPHE. Thus, it is expected that BPHE-A3 would have the lowest asymptotic fouling resistance value if this BPHE has an identical aspect ratio as the other two plates.

One of the objectives of this project is to study the effect of aspect ratio of BPHE on fouling resistance. To recall, aspect ratio is defined as the ratio of length to width of a BPHE. When two BPHEs with identical geometries except the width are tested with the same test conditions, according to Equation (5-2), the wider BPHE tends to foul more because the width of the BPHE is inversely proportional to fluid velocity in a BPHE. Low velocity results in high fouling resistance. The three test BPHEs that have been tested have the same width, so this theory can only be confirmed only after the next test BPHE-A4 is tested.

Effect of suspended solids

Suspended solids can come from different sources. Three possible sources are:

1) The undissolved minerals during the creation of low fouling potential water

2) Precipitation that occur in bulk of fluid

3) The removed particles from the deposits on the surface

Throughout the evaporation process, the cooling tower water becomes saturated with minerals. As a result, the water becomes unstable such that slight temperature or pH increase might cause precipitation anywhere in the system. Suspended solids are evidently present in the system. The structure of the deposit due to the suspended solids is flakier and can be removed easily; whereas the deposit due to precipitation is more solid and harder to be removed. Particulate fouling was found on the RTD probes to measure inlet and outlet water temperature as shown in Fig. 5-8.

Fig. 5-8: Deposit on a RTD probe that measures outlet water temperature

Suspended solids are also found in the post-cooler. Before starting the test for BPHE-A3, a gradual decline of water flow rate was noticed. It was found that the identified problem came from the post-cooler that had been operating for almost 9 months. The post cooler had never been cleaned since the first test was done. Severe fouling was observed in the inlet and outlet ports of the post-cooler. From observations, there were 2 types of fouling identified. On the top layer of deposit, the fouling appeared to be caused by particulate fouling as the structure of the deposit were flaky and less dense. The bottom layer of the deposit is harder to remove, which is a strong indication of precipitation fouling.

Theoretically, precipitation of inversely soluble minerals occurs at the warmest part of the system. The warmest part of the system is not the test condenser but the

heating elements of a 6 kW immersion heater that is used to maintain entering water temperature at 29.44°C (85°F) to the test BPHE. Therefore, in order to eliminate cross contamination of suspended solids between tests, a cleaning procedure using a de-scaler solution needs to be implemented at the end of each test in the future.

5.3 Proposed alternative approach of LMTD calculations

In this project, the refrigerant enters the test condenser at 18.3°C (65°F) above condensing temperature and exits at approximately 0°C (32°F) to 10.6°C (19°F) below the condensing temperature depending on the BPHE model. Hence, the AHRI LMTD calculation method, which utilizes only refrigerant condensation process, does not give entirely accurate representations of the actual performance of test BPHEs. It is also noticed that from the reference clean UA correlations, the correlations do not give the expected trends because as the water flow rate increases, the UA values decreases. Higher refrigerant saturation pressure and water flow rate should enhance the heat transfer rates and therefore increase the UA values. There are two alternative approaches for LMTD calculation proposed in this section. Both approaches include the effect of superheat and sub-cooling regions in a BPHE.

5.3.1 Overall LMTD calculation

The first approach is referred to here as the “overall LMTD” method. The overall LMTD approach utilizes the traditional definition of LMTD (Equation (4-2)). Overall LMTD is defined as:

$$LMTD_{overall} = \frac{(T_{ERT} - T_{ExWT}) - (T_{ExRT} - T_{EWT})}{\ln\left(\frac{T_{ERT} - T_{ExWT}}{T_{ExRT} - T_{EWT}}\right)} \quad (5\text{-}4)$$

Where: $LMTD_{overall}$ = Overall method of Log Mean Temperature Difference (°C) or (°F)

T_{ERT} = Entering Refrigerant Temperature (°C) or (°F)

T_{ExRT} = Exiting Refrigerant Temperature (°C) or (°F)

T_{ExWT} = Exiting Water Temperature (°C) or (°F)

T_{EwT} = Entering Water Temperature (°C) or (°F)

This LMTD equation takes both superheat and sub-cooling effects in a BPHE into consideration. In this approach, T_{sat} (P_{sat}) is not explicitly used in the calculation. However, it is noticed that when the refrigerant entering water temperature is set to a constant at 76.7°C (170°F) as stated in the low heat flux test conditions, the change of saturation pressure alters the exiting refrigerant temperature. As P_{sat} is increased from 1000.1 kPa (145.05 psi) to 1027.9 kPa(147.09 psi) while setting the water mass flow rate at 17.42 kg/min (38.4 lb/min) and maintaining the other test conditions, the outlet refrigerant temperature is reduced by 0.46°C (0.82°F). The reason behind this instance is that higher P_{sat} or T_{sat} causes less superheat as the inlet refrigerant temperature is always set at a constant temperature. In addition, higher T_{sat} creates more temperature difference between refrigerant and water, which drives higher heat transfer rate between the two fluids. As a result, for higher P_{sat}, the outlet refrigerant temperature is lowered by 0.46°C (0.82°F) and the exiting water temperature is increased by 0.33°C (0.6°F). The data that were collected for clean UA correlations method are used to compute the UA values using the overall LMTD method. The results are plotted and compared with the results

that are computed using the LMTD method defined by AHRI as shown in Fig. 5-9 to Fig. 5-11.

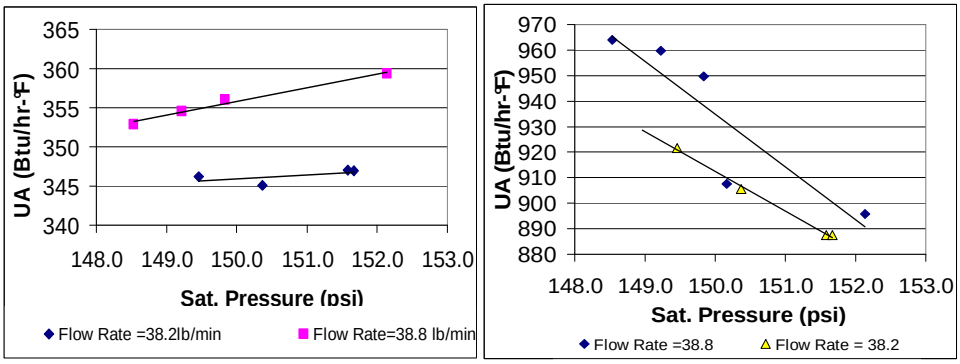

(a) **(b)**

Fig. 5-9 :**(a)** UA calculated with overall LMTD method vs. saturation pressure for BPHE A-1. **(b)** UA calculated with AHRI LMTD method vs. saturation pressure for BPHE-A1.

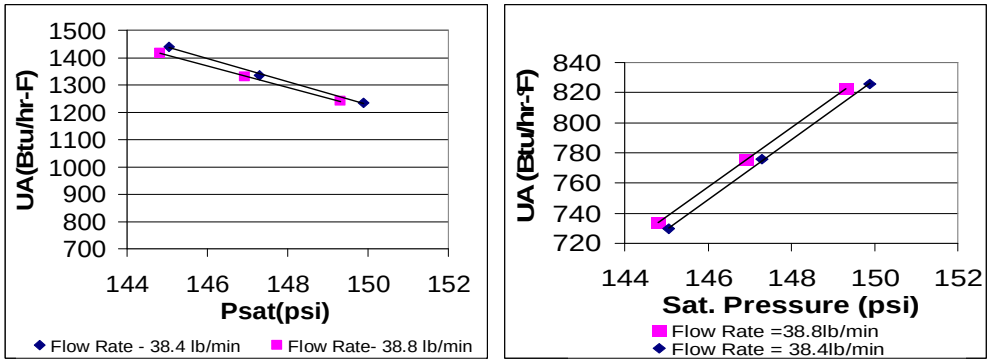

(a) **(b)**

Fig. 5-10:**(a)** UA calculated with overall LMTD method vs. saturation pressure for BPHE A-2. **(b)** UA calculated with AHRI LMTD method vs. saturation pressure for BPHE-A2.

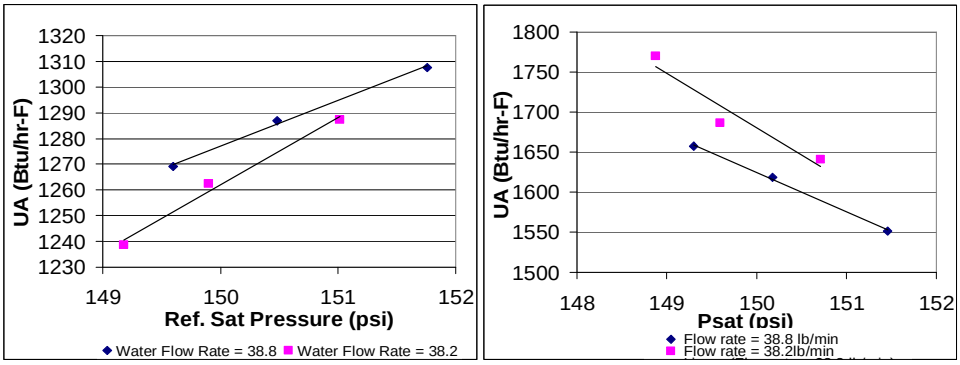

(a) **(b)**

Fig. 5-11 :**(a)** UA calculated with overall LMTD method vs. saturation pressure for BPHE A-3. **(b)** UA calculated with AHRI LMTD method vs. saturation pressure for BPHE-A3.

It can be seen from Fig. 5-9 (a) to Fig. 5-11 (a) that the computed UA values using overall LMTD follow the expected trends, which are increases of UA values as the water flow rates and refrigerant saturation pressure are increased. On the other hand, Fig. 5-9 (b) to Fig. 5-11(b) show unusual trends which are decreases in UA values when saturation pressure and water mass flow rates are increased. The computed UA values using overall LMTD are consistent with the fact that the overall heat transfer coefficients increase proportionally with water mass flow rates and refrigerant saturation pressures.

The collected data for all three test BPHEs are used to compute fouling resistances by using the overall LMTD method. Then, the results are plotted in Fig. 5-12, 5-13, and 5-14 and compared with fouling resistances that are calculated using an AHRI definition of LMTD (Equation 4-3).

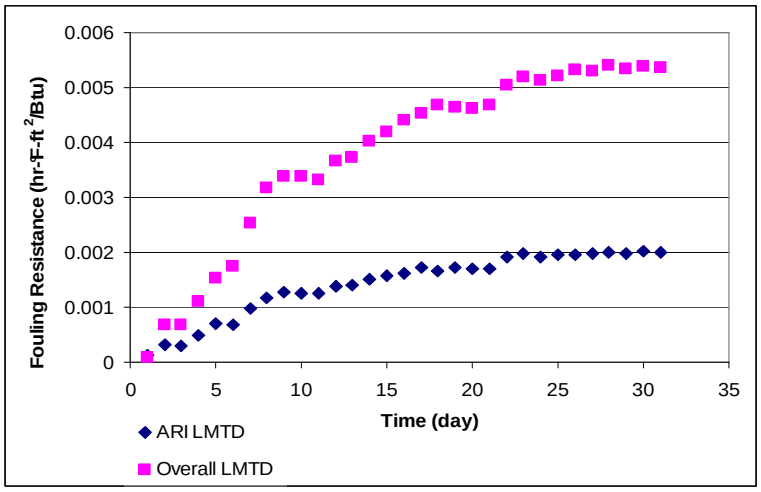

Fig. 5-12: Comparison of fouling curves computed using overall LMTD and AHRI LMTD approaches for BPHE-A1

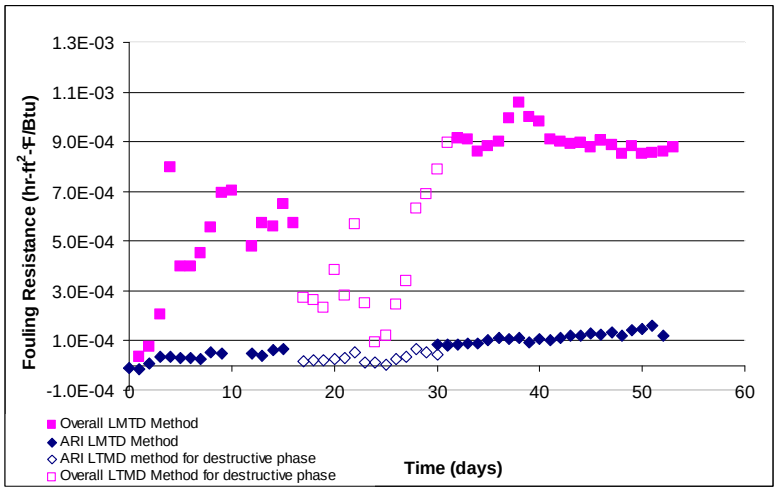

Fig. 5-13: Comparison of fouling curves computed using overall LMTD and AHRI LMTD approaches for BPHE-A2

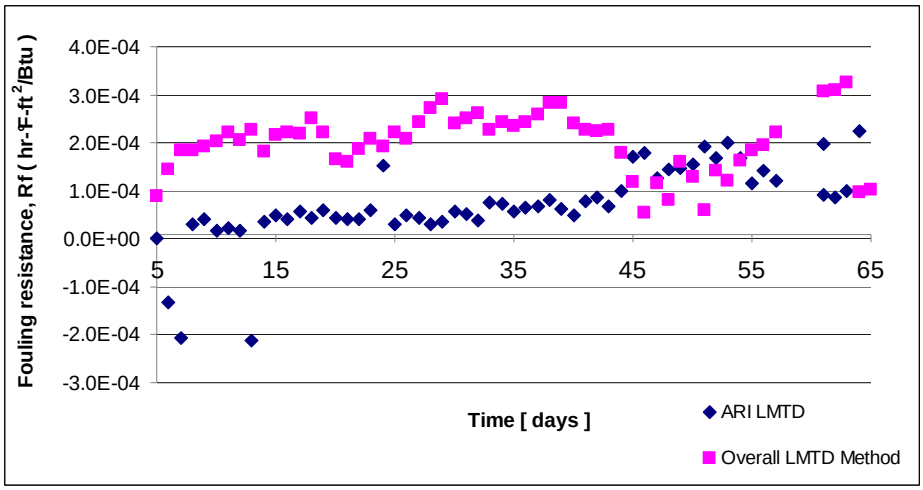

Fig. 5-14: Comparison of fouling curves computed using overall LMTD and AHRI LMTD approaches for BPHE-A3

As seen in Fig. 5-9 to Fig. 5-11 that asymptotic fouling resistances that are computed by overall LMTD method are approximately two to eight times higher than the fouling resistances computed by using AHRI LTMD calculation method. The overall LMTD method is expected to give higher fouling resistances because of higher LMTD values. The computed LMTD values now have larger temperature difference at the inlet and outlet of the BPHE since now the inlet and outlet refrigerant temperature are used in the calculations. Higher LMTD values result in lower overall heat transfer coefficients and higher fouling resistance values.

The general LMTD method is used to analyze a heat transfer rate of a heat exchanger using the entering and exiting fluid temperatures of both fluids and the heat transfer area. The analysis is subject to the assumptions that the variations of specific heats and the overall heat transfer coefficients of the 2 fluids are negligible. However, in this project, the refrigerants undergo phase changes from vapor to two-phase and eventually to liquid phase depending on the BPHE models. The overall heat transfer

coefficients for each refrigerant phase are different and may not be accurate if the variations are neglected.

5.3.2 3-Region LMTD calculation

The second approach is referred to here as the "3-region LMTD" method. This approach analyzes overall heat transfer individually that occur in the three refrigerant regions – superheat, condensation, and sub-cooling by utilizing the conventional LMTD definition (Equation (4-2)). The three regions are shown in Fig. 5-15.

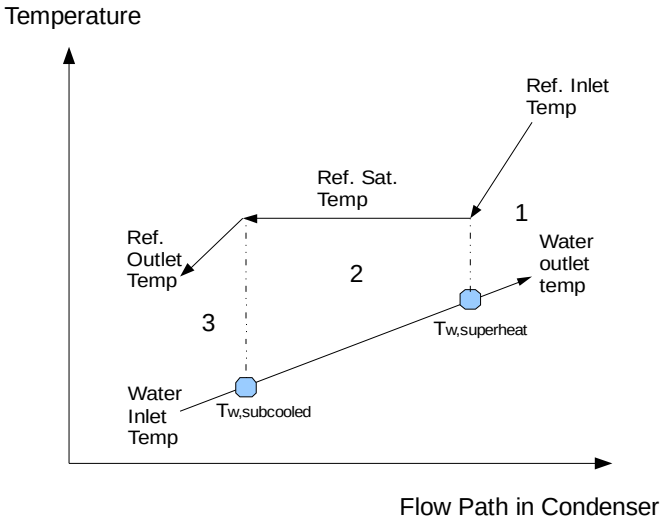

Fig. 5-15: Schematic of flow paths with different regions

Region 1 indicates where the condition of the refrigerant is in superheat condition, Region 2 indicates the region in which refrigerant occurs in two-phase stage and Region 3 indicates the condition of the refrigerant is in sub-cooling. The pressure and temperatures of the refrigerant and water are measured at the inlet and outlet of the test condenser. Thus, the corresponding water temperatures in which water is in contact with refrigerant transition from single phase to two-phase and vice versa have to be calculated (these temperatures are denoted by blue dots in Fig. 5-12). Since the refrigerant at the

inlet and outlet of the BPHE is in single phase, the enthalpy can be obtained from an R134a property table by using the pressure and temperature measurements. The intermediate water temperature for Region 1 can be calculated by using heat balance equation:

$$T_{w,superheat} = T_{ExWT} - \left(\frac{\dot{m}_{ref}(h_{in} - h_{sat,vap})}{\dot{m}_w c_p} \right) \tag{5-5}$$

Where: $T_{w,superheat}$ = entering water temperature to a superheat region (°C) or (°F)

T_{ExWT} = Exiting Water Temperature (°C) or (°F)

$\dot{m}_{ref}$ = refrigerant mass flow rate (kg/s) or (lb/min)

$\dot{m}_w$ = water mass flow rate (kg/s) or (lb/min)

c_p = specific heat of water (kJ/kg-K) or (Btu/lb-°F)

h_{in} = enthalpy entering refrigerant (kJ/kg) or (Btu/lb)

$h_{sat,vap}$ = enthalpy saturated vapor (kJ/kg) or (Btu/lb)

The amount of heat transfer on the water side due to the superheat refrigerant can be calculated in the following equation:

$$\dot{q}_{w,superheat} = \dot{m}_w c_p \left(T_{ExWT} - T_{w,superheat} \right) \tag{5-6}$$

Where: $\dot{q}_{w,superheat}$ = heat transfer rate in the superheat region (kW) or (Btu/min)

$\dot{m}_w$ = water mass flow rate (kg/s) or (lb/min)

c_p = specific heat of water (kJ/kg-K) or (Btu/lb-°F)

T_{ExWT} = Exiting Water Temperature (°C) or (°F)

$T_{w,superheat}$ = entering water temperature to a superheat region (°C) or (°F)

The LMTD of region 1 can be calculated as follows:

$$LMTD_{superheat} = \frac{(T_{ref,in} - T_{ExWT}) - (T_{ref,vap} - T_{w,superheat})}{\ln\left(\frac{T_{ref,in} - T_{ExWT}}{T_{ref,vap} - T_{w,superheat}}\right)} \quad (5\text{-}7)$$

Where: $LMTD_{superheat}$ = LMTD in superheat region (°C) or (°F)

$T_{ref,in}$ = refrigerant entering temperature (°C) or (°F)

$T_{ref,vap}$ = refrigerant saturated vapor temperature (°C) or (°F)

T_{ExWT} = Exiting Water Temperature (°C) or (°F)

$T_{w,superheat}$ = entering water temperature to a superheat region (°C) or (°F)

The overall heat transfer coefficient of the superheat region can be calculated as follows:

$$UA_{superheat} = \frac{\dot{q}_{w,superheat}}{LMTD_{superheat}} \quad (5\text{-}8)$$

Where: $UA_{superheat}$ =overall heat transfer coefficient for superheat region

$$\left(\frac{W}{^{o}C}\right) \text{ or } \left(\frac{Btu}{hr-^{o}F}\right)$$

$\dot{q}_{w,superheat}$ = heat transfer rate in the superheat region (kW) or (Btu/min)

$LMTD_{superheat}$ = LMTD in superheat region (°C) or (°F)

The two-phase and sub-cooled regions are analyzed the same way as the superheat region using Equation 5-5 to 5-8. The total overall heat transfer coefficients of each BPHE are computed by adding the computed UA values for each region (Sapali, 2009) . The

contribution to the overall heat transfer coefficient for each region to the total UA values is evaluated. This analysis is done by using the data collected for one of the UA correction methods explained in Section 4.3.2. Table 5-2 summarizes the results for the three test BPHEs.

Table 5-2: Summary of results for clean heat exchangers analyzed with 3-region LTMD approach

BPHE-A1

m_{ref}	m_{water}	P_{sat}	$T_{w,in}$	$T_{w,out}$	UA_{total}	$UA_{subcooled}$	$UA_{superheat}$	$UA_{condensing}$			
[lb/min]	[lb/min]	[psi]	[℉]	[℉]	[Btu/hr-℉]	[Btu/hr-℉]	[Btu/hr-℉]	[Btu/hr-℉]	% of $UA_{subcooled}$	% of $UA_{superheat}$	% of $UA_{condensing}$
3.5	38.2	150	85.0	91.6	951.8	3.4	92.0	856.5	0.4	9.7	90.0
3.5	38.1	150	85.0	91.6	929.6	1.1	91.3	837.3	0.1	9.8	90.1
3.5	38.1	152	85.1	91.7	900.1	3.1	89.2	807.8	0.3	9.9	89.7
3.5	38.1	152	85.0	91.7	903.1	3.2	89.6	810.3	0.4	9.9	89.7
3.5	38.8	149	85.2	91.7	981.9	1.8	93.8	886.3	0.2	9.6	90.3
3.5	38.9	149	85.4	91.9	976.2	3.1	93.3	879.8	0.3	9.6	90.1
3.5	38.8	150	85.4	91.9	956.5	0.2	92.5	863.8	0.0	9.7	90.3
3.5	38.8	150	85.0	91.5	928.8	0.7	91.0	837.0	0.1	9.8	90.1
3.5	38.8	152	85.1	91.7	892.4	4.0	88.4	800.0	0.4	9.9	89.6

BPHE-A2

m_{ref}	m_{water}	P_{sat}	$T_{w,in}$	$T_{w,out}$	UA_{total}	$UA_{subcooled}$	$UA_{superheat}$	$UA_{condensing}$			
[lb/min]	[lb/min]	[psi]	[℉]	[℉]	[Btu/hr-℉]	[Btu/hr-℉]	[Btu/hr-℉]	[Btu/hr-℉]	% of $UA_{subcooled}$	% of $UA_{superheat}$	% of $UA_{condensing}$
3.5	38.4	145	85.2	93.4	1270.0	100.4	106.3	1063.0	7.9	8.4	83.7
3.5	38.4	147	85.1	93.3	1204.0	119.5	101.7	982.5	9.9	8.4	81.6
3.5	38.4	150	85.1	93.3	1143.0	140.6	96.8	905.5	12.3	8.5	79.2
3.5	38.8	147	85.0	93.1	1203.0	120.8	101.3	980.8	10.0	8.4	81.5
3.5	38.9	145	85.0	93.1	1254.0	103.5	104.9	1046.0	8.3	8.4	83.4
3.5	38.8	149	85.0	93.1	1151.0	139.8	97.1	913.7	12.1	8.4	79.4

BPHE-A3

m_{ref}	m_{water}	P_{sat}	$T_{w,in}$	$T_{w,out}$	UA_{total}	$UA_{subcooled}$	$UA_{superheat}$	$UA_{condensing}$			
[lb/min]	[lb/min]	[psi]	[℉]	[℉]	[Btu/hr-℉]	[Btu/hr-℉]	[Btu/hr-℉]	[Btu/hr-℉]	% of $UA_{subcooled}$	% of $UA_{superheat}$	% of $UA_{condensing}$
3.5	38.8	149	85.0	95.0	1287.0	195.6	104.4	987.5	15.2	8.1	76.7
3.5	38.8	150	85.0	95.1	1273.0	202.5	103.3	966.8	15.9	8.1	75.9
3.5	38.8	152	85.0	95.1	1246.0	212.4	101.5	932.4	16.5	8.1	74.8
3.5	38.2	149	85.0	95.5	1291.0	175.8	106.3	1009	13.6	8.2	78.2
3.5	38.2	150	85.0	95.4	1298.0	192.1	106.1	999.7	14.9	8.2	77.0
3.5	38.2	151	85.0	95.4	1269.0	198.1	104.1	966.9	15.6	8.2	76.2

As seen from Table 5-2 that the tested BPHEs have differing sizes of superheat and sub-cooled regions. For instance, the fraction of UA value due to sub-cooling region to the total UA in BPHE-A1 is almost negligible; whereas for BPHE-A2 and BPHE-A3, the total UA values are contributed by 10 to 16% of UA values in sub-cooled region. From

the percentage distribution, it is expected that most of the heat transfer occur in the two-phase region and this would be a rationale for using the AHRI LMTD method.

Fouling resistances are computed by implementing the 3-region LMTD approach method. BPHE-A1 has been selected to obtain preliminary results in the fouling resistance computation using the proposed method. As seen in Table 5-2, the sub-cooling effect is negligible, so there are only two regions considered in the analysis of BPHE-A1. Fouling resistances are computed based on individual region.

The UA values are computed by substituting the measurements taken during the three hour intensive data collection period into Equation 5-6 to 5-8. As seen from the above equations that in order to compute fouling resistances, surface areas of each region need to be known. Thus, to compute for areas, refrigerant and water convective heat transfer coefficients need to be determined. However, since a Wilson plot procedure has never been performed in the tests, the appropriate correlations for convective coefficients for water and refrigerant have to be selected from a literature review.

Water convective heat transfer coefficient

Wanniarachchi et al. (1995b) presented a correlation in terms of internal geometric parameters of a BPHE. From their experimental data, they developed correlations that fit laminar, transition, and turbulent flow regions. The equations are listed as follows:

$$Nu_T = \left[Nu_1^3 + Nu_t^3\right]^{1/3} \mathrm{Pr}^{1/3} (\mu / \mu_w)^{0.17} \tag{5-9}$$

$$Nu_l = 3.65[\beta]^{-0.455}[\phi]^{0.661}\,\mathrm{Re}^{0.339} \tag{5-10}$$

$$Nu_t = 12.6\left[\beta\right]^{-1.142}[\phi]^{1-m}\,\mathrm{Re}^{m} \tag{5-11}$$

$$m = 0.646 + 0.0011[\beta] \tag{5-12}$$

Where: Nu_T = Total Nusselt number

Nu_l = Nusselt number for laminar region

Nu_t = Nusselt number for turbulent region

μ = dynamic viscosity $\left(\frac{kg}{m-s}\right)$ or $\left(\frac{lb}{ft-hr}\right)$

μ_w = dynamic viscosity at the wall $\left(\frac{kg}{m-s}\right)$ or $\left(\frac{lb}{ft-hr}\right)$

Re = Reynolds number

β = chevron angel (°)

ϕ = ratio of developed length to protracted length (enlargement factor)

The correlation is valid for $1 \le \mathrm{Re} \le 10^4$ and $20° \le \beta \le 62^\circ, \beta \rangle 62^\circ = 62^\circ$.

Refrigerant convective heat transfer coefficient

According to Webb, when refrigerant vapor enters BPHE, a small fraction of vapor is immediately condensated at the surface of heat exchanger. Thus, there are two components to be considered in the calculations of convective condensation of superheated vapor. Webb (1994) proposed a methodology to calculate heat transfer coefficient for convective condensation of superheated vapor for enhanced tubes and shell-side condensation. It is as follows:

$$h_{sup} = h_{fc}\frac{(T_b - T_{sat})}{(T_{sat} - T_w)} + h_{sat} \qquad (5\text{-}13)$$

Where: h_{sup} = condensation convective coefficient for superheated vapor

$\left(\frac{W}{m^2 - {}^\circ C}\right)$ or $\left(\frac{Btu}{hr - ft^2 - {}^\circ F}\right)$

T_{sat} = saturation temperature (°C) or (°F)

h_{fc} = heat transfer coefficient for forced convection to a gas

$\left(\frac{W}{m^2-^oC}\right)$ or $\left(\frac{Btu}{hr-ft^2-^oF}\right)$

T_b =superheated temperature (°C) or (°F)

T_w =wall temperature (°C) or (°F)

h_{sat} = convective condensation of saturated vapor $\left(\frac{W}{m^2-^oC}\right)$ or $\left(\frac{Btu}{hr-ft^2-^oF}\right)$

Convective condensation of saturation vapor (h_{sat}) and heat transfer coefficient for forced convection to a gas (h_{fc}) are computed using the following models:

1. Yan et al.(1999) proposed an experimental-based model of convective condensation of saturated vapor (h_{sat}), which is given as follows:

$$h_r = \left(\frac{k_L}{D_h}\right) 4.118 * \mathrm{Re}_{eq}^{0.4}\, \mathrm{Pr}_L^{1/3} \tag{5-14}$$

$$Re_{eq} = \frac{G\left(1 - X_m + X_m\left(\frac{\rho_L}{\rho_v}\right)^{1/2}\right)\cdot D_h}{\mu_L} \tag{5-15}$$

Where: h_r = refrigerant convective heat transfer coefficient $\left(\frac{W}{m^2-^oC}\right)$ or

$\left(\frac{Btu}{hr-ft^2-^oF}\right)$

k_L = conductivity of refrigerant in liquid phase $\left(\frac{W}{m-^oC}\right)$ or $\left(\frac{Btu}{ft-hr-^oF}\right)$

Re_{eq} = equivalent Reynolds number

Pr = Prandtl number

G = refrigerant mass flux (kg/m^2-s) or (lb/ft^2-s)

X_m = vapor quality between inlet and outlet of the BPHE

D_h (hydraulic diameter) $= \frac{2e}{\phi}$ (mm) or (inch)

μ_L = dynamic viscosity in liquid phase $\left(\frac{kg}{m-s}\right)$ or $\left(\frac{lb}{ft-hr}\right)$

2. h_{fc} is calculated by using equation for single phase convective R-134a in an condenser by Longo (2008).

$$h_{fc} = 0.2267\left(\frac{\lambda_G}{d_h}\right)\mathrm{Re}_G^{0.631}\,\mathrm{Pr}_G^{1/3} \tag{5-16}$$

Where: h_{fc} = heat transfer coefficient for forced convection to a gas flowing

$\left(\frac{W}{m^2-{}^oC}\right)$ or $\left(\frac{Btu}{hr-ft^2-{}^oF}\right)$

λ_G = thermal conductivity $\left(\frac{W}{m-{}^oC}\right)$ or $\left(\frac{Btu}{ft-hr-{}^oF}\right)$

Re_G = Reynolds number in vapor phase

Pr_G= Prandtl number in vapor phase

Once the convective coefficient of refrigerant and water are computed, the overall heat transfer coefficient for superheat region can be calculated using Equation 5-17.

$$\frac{1}{U_{superheat}} = \frac{1}{h_{w,sup}} + \frac{t}{k_{material}} + \frac{1}{h_{ref,sup}} \tag{5-17}$$

Where: $U_{superheat}$ = heat transfer coefficient in the superheat region

$$\left(\frac{W}{m^2-K}\right) \text{or} \left(\frac{Btu}{ft^2-hr-R}\right)$$

$h_{w,sup}$ = water convective heat transfer coefficient in superheat region

$$\left(\frac{W}{m^2-^oC}\right) \text{ or } \left(\frac{Btu}{hr-ft^2-^oF}\right)$$

t = plate wall thickness (m) or (ft)

$k_{material}$ = plate conductivity $\left(\frac{W}{m-K}\right)$ or $\left(\frac{Btu}{ft-hr-R}\right)$

$h_{ref,sup}$ = refrigerant heat transfer coefficient in superheat region

$$\left(\frac{W}{m^2-^oC}\right) \text{ or } \left(\frac{Btu}{hr-ft^2-^oF}\right)$$

When the heat transfer coefficient in the superheat region is determined, the surface area of superheat region is calculated by using the following equation:

$$A_{superheat} = \frac{\dot{m}_{ref}(h_{in} - h_{sat,vapor})}{U_{superheat} \cdot LMTD_{superheat}} \tag{5-18}$$

Where: $A_{superheat}$ = area of heat transfer in superheat region (m^2) or (ft^2)

$\dot{m}_{ref}$ = refrigerant mass flow rate (kg/min) or (lb/min)

h_{in} = enthalpy entering refrigerant (kJ/kg) or (Btu/lb)

$h_{sat,vap}$ = enthalpy saturated vapor (kJ/kg) or (Btu/lb)

$LMTD_{superheat}$ = LMTD in superheat region (°C) or (°F)

The computed area of superheat region is 0.24 cm^2 (2.6 x 10^{-4} ft^2), which is almost negligible. The area of the condensing region can then be determined by subtracting the

nominal heat transfer area with the superheat area. Since, there are separate clean and fouled overall coefficients in each region, fouling resistances in superheat and condensation regions are computed using Equation 5-19 and 5-20.

$$R_{f,superheat} = A_{superheat}\left(\frac{1}{UA_{f,superheat}} - \frac{1}{UA_{C,superheat}}\right) \tag{5-19}$$

Where: $R_{f,superheat}$ = fouling factor in superheat region $\left(\frac{m^2 - {}^oC}{W}\right)$ or $\left(\frac{hr - {}^oF - ft^2}{Btu}\right)$

$UA_{f,superheat}$ = overall heat transfer coefficient in fouling condition for superheat region $\left(\frac{W}{{}^oC}\right)$ or $\left(\frac{Btu}{hr - {}^oF}\right)$

$UA_{C,superheat}$ = overall heat transfer coefficient in clean condition for superheat region $\left(\frac{W}{{}^oC}\right)$ or $\left(\frac{Btu}{hr - {}^oF}\right)$

$A_{superheat}$ = nominal heat transfer area (m^2) or (ft^2)

$$R_{f,condensing} = A_{condensing}\left(\frac{1}{UA_{f,condensing}} - \frac{1}{UA_{C,condensing}}\right) \tag{5-20}$$

Where: $R_{f,condensing}$ = fouling factor in superheat region $\left(\frac{m^2 - {}^oC}{W}\right)$ or $\left(\frac{hr - {}^oF - ft^2}{Btu}\right)$

$UA_{f,condensing}$ = overall heat transfer coefficient in fouling condition for superheat region $\left(\frac{W}{{}^oC}\right)$ or $\left(\frac{Btu}{hr - {}^oF}\right)$

$UA_{C,condensing}$ = overall heat transfer coefficient in clean condition for superheat

region $\left(\frac{W}{^{o}C}\right)$ or $\left(\frac{Btu}{hr-^{o}F}\right)$

$A_{condensing}$ = nominal heat transfer area (m^2) or (ft^2)

Fouling resistances computed using 3-region LMTD approach and compared with the fouling resistances computed by the overall LMTD approach from previous section and the LMTD defined by AHRI in Fig. 5-16.

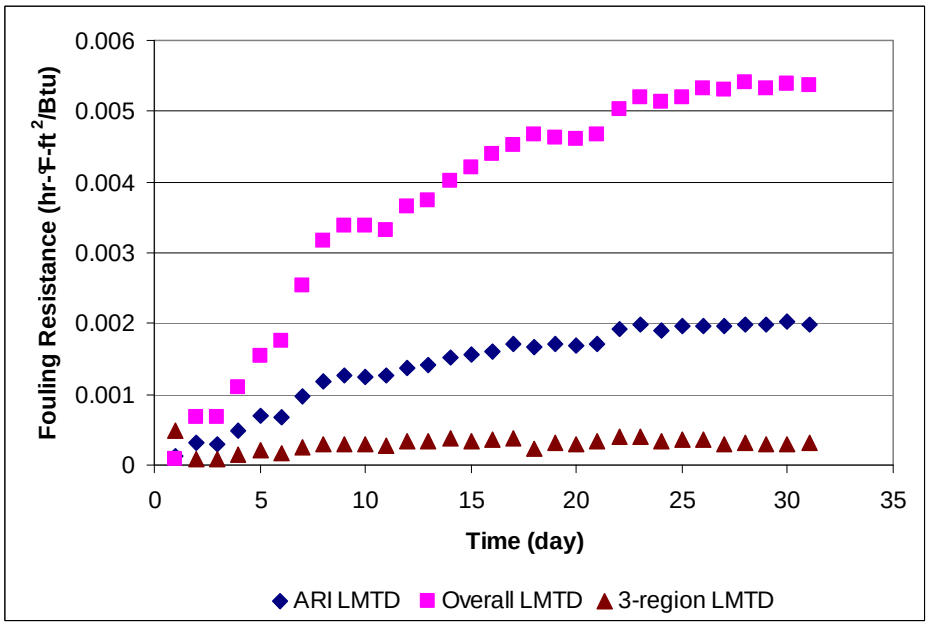

Fig. 5-16: Comparison of fouling curves computed using 3-region LTMD, overall LMTD and AHRI LMTD approaches for BPHE-A1

The 3-region LTMD calculation approach is derived from the conventional LTMD definition for each refrigerant phase that occurs inside BPHEs. As seen in Fig. 5-16 that asymptotic fouling curve that is computed by using 3-region LMTD method has the lowest asymptotic fouling. There are several assumptions made for the proposed approach:

- This approach assumes that the surface area of heat exchanger that is exposed to each refrigerant phase does not change throughout the fouling process.

- The computed refrigerant convective coefficient is a function of change of refrigerant quality in the condensation phase as seen in Equation 5-17. It is assumed that the quality of the refrigerant in clean and fouled conditions did not change. However, it was noticed that the exiting temperature of the refrigerant of the test BPHE changed in fouled condition.

The 3-region LMTD approach serves as a consistent method for comparing the actual performance of a BPHE in which one of the fluids inside the BPHE experience a phase change. This approach shows a distribution of heat load between each region. The limitation of the 3-region LTMD approach is in the use of correlations to determine the convective heat transfer coefficients for different refrigerant phases and water.

CHAPTER VI

CONCLUSIONS AND RECOMMENDATIONS

6.1 Conclusions

A test facility to measure fouling on the water side of a brazed plate type condenser in cooling tower application has been designed and constructed. This test facility was built because even though BPHEs are widely used in the refrigeration cycles used as water-cooled condensers, fouling characteristics of BPHE are not well understood. In addition, previous fouling studies of similar heat exchangers that have been conducted did not implement water that was representative of water that can be found in cooling towers in the United States. The presently conducted tests are considered as the accelerated tests because the tests do not implement blowdown (purging) processes as in actual operation of cooling towers.

A procedure to create high fouling potential water was developed by introducing an evaporation process in the system. The high fouling potential cooling tower water is created by cycling low fouling potential water through a cooling tower. As the water is evaporated, the concentrations of dissolved salts in the water increases until the water is supersaturated stage. Low fouling potential is used as baseline water and make-up water to replace the loss due to evaporation. Water pH needs to be monitored daily and

maintained at pH=9.3 for high fouling potential water as LSI depends greatly on the actual measured water pH. The facility was able to reach LSI values of 3.5 and higher.

A thorough uncertainty analysis was performed to study the effect of sensor error on the uncertainty of computed fouling resistances. Outlet water temperature and refrigerant pressure measurements were found to be the critical measurements as small drifts result in high errors in fouling resistances that are computed with the AHRI definition of LTMD. Three approaches to compensate for the drift in test conditions have been developed and implemented in the fouling resistance calculations.

Experiments of duration 31-53 days were performed to study fouling on water side brazed type of condensers in cooling tower application. Three BPHEs were tested – model BPHE-A1 and BPHE-A2 have the same aspect ratio but different chevron angle, and BPHE-A3 has different aspect ratio from BPHE-A1 and BPHE-A2 but the same chevron angle as BPHE-A2. The asymptotic fouling resistance for BPHE-A1 and BPHE-A2 are 0.000351 m^2-°C/W (1.991x10^{-3} hr-°F-ft2/Btu) and 0.0000209 m^2-°C/W(1.186 x 10^{-4} hr-°F-ft2/Btu) respectively. As of April 16, 2010, the test of BPHE-A3 is still in progress. The fouling resistance for BPHE-A3 has reached 0.00001735 m^2-°C/W (0.9854 x 10^{-4} hr-°F-ft2/Btu).

Although only 3 tests were performed (total test duration is 148 days), several preliminary conclusions are drawn from the tests:

- Internal geometry of BPHE is a crucial parameter that affects fouling resistance. The experimental data obtained in the tests show that BPHE with high chevron angle has an asymptotic fouling resistance 10 times higher than that of the BPHE with the low chevron angle.

- The test results are consistent with the hypothesis that velocity is another parameter that affects fouling in a BPHE because velocity affects the shear stress on heat exchanger surface. High water velocity induces higher shear stress that results in higher removal rates.
- Fouling resistance gradually increases during Phase II of evaporation process. In this phase, LSI of water continually increases from LSI ≈ 2 to LSI ≈ 3 as the water in the system is continually evaporated.
- The uncertainty of fouling resistance associated with initial RTD accuracy is undesirably large. Before the recalibration, the accuracies of RTD that measured entering and exiting water temperature to the test BPHE were ± 0.06°C (0.11°F) and ± 0.08°C (0.14°F) respectively. Before testing BPHE-A3, the RTDs were calibrated to ±0.05°C (0.09°F). The calibration is successful in reducing the uncertainty of asymptotic fouling resistance for BPHE-A3 can be reduced from 38.9 % to 26.6 %. Therefore, calibration of RTDs is recommended before a new test is started.
- The presence of suspended solids cannot be neglected as it affects the net deposited minerals on the heat exchange surface areas.

6.2 Recommendations

There are several suggestions to improve the facility performance:

- From the inverse solubility theory, the inversely soluble minerals are expected to precipitate in the warmest part of the system. In an actual cooling tower loop, the warmest part of the loop is in a condenser; however, in this test facility, the

warmest part of the loop is located in on the heating elements of an immersion heater that is used to maintain water temperature to the inlet test BPHE at 29.44°C (85°F). It was observed that there is a mineral deposit layer on the heating elements and on the wall of the tank where the heater is located. In order to prevent the precipitated minerals to settle and be deposited on the elements, a stirring mechanism should be introduced in the solution tank.

- To eliminate cross contamination of suspended solids between tests, a thorough cleaning procedure using a de-scaler solution needs to be implemented at the end of each test in the future.
- Recalibrate all the RTDs used in the system to ensure the accuracies. RTDs that are used to measure refrigerant temperatures have not been calibrated since the beginning of the project. All the RTDs need to be calibrated within ± 0.05°C (0.09°F).
- Fouling resistances that are computed by using LMTD equation specified by AHRI are very sensitive to the refrigerant saturation pressure drift. If the measured pressure drifts by 1 psi above the desired saturation pressure, the error in the computed fouling resistance is approximately 50%. Therefore, an accumulator or similar to dampen device should be installed to reduce the fluctuations in refrigerant pressure.

REFERENCES

Amjad, Z. (1988). Calcium sulfate dihydrate (Gypsum) scale formation on heat exchanger surfaces: the influence of the scale inhibitors. *Journal of Colloid and Interface Science, 123*(2), 523-536.

Andritsos, N., Kontopoulou, M., Karabelas, A. J., & Koutsoukos, P. G. (1996). Calcium carbonate deposit formation under isothermal conditions. *Canadian Journal of Chemical Engineering, 74*(6), 911-919.

ARI. (1997). Fouling Factors: A Survey of Their Application in Today's Air Conditioning and Refrigeration Industry (pp. 5). Arlington, Virginia: Air-Conditioning and Refrigeration Institute.

ARI. (2007). Performance Rating of Water-cooled Refrigerant Condensers, Remote Type (Vol. Standard 450). Arlington, Virginia: Air-Conditioning & Refrigeration Institute.

Ayub, Z. H. (2003). Plate heat exchanger literature survey and new heat transfer and pressure drop correlations for refrigerant evaporators. *Heat Transfer Engineering, 24*(5), 3-16.

Bansal, B., & Muller-Steinhagen, H. (1993). Crystallization fouling in plate heat exchangers. *Journal of Heat Transfer, Transactions ASME, 115*(3), 584-591.

Bansal, B., Muller-Steinhagen, H., & Chen, X. D. (1997). Effect of suspended particles on crystallization fouling in plate heat exchangers. *Journal of Heat Transfer, 119*(3), 568-574.

Bossan, D., Grillot, J. M., Thonon, B., & Grandgeorge, S. (1995). Experimental study of particulate fouling in an industrial plate heat exchanger. *Journal of Enhanced Heat Transfer, 2*(Compendex), 167-175.

Briggs, J. F. F. a. J. C. (1977). *Quality of Rivers of the United States, 1975 Water Year; based on National Stream Quality Accounting Network (NASQAN).*

Chamra, L. M. (2006). *Waterside Fouling Inside Smooth and Augmented Copper Alloy Condenser Tubes in Cooling Tower Applications*: Mississippi State University.

Chamra, L. M., & Webb, R. L. (1993). Effect of particle size and size distribution on particulate fouling in enhanced tubes. *Journal of Enhanced Heat Transfer, 1*(1), 65-75.

Chenoweth, J. M. (1990). Final report of the HTRI/TEMA joint committee to review the fouling section of the TEMA standards. *Heat Transfer Engineering, 11*(1), 73-107.

Churchill, S. W. (1977). Friction-factor equation spans all fluid-flow regimes. *Chemical Engineering Progress, 84*(24).

GEA. (2010). GEA FlatPlate Select. from http://www.flatplate.com

Gudmundsson, J. S. (1981). *Fouling of Heat Transfer Equipment.* Washington D.C: Hemisphere.

Hasson, D. (1962). Rate of Decrease of Heat Transfer due to Scale. *DECHEMA Monogr., 47*, 233-282.

Hasson, D., & Zahavi, J. (1970). Mechanism of calcium sulfate scale deposition on heat-transfer surfaces. *9*(1), 1-10.

Heavner, R. L., Kumar, H., & Wanniarachchi, A. S., *AIChE Symposium Series B2 - AIChE Symposium Series)*. New York: AIChE.

Kemmer, F. (1979). *The NALCO Water Handbook*: McGRAW-Hill Book Company.
Kern, D. Q. a. S., R.A. (1959). A theoretical analysis of thermal surface fouling. *Br. Chem. Eng, no. 4*
p.228-262.
Klepetsanis, P. G., & Koutsoukos, P. G. (1991). Spontaneous precipitation of calcium sulfate at conditions of sustained supersaturation. *Journal of Colloid and Interface Science, 143*(2), 299-308.
Klima, W. F., & Nancollas, G. H. (1987). *GROWTH OF GYPSUM.* Paper presented at the Fundamental Aspects of Crystallization and Precipitation Processes. Papers Presented at the National AIChE Meetings, 1985 and 1986., Chicago, IL, USA.
Knudsen, J. G., & Story, M. (1978). Effect of heat transfer surface temperature on the scaling behavior of simulated cooling tower water. *AIChE Symposium Series, 74*(174), 25-30.
Langelier, W. F. (1936). The analytical control of anti-corrosive water treatment. *Journal of American Water Works Association, 28*, 1500-1504.
Larson, T. E., Buswell, A.M. (1942). Calcium carbonate saturation index and alkalinity interpretations. *Journal of The American Water Works Association, 34*(11).
Li, W., & Webb, R. L. (2000). Fouling in enhanced tubes using cooling tower water Part II: Combined particulate and precipitation fouling. *International Journal of Heat and Mass Transfer, 43*(19), 3579-3588.
Longo, G. A. (2008). Refrigerant R134a condensation heat transfer and pressure drop inside a small brazed plate heat exchanger. *International Journal of Refrigeration, 31*(5), 780-789.
Luan, Z.-j., Zhang, G.-m., Tian, M.-c., & Fan, M.-x. (2008). Flow resistance and heat transfer characteristics of a new-type plate heat exchanger. [doi: DOI: 10.1016/S1001-6058(08)60089-X]. *Journal of Hydrodynamics, Ser. B, 20*(4), 524-529.
McQuiston, F. C., Parker, Jerald D., Spitler, Jeffrey D. (2005). *Heating, Ventilating, and Air Conditioning Analysis and Design* (Vol. 6th): Wiley.
Morse, R. W., & Knudsen, J. G. (1977). Effect of alkalinity on the scaling of simulated cooling tower water. *The Canadian Journal of Chemical Engineering, 55*(3), 272-278.
Muley, A., & Manglik, R. M. (1999). (Vol. 121).
Muller-Steinhagen, H., Reif, F., Epstein, N., & Watkinson, A. P. (1988). Influence of Operating Conditions on Particulate Fouling. *Canadian Journal of Chemical Engineering, 66*(1), 42-50.
Muller-Steinhagen, H. M., & Middis, J. (1989). Particulate fouling in plate heat exchangers. *Heat Transfer Engineering, 10*(4), 30-36.
Papavergos, P. G., & Hedley, A. B. (1984). PARTICLE DEPOSITION BEHAVIOUR FROM TURBULENT FLOWS. *Chemical Engineering Research and Design, 62*(5), 275-295.
Pearson, B. (2010). LSI Spreadsheet. In L. Cremaschi (Ed.).
Ramesh, A. (2010). *Design of An Experimental Facility to Determine Fouling Resistance of Water Cooled Brazed Plate Heat Exchangers Using Cooling Tower Water* Oklahoma State University, Stillwater.
Ritter, R. B. (1981). Crystalline Fouling Studies. *American Society of Mechanical*

Engineers, Heat Transfer Division, (Publication) HTD, 17, 67-72.
Sapali, S. N. (2009). Two-Phase Condensation Heat Transfer Coefficients and Pressure Drops of R-404A for Different Condensing Temperatures in A Smooth and Micro-Fin TUbe. *International Journal of Engineering Science and Technology, 1(2)*, 43-58.
Taborek, J., Aoki, T., Ritter, R. B., Palen, J. W., & Knudsen, J. G. (1972). Fouling. The major unresolved problem in heat transfer. *Chemical Engineering Progress, 68*(2), 59-67.
Taylor, N., Kuyatt, C.E. (1994). Guidelines for Evaluating and Expressing the Uncertainty of NIST Measurement Results: NIST Technical Note 1297.
Thonon, B., Grandgeorge, S., & Jallut, C. (1999). Effect of geometry and flow conditions on particulate fouling in plate heat exchangers. *Heat Transfer Engineering, 20*(3), 12-24.
Wanniarachchi, A. S., Ratnam, U., Tilton, B. E., & Dutta-Roy, K. (1995a). *30th National Heat Transfer Conference B2 - 30th National Heat Transfer Conference).* New York: ASME.
Wanniarachchi, A. S., Ratnam, U., Tilton, B. E., & Dutta-Roy, K. (1995b). *Approximate correlations for chevron-type plate heat exchangers.* Paper presented at the Proceedings of the 1995 30th National Heat Transfer Conference. Part 14, August 6, 1995 - August 8, 1995, Portland, OR, USA.
Watkinson, A. P., & Martinez, O. (1975). Scaling of Heat Exchanger Tubes by Calcium Carbonate. *Journal of Heat Transfer, 97 Ser C*(4), 504-508.
Webb, R. L. (1994). *Principle of Enhanced Heat Transfer*. Michigan: Wiley.
Wiechers, H. N. S., Sturrock, P., & Marais, G. v. R. (1975). Calcium carbonate crystallization kinetics. [doi: DOI: 10.1016/0043-1354(75)90143-8]. *Water Research, 9*(9), 835-845.
Y, S. G., & K, A. J. (1995). Detachment of Spherical Microparticles Adhering on Flat Surfaces by Hydrodynamic Forces. [doi: DOI: 10.1006/jcis.1995.0009]. *Journal of Colloid and Interface Science, 176*(1), 74-85.

APPENDICES

Appendix A: Moving Average Program

```
!  SlidingWindow.f90
!
!  FUNCTIONS:
!     SlidingWindow      - Entry point of console application.
!
!

!****************************************************************************
******
!
!  PROGRAM: SlidingWindow
!
!  PURPOSE:  To find a subset size for UA computations.
!
!****************************************************************************
******

      program SlidingWindow

      integer maxnum

!     parameter maxnum=10000

      real Psat(20000),EFT(20000),ExFT(20000),mdot(20000)
      real ERT(20000), ExRT(20000)

      real PsatSum,EFTSum,ExFTSum,mdotSum, DPTSum, ERTSum, ExRTSum
      real mREFSum

      real PsatAvg(20000),EFTAvg(20000),ExFTAvg(20000),mdotAvg(20000)
      real ERTAvg(20000), ExRTAvg(20000)


      integer WinSize, NumDP, MaxStart, i, j

      print*, 'Enter number of points for sliding window'

      read*, WinSize

      print*, 'Enter number of data points'

      read*, NumDP
```

```
      open (Unit=7, FILE= 'datapts.csv')

      read(7,*) NumDP

      do 100 i=1,NumDP
          read(7,*) Psat(i),EFT(i),ExFT(i),mdot(i), ExRT(i), ERT(i)

100    continue


      MaxStart=NumDP-WinSize+1

       do 200 i=1,MaxStart
          EndAvg=i+WinSize-1
          PsatSum=0
            EFTSum=0
            ExFTSum=0
            mdotSum=0
            ExRTSum=0
            ERTSum=0

            do 150 j=i,EndAvg
             PsatSum=PsatSum+Psat(j)
               EFTSum=EFTSum+EFT(j)
               ExFTSum=ExFTSum+ExFT(j)
               mdotSum=mdotSum+mdot(j)
               ExRTSum= ExRTSum+ExRT(j)
               ERTSum=ERTSum+ERT(j)
150         continue

             PsatAvg(i)=PsatSum/Float(WinSize)
               EFTAvg(i)=EFTSum/Float(WinSize)
               ExFTAvg(i)=ExFTSum/Float(WinSize)
               mdotAvg(i)=mdotSum/Float(WinSize)
               ExRTAvg(i)= ExRTSum/Float(WinSize)
               ERTAvg(i)=ERTSum/Float(WinSize)

200    continue



      open (Unit=8, FILE='SlidingWindow.csv')
      do 300 i=1, MaxStart
      write(8,*)PsatAvg(i),EFTAvg(i),ExFTAvg(i),mdotAvg(i), ExRTAvg(i),
     & ERTAvg(i)
300      continue

      end program SlidingWindow
```

Appendix B: BPHE Model to Determine Uncertainty

```
"B - Procedure to Compute UA in uncertainty mode "
{Procedure find_UA_uncertainty
(R$,P_sat_ref,T_ref_in,DeltaT_subcooling_ref,T_water_in,DELTAT_water_F,P_water,V_dot_wat
er_designed, Area_ht, m_dot_ref: m_dot_water, LMTD, UA,q_dot, T_water_out, x_ref_out,
q_flux, V_dot_ref_designed)}

Procedure find_UA_uncertainty
(R$,P_sat_ref,T_ref_in,T_ref_out,T_water_in,T_water_out,P_water,m_dot_water, Area_ht,
m_dot_ref: LMTD, UA,q_dot, x_ref_out, q_flux, V_dot_ref_designed)

{CF1:=(5/9)    [C/F]}

T_sat_ref:=Temperature(R$,P=P_sat_ref,x=1)

rho_ref_out:=density(R$, p=P_sat_ref, T=T_ref_out)

V_dot_ref_designed:=m_dot_ref/rho_ref_out
DELTAT_water_F=T_water_out-T_water_in
rho_water_in:=density(Water, p=P_water, T=T_water_in)

m_dot_water_hr:=m_dot_water*convert(lb_m/min, lb_m/hr)
c_water:=Cp(Water,T=T_water_in,P=P_water)
q_dot_min:=m_dot_water*c_water*DELTAT_water_F
q_ref=m_dot_ref*(h_ref_in-h_ref_out)
q_avg=(q_ref+q_dot_min)*0.5
q_dot=q_avg*convert(Btu/min, Btu/hr)
q_flux=q_dot/Area_ht

h_ref_in:=Enthalpy(R$,T=T_ref_in,P=P_sat_ref)

h_ref_out:=h_ref_in-(q_dot_min/m_dot_ref)

h_sat_liquid:=Enthalpy(R$,T=T_sat_ref,x=0)

if(h_ref_out<=h_sat_liquid) then
    x_ref_out=0
else x_ref_out=Quality(R$,P=P_sat_ref,h=h_ref_out)

LMTD=((T_sat_ref-T_water_out)-(T_sat_ref-T_water_in))/ln((T_sat_ref-T_water_out)/(T_sat_ref-
T_water_in))
UA_min:=m_dot_water*c_water*(T_water_out-T_water_in)/LMTD
UA=UA_min*convert(Btu/min-F, Btu/hr-F)


END find_UA_uncertainty
```

```
"----------Data Input----------"
R$='R134a'

Area_ht=4.6[ft^2]
T_water_in=85[F]
P_sat_ref=149.7[F]
T_sat_ref=T_sat(R134a,P=P_sat_ref)
P_water=14.7[psi]
T_ref_in = 169.638 [F]
T_ref_out=88 [F]

T_water_out=92.8[F]
m_dot_ref=3.5[lb_m/min]
m_dot_water=38.8
"Water side"
rho_water_in=density(Water, p=P_water, T=T_water_in)

c_water=Cp(Water,T=T_water_in,P=P_water)
q_dot_min=m_dot_water*c_water*(T_water_out-T_water_in)
q_ref=m_dot_ref*(h_ref_in-h_ref_out)
q_avg=(q_ref+q_dot_min)*0.5
q_dot=q_dot_min*convert(Btu/min, Btu/hr)
q_flux=q_dot/Area_ht

"Refrigerant side"
h_ref_in=Enthalpy(R$,T=T_ref_in,P=P_sat_ref)

h_ref_out=h_ref_in-(q_dot_min/m_dot_ref)

h_sat_liquid=Enthalpy(R$,T=T_sat_ref,x=0)

rho_ref_out=density(R$, p=P_sat_ref, T=T_ref_out)

V_dot_ref_designed=m_dot_ref/rho_ref_out

"Calculate LMTD"
LMTD=((T_sat_ref-T_water_out)-(T_sat_ref-T_water_in))/ln((T_sat_ref-T_water_out)/(T_sat_ref-
T_water_in))
UA = q_dot/LMTD

Rf=Area_ht*(1/UA-1/UA_0)
```

VITA

Ellisa Lim

Candidate for the Degree of

Master of Science

Thesis: A PRELIMINARY INVESTIGATION OF FOULING IN BRAZED PLATE HEAT EXCHANGERS

Major Field: Mechanical Engineering

Biographical:

Education: Graduated from Canadian International School (Singapore) in 2001. Received Bachelor of Science in Mechanical Engineering from Seattle University in June 2006. Completed the requirements for Master of Science in Mechanical Engineering at Oklahoma State University, Stillwater, Oklahoma in July 2010.

Experience: Employed as an Engineering Intern at Spiration, Inc. (Redmond, WA) from June 2005 to August 2005. Employed as a Mechanical Designer by The Greenbusch Group (Seattle, WA) from August 2006 to August 2007. Employed as a Graduate Teaching and Research Assistant by Mechanical an Aerospace Engineering Department at Oklahoma State University from January 2008 to July 2010.

Professional Memberships: American Society of Heating Refrigerating and Air Conditioning Engineers (ASHRAE), American Society of Mechanical Engineers (ASME).

Name: Ellisa Lim Date of Degree: July 2010

Institution: Oklahoma State University Location: OKC or Stillwater, Oklahoma

Title of Study: A PRELIMINARY INVESTIGATION OF FOULING IN BRAZED PLATE HEAT EXCHANGERS

Pages in Study: 152 Candidate for the Degree of Master of Science

Major Field: Mechanical Engineering

Scope and Method of Study: This thesis reports a preliminary investigation of combined particulate and precipitation fouling on the water-side of brazed plate heat exchangers (BPHE) used as water-cooled condensers. An experimental facility to study fouling on water-side of brazed plate-type (BPHE) condensers has been designed and constructed. The test facility was designed based on standard rating conditions to measure performance of water-cooled refrigerant condensers. This thesis also covers a methodology to compose high fouling potential water.

Findings and Conclusions: Experiments were performed on three BPHEs that have different geometries and chevron angles using high fouling potential water. The experimental results show that the fouling resistances gradually increase with Langlier Saturation Index (LSI) values, which is an index used to determine the saturation level of $CaCO_3$ in water. In addition, a strong effect of internal geometry of the plates on the asymptotic fouling resistances was observed. The asymptotic fouling resistance for the BPHE with a 60° chevron angle is almost 10 times more than the asymptotic fouling resistances of the BPHEs that have 27° chevron angles.

ADVISER'S APPROVAL: Dr. Jeffrey Spitler